DETERMINATION OF LARGE-SCALE RESERVOIR PROPERTIES USING GLOBAL AND LOCAL UPSCALING APPROACHES

Mr. Pakarang Yimpoonsap

A Thesis Submitted in Partial Fulfillment of the Requirements
for the Degree of Master of Engineering in Petroleum Engineering
Department of Mining and Petroleum Engineering
Faculty of Engineering
Chulalongkorn University
Academic Year 2004
ISBN 974-53-1114-6

การหาค่าคุณสมบัติขนาดใหญ่ของแหล่งกักเก็บโดยใช้วิธีการขยายขนาดการแบ่งส่วนแบบทั้งหมด และการขยายขนาดการแบ่งส่วนแบบเฉพาะที่

นาย ปะการัง ยิ้มพูลทรัพย์

วิทยานิพนธ์นี้เป็นส่วนหนึ่งของการศึกษาตามหลักสูตรปริญญาวิศวกรรมศาสตรมหาบัณฑิต
สาขาวิชาวิศวกรรมปิโตรเลียม ภาควิชาวิศวกรรมเหมืองแร่และปิโตรเลียม
คณะวิศวกรรมศาสตร์ จุฬาลงกรณ์มหาวิทยาลัย
ปีการศึกษา 2547
ISBN 974-53-1114-6

Thesis Title	DETERMINATION OF LARGE-SCALE RESERVOIR PROPERTIES USING GLOBAL AND LOCAL UPSCALING APPROACHES
By	Mr. Pakarang Yimpoonsap
Field of Study	Petroleum Engineering
Thesis Advisor	Suwat Athichanagorn, Ph.D.
Thesis Co-advisor	Sunthorn Pumjan, Ph.D.

Accepted by the Faculty of Engineering, Chulalongkorn University in Partial Fulfillment of the Requirements for the Master 's Degree

…….. Dean of the Faculty of Engineering
(Professor Direk Lavansiri, Ph.D.)

THESIS COMMITTEE

…… Chairman
(Associate Professor Yingyos Khemayodhin)

…… Thesis Advisor
(Assistant Professor Suwat Athichanagorn, Ph.D.)

…… Thesis Co-advisor
(Sunthorn Pumjan, Ph.D.)

…… Member
(Jirawat Chewaroungroaj, Ph.D.)

ปะการัง ยิ้มพูลทรัพย์: การหาค่าคุณสมบัติขนาดใหญ่ของแหล่งกักเก็บโดยใช้วิธีการขยายขนาดการแบ่งส่วนแบบทั้งหมด และการขยายขนาดการแบ่งส่วนแบบเฉพาะที่ (DETERMINATION OF LARGE-SCALE RESERVOIR PROPERTIES USING GLOBAL AND LOCAL UPSCALING APPROACHES) อาจารย์ที่ปรึกษา: ผศ.ดร. สุวัฒน์ อธิชนากร, อาจารย์ที่ปรึกษาร่วม: อ.ดร. สุนทร พุ่มจันทร์ จำนวนหน้า 107 หน้า, ISBN 974-53-1114-6

การกระจายตัวของค่าคุณสมบัติของแหล่งกักเก็บที่ได้จากการทำธรณีสถิตินั้น มีการแบ่งส่วนที่ละเอียดมาก โดยรายละเอียดนี้จะมีมากเกินกว่าความสามารถในการจำลองการไหลในแหล่งกักเก็บ ดังนั้นจึงต้องมีการขยายขนาดการแบ่งส่วน (Upscaling) ค่าคุณสมบัติของการแบ่งส่วนที่ใหญ่ขึ้นซึ่งให้ผลของการจำลองการไหลที่ใกล้เคียงกับผลที่ได้จากการจำลองการไหลของค่าคุณสมบัติของแหล่งกักเก็บก่อนที่จะมีการขยายขนาด วิธีการที่ใช้ในการหาค่าคุณสมบัติสำหรับการแบ่งส่วนที่ใหญ่ขึ้นในปัจจุบันเป็นวิธีที่ใช้เวลามาก งานวิจัยนี้ได้เสนอวิธีการหาค่าคุณสมบัติสำหรับการแบ่งส่วนที่ใหญ่ขึ้นแบบใหม่โดยใช้การขยายขนาดการแบ่งส่วนแบบเฉพาะที่ ซึ่งจะหาค่าคุณสมบัติขนาดใหญ่ของแหล่งกักเก็บเฉพาะตำแหน่งที่มีข้อมูลอยู่และใช้ธรณีสถิติในการกระจายค่าคุณสมบัติสำหรับการแบ่งส่วนที่ขยายแล้วไปสู่จุดต่างๆในแหล่งกักเก็บ

ในงานวิจัยนี้ ความสามารถในการซึมผ่านถูกใช้เป็นค่าคุณสมบัติของแหล่งกักเก็บที่ต้องการศึกษา ความสามารถในการซึมผ่านสำหรับแหล่งกักเก็บ 3 แหล่งได้ถูกสร้างขึ้นโดยใช้ธรณีสถิติ โดยแหล่งที่หนึ่งและสองใช้ Krigging estimation และแหล่งที่สามใช้ Sequential Gaussian Simulation ข้อมูลที่ได้จากแหล่งกักเก็บเหล่านี้ นำมาทำการขยายขนาดการแบ่งส่วนแบบทั้งหมด และขยายขนาดการแบ่งส่วนแบบเฉพาะที่ โดยใช้วิธี Harmonic-arithmetic averaging ค่าความสามารถในการซึมผ่านที่ทำการขยายขนาดการแบ่งส่วนแบบทั้งหมดและแบบเฉพาะที่ ได้ถูกนำมาเปรียบเทียบกัน นอกจากนั้นยังมีการเปรียบเทียบผลที่ได้จากการจำลองการไหลโดยใช้ค่าความสามารถในการซึมผ่านที่ได้จากการทำการขยายขนาดการแบ่งส่วนแบบทั้งหมดและแบบเฉพาะที่ กับผลที่ได้จากการจำลองการไหลโดยใช้ค่าความสามารถในการซึมผ่านที่ไม่ได้ทำการขยายการแบ่งส่วน ผลที่ได้จากการศึกษาในครั้งนี้ได้แสดงให้เห็นว่า การหาค่าคุณสมบัติขนาดใหญ่ของแหล่งกักเก็บโดยใช้วิธีการขยายขนาดการแบ่งส่วนแบบเฉพาะที่ มีประสิทธิภาพดีเท่ากับการขยายขนาดการแบ่งส่วนแบบทั้งหมด

ภาควิชา วิศวกรรมเหมืองแร่และปิโตรเลียม	ลายมือชื่อนิสิต……
สาขาวิชา วิศวกรรมปิโตรเลียม	ลายมือชื่ออาจารย์ที่ปรึกษา.....
ปีการศึกษา 2547	ลายมือชื่ออาจารย์ที่ปรึกษาร่วม.....

4471617121 : MAJOR PETROLEUM ENGINEERING
KEY WORD : /GEOSTATISTICS/ UPSCALING/ PERMEABILITY DISTRIBUTION/ SEQUENTIAL GAUSSIAN SIMULATION

PAKARANG YIMPOONSAP. DETERMINATION OF LARGE-SCALE RESERVOIR PROPERTIES USING GLOBAL AND LOCAL UPSCALING APPROACHES. THESIS ADVISOR: SUWAT ATHICHANAGORN, PH.D., THESIS CO-ADVISOR: SUNTHORN PUMJAN, PH.D., 107 pp.
ISBN 974-53-1114-6

Fine-scale reservoir properties obtained from Geostatistics generally cannot be handled by dynamic reservoir simulator. Reservoir properties for larger grid blocks are therefore. These larger grid blocks must produce similar results to those obtained from fine scale simulation. Conventional methods used to compute properties of coarse blocks are performed for the entire field and take a lot of computational time. This study introduces a new method to determine properties of large grid blocks. Local upscaling is performed at data locations, and then upscaled properties are populated for the entire reservoir using Geostatistics.

In this study, permeability was chosen as a parameter of interest. Three reservoir models were generated using Geostatistics. The permeability fields of Reservoir I and II were generated based on Krigging estimation while that of Reservoir III was generated based on Sequential Gaussian Simulation. The permeabilities of these reservoirs were upscaled by using harmonic-arithmetic averaging method. The coarse-scale permeability distributions based on global and local upscaling were compared using values of permeability. In addition, results of coarse-scale simulations based on global and local upscaling were compared with results from fine-scale simulation. The results of the study show that the new algorithm to determine large-scale permeability distribution based on local upscaling is as effective as the procedure based on global upscaling.

Department of Mining and Petroleum Engineering	Student's signature…….
Field of study: Petroleum Engineering	Advisor's signature……
Academic year: 2004	Co-advisor's signature……

ACKNOWLEDGEMENTS

I would like to express my appreciation to my advisor, Dr. Suwat Athichanagorn and my co-advisor, Dr. Sunthorn Pumjan, for their advice, guidance throughout the course of this study. I would like to thank Associate Professor Yingyos Khemayodhin and Dr. Jirawat Chewaroungroaj, who are the thesis committee for their revision of the manuscript of this thesis and suggestions.

I would like to thank my mother to be my inspiration, even through she passed away, and my sisters for her love and encouragement, which helped me to pass through the hard time of this study. Finally, I also would like to thank Mr. Worapot Laopom, my folk in the class, to help me as another adviser.

CONTENTS

Page

Page

Page

LIST OF TABLES

Table **Page**

LIST OF FIGURES

Figure **Page**

Figure **Page**

Figure **Page**

Figure **Page**

NOMENCLATURE

a	range distance
$C(h)$	covariance function
C_0	nugget value
C_1	sill value
$F_Z(Z)$	cumulative distribution function
h	lag distance
KI	Upscaled absolute permeability in the I-direction
r	correlation coefficient
ReV	Regionalized variables
RF	Random function
RV	Random variables
$\overline{x}$	mean of variable x
$\overline{y}$	mean of variable y
V_i	estimated volume of the cell i
$Z(x_i)$	Realization
z_{xi}	simple kriging estimator at location u
$Z^*_{SK}(u)$	the linear regression estimation

GREEK LETTERS

$\gamma(\boldsymbol{h})$	variogram function
λ_α	weight for α sample ($\alpha = 1,...,n$)
$\phi(x)$	scaling function
$\sigma^2_{SK}(u)$	simple kriging variance at location u

CHAPTER I

INTRODUCTION

1.1 General Statement

In general, hydrocarbon reservoirs have a certain degree of heterogeneity of reservoir properties. To describe the distribution of reservoir properties, geostatistical methods are often used. Geostatistics is the most effective technique to characterize reservoir properties since it can deal with fine scale heterogeneities and give high-resolution images of the reservoir. Due to the fact that the number of geostatistical cells is tremendous, reservoir properties generated by Geostatistics cannot be handled by a dynamic reservoir simulator really well.

In fact, larger grid blocks are needed for reservoir simulation. Reservoir properties of coarse blocks must be determined. These properties have to produce similar results to the results of fine scale simulation. The coarse scale models are supposed to maximize the computational efficiency by minimizing the grid block number needed to simulate the reservoir.

Conventional methods to compute properties of coarse blocks rely on upscaling of properties of fine-scale blocks. In general, upscaling is performed for the entire field. This approach is called global upscaling in this study. The drawback of global upscaling is that it takes a lot of computational time since it has to be performed for the entire field. In order to overcome this problem, we introduce a new method to determine properties of large grid blocks based on local upscaling. In this method, upscaling is performed at only data locations to determine the properties at coarse scale for these blocks. After that, the properties of the entire field can be determined using geostatistical method.

1.2 Objective

The purpose of this study is to find the best way to reduce computational time to prepare raw data to be used in reservoir simulation. Two different approaches which are based on traditional global fine-scale upscaling and local fine-scale upscaling are investigated.

1.3 Outline of Approach

To compare two different approaches, there are four steps as following:

1. Create raw data for three reservoir models. A data set of permeability is constructed in the same nature as the real field data such as the spacing of wells. All data in these three models are artificially created. In the first and second model, the raw data are 14 permeability values sampled from 14 vertical wells. The study area covers 4,020 feet in the north-south direction and 4,010 ft in the east-west direction. In the third model, the raw data are 28 permeability values sampled from 16 vertical wells and 3 horizontal wells. The study area covers 2,000 feet in the north-south direction and 2,000 ft in the east-west direction.
2. Create three reservoir models. Three reservoir models are created using Geostatistics. Omnidirectional variogram model, representing all directions, is used to find the variogram model in this step to examine the correlation between the data set and distance among data. In the first and second model, Krigging estimation is used to generate fine scale permeability distribution. In the third model, Sequential Gaussian Simulation is used to generate 60 realizations of fine scale permeability distribution.
3. Determine coarse scale permeability distribution based on global and local upscaling. After fine scale distribution is found, two different approaches based on global upscaling and local upscaling are applied to generate coarse scale permeability distribution. The upscaling process is based on Harmonic-Arithmetic average.

4. Compare results. Two methods are used to compare the results which are comparison based on values of permeability and comparison based on results of reservoir simulation. In comparison based on values of permeability, the correlation between coarse scale permeability values based on global and local upscaling are determined for the three reservoir models. In the comparison based on results of reservoir simulation, only coarse scale permeability distribution for Reservoir I and II are used as reservoir properties to perform reservoir simulation. There are too many realization of coarse scale permeability distribution for Reservoir III. Each realization contains a certain degree of randomness. Therefore, it is impossible to compare the results.

PETREL and GSLIB softwares were used in the geostatistical modeling while REDUCE++ program was used for reservoir simulation.

1.4 Dissertation Outline

Chapter II reviews previous works concerning with this study.

Chapter III introduces the methodology used in this study including Geostatistics, and upscaling. This chapter is divided into three sections, which are presented as follows:

- Section 3.1 discusses the principle of Geostatistics. The theory of Geostatistics is first presented. After that, a procedure to determine the relationship among the set of data and the separating distance is introduced in term of variogram analysis. In addition, discussion on Krigging estimation and Sequential Gaussian Simulation is included to explain how to estimate the variable value at each location of interest. All of the topics in this chapter can be applied to any variable of interest that exhibit a certain spatial relationship, including porosity, permeability, water saturation, and etc.

- Section 3.2 introduces the upscaling process. It briefly presents the theory of upscaling. Two main types of upscaling techniques are also discussed.

- Section 3.3 discusses two different approaches used to determine coarse scale permeability distribution which are based on global and local upscaling of fine scale permeabilities.

Chapter IV presents the approach taken in this study including generating raw data, simulating realizations from the data using Krigging estimation and Sequential Gaussian Simulation, coarse scale permeability distribution based on global and local upscaling and comparing the result using reservoir performance and similarity between generated properties.

Chapter V summarizes the results of this study. The conclusions and recommendations are also presented.

CHAPTER II

LITERATURE REVIEWS

In order to efficiently manage hydrocarbon reservoirs, field scale simulations are performed. Small-scale heterogeneities in the reservoir have a significant effect in the performance of reservoir. However, limitations of calculation process for today's reservoir simulator prevent us from performing fine-scale simulation. Therefore, there is a need to perform reservoir simulation at a larger scale, and the rock properties have to be upscaled well enough to provide a good result.

Upscaling is a technique that transforms a detailed geological model to a coarser grid simulation model such that the fluid flow behaviors in the upscaled system are at best preserved. Upscaling consists of two parts: gridding and averaging (1). Gridding is the part that fine-scale grids are redrawn into coarser grids. Averaging is the step to calculate effective properties of the coarse grid blocks while preserving fine grid fluid flow dynamics (pressure and flow rates etc.) within the coarse grid blocks. Lozano, J.A(2) presented that there are three main techniques of permeability averaging, ranged from the simplest techniques which are analytical techniques (arithmetic, harmonic, and geometric means) to intermediate techniques such as renormalization(3) and the most complicate techniques which are numerical techniques (pressure solver method(4)). Simple and intermediate techniques are fast but less accurate while numerical techniques are accurate but time consuming and costly.

For analytical techniques, it is well known that the *arithmetic mean* is derived for flows parallel to the layering direction and the *harmonic mean* is derived for flows perpendicular to the layering direction(5). However, Cardwell and Parsons(6) commented that the arithmetic and harmonic mean give only the upper and lower limits of the effective permeabilities rather than the effective permeabilities themselves. Warren and Price(7) conducted several numerical experiments to

investigate the effective permeability and concluded that the effective permeability of randomly generated three-dimensional permeable medium equals the *geometric mean*

of the individual permeabilities. However, their conclusion is only good for purely uncorrelated permeability fields that seldom exist in the real world.

Tang(8) conducted a study to compare coarse model performances of the combination of analytical techniques which are *Arithmetic-Harmonic* and *Harmonic-Arithmetic* average. His study shows that the results of *Harmonic-Arithmetic* average are more accurate than the results of *Arithmetic-Harmonic* average. Therefore, *Harmonic-Arithmetic* average was used in this thesis to upscale permeabilities.

Christie(9) stated that in the pressure-solver method, Christie sets up a single-phase-flow calculation with specified boundary conditions and then determine the value of effective permeability that yields the same flow rate as the fine-grid calculation. The results depend on the assumptions made, particularly with regard to boundary conditions. The most common assumption is that there is no-flow boundary condition.

There are several intermediate averaging techniques between the traditional simple averaging methods and the pressure solver techniques. A frequently used intermediate method is renormalization. Renormalization includes a series of multiple step calculations using an equivalent resistor network approach. There are two major problems for the renormalization technique. First, it is not flexible and not accurate for some cases. This problem arises because the renormalization technique requires that the fine grid blocks must be grouped in a particular fashion, e.g., 2x2 that makes solving a three-dimensional problem using the renormalization method quite difficult. Second, the unrealistic boundary conditions used in the renormalization technique sometimes result in estimation errors over 100%(10).

CHAPTER III

Methodology

This chapter presents the theory and technique of geosatistic and upscaling. This involves two steps, which are geostatistical analysis and upscaling analysis.

3.1 Geostatistics

The enormous expense of developing heterogeneous offshore fields and the desire to increase ultimate recovery force oil companies to use innovative reservoir characterization techniques to determine how various properties are distributed throughout a reservoir. Geostatistics is one of many new technologies often incorporated into the reservoir characterization process. It is used as a means of calculating the values of properties between the actual measured data points (interpolation), thereby creating a grid of values which can be used to create maps, cross-sections, and flow models. Geostatistics may be defined as a study of spatial correlation between variables. This rapidly growing branch of applied statistics and mathematics offers a collection of tools aimed at understanding and modeling spatial variability.

Spatial variability includes scales of connectivity (heterogeneity) as well as directionality within the data sets. Reservoir data show spatial connectivity to greater or lesser degrees because as the distance between two data points increases, the similarity between the two measurements decreases. Moreover, the similarity between two measurements will also change with direction. By understanding how data values vary with distance and direction, we can interpolate values at unsampled locations throughout our study area.

3.1.1 The basic of the regionalized variable and spatial correlation

The main purpose of regionalized variables and spatial correlation is to estimate the continuity of sample properties with distance and direction. For example, two wells in same vicinity are more likely to have similar reservoir properties than two wells which are further apart; however there are the limitation of distance and direction, needed to be considered. Spatial correlation analysis is one of the most important steps in Geostatistics because it conditions subsequent processes, such as kriging and conditional simulation results, and their associated uncertainties.

A Regionalized Variable is any variable distributed in space or sometime time. Any measurement of Regionalized Variable can be viewed as a realization of random function. The theory introduces four definitions, which are Regionalized Variables (ReV), Realization $Z(x_i)$, Random Variable (RV), and Random Function (RF). Regionalized Variables are measurable quantities which characterize the natural phenomena such as porosity of rock, ore grade, level of ground surface, etc. Realization is defined as a collected value of the Regionalized Variables. Random Variable is defined as a variable that takes a certain number of numerical values according to a certain probalility distribution or in specific a univariate distribution function. And, Random Function is the set of auto-correlated random variables or in specific a multivariate distribution function with n Random Variables ($n \in D$; D = study domain). From the definition of Random Function, the phenomenon of study domain is completely described by RF. In reality, it is impossible to have a complete data to characterize natural phenomena. However, it can be said that the Random Function model is an effective way to characterize uncertainty inherited in the model. The spatial variability structure can be found from the Random Function model. Spatial correlation describes the relationship between regionalized variables sampled at different locations. Samples that are correlated are not independent with distance. The closer two variables are to each other in space the more likely they are related. In fact, the value of a variable at one location can be

predicted from values sampled at other (nearby) locations. The two common measures of spatial continuity are the variogram and its close relative.

3.1.2 Variogram analysis

Regionalized variable theory uses the concept of semivariance or variogram[11] to express the relationship between different points on a surface. Semivariance is defined as:

$$\gamma(\boldsymbol{h}) = [1/2N(\boldsymbol{h})] \Sigma [(Z_{xi}) - Z(xi+\boldsymbol{h})]^2 \quad (3.1)$$

Where:

$\gamma(\boldsymbol{h})$	=	variogram value at distance $\boldsymbol{h}$
$\boldsymbol{h}$	=	lag (separation distance)
z_{xi}	=	value of sample located at *point xi*
$z_{xi}+\boldsymbol{h}$	=	value of sample located at *point xi*+$\boldsymbol{h}$
$N(\boldsymbol{h})$	=	total number of sample pairs for the lag interval $\boldsymbol{h}$.

Variogram is used to describe the rate of change of a regionalized variable as a function of distance. Variogram value is evaluated by calculating $\gamma(\boldsymbol{h})$ for all pairs of points in the data set and assigning each pair to a lag interval $\boldsymbol{h}$. The plot of variogram values versus lag distance, called experimental variogram. The experimental variogram is based on the values contained in the data set, and is computed as a preliminary step in the kriging process. The experimental variogram serves as a template for the model variogram. Fig. 3.1 shows the basic components of a variogram model.

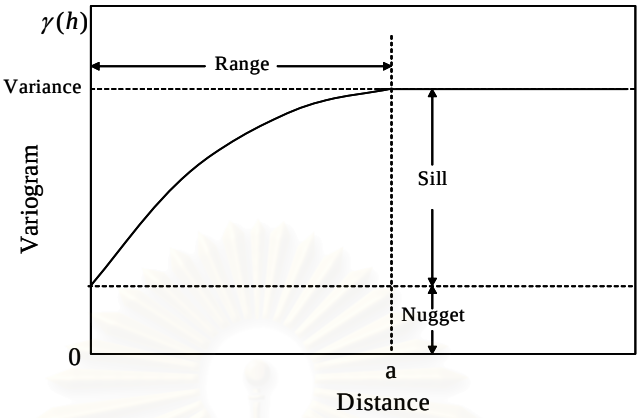

Figure 3.1: Basic components of a variogram.

As seen in Fig.3.1, there are three major components of variogram which are sill, range, and nugget. The sill represents the maximum variance of the measured spatial process being modeled. The lag distance at which the sill is reached by the variogram is called the range, which represents the maximum separation distance at which one data point will be able to correlate with any other point in the data set. Nugget represents the variation at small scale and should be zero at zero distance. But in practice, nugget value comes from two sources, measurement error and small scale variation.

3.1.2.1 Variogram search strategies

When computing the experimental variogram, the following search parameters must be taken into account. Fig 3.2 shows the example of search strategy along azimuths 45 and 135 degrees.

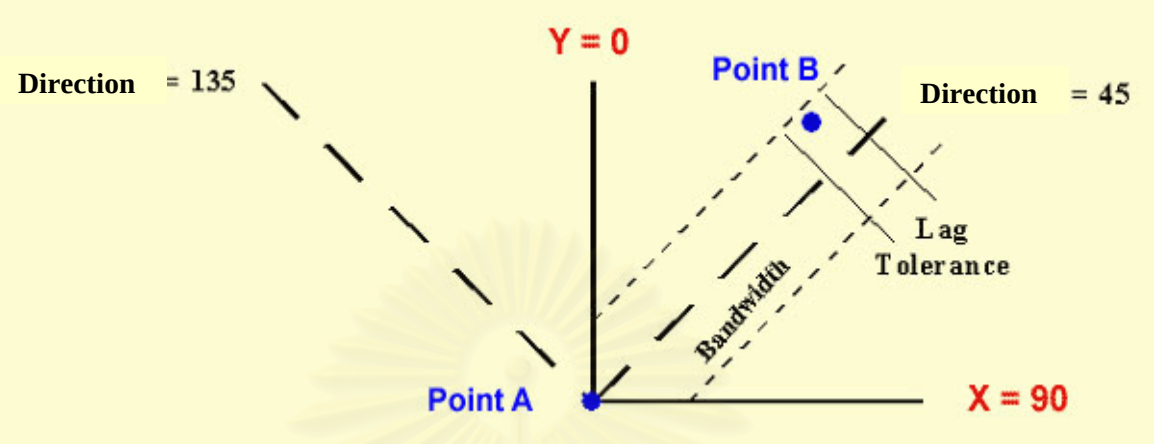

Figure 3.2: Search strategy along directions 45 and 135 degrees.

- Lag: the lag distance is the separation distance, ***h***, between sample points used in calculating the experimental model.
- Search direction: because reservoir data often exhibit directional properties, a certain direction for the search strategy needs to be specified. Such is the case when the continuity of a reservoir property is more prevalent in one direction than in another direction. The search direction also has a direction tolerance.
- Bandwidth: the bandwidth restricts the limits (width) of the direction tolerance at large lag distances.

In Fig. 3.2, point A is compared to point B. The bandwidth is indicated by a light dashed line about the search direction (heavy dashed line) of 45 degrees. Point B lies within one of the search bins designated by the lag tolerance.

3.1.2.2. Common Variogram Models

There are four common variogram models; Spherical model, Power model, Exponential model and Gaussian model.

(i) Power Model

The power model has no sill, so it is called non-transition; its equation is defined as:

$$\gamma(h) = Co + Wh^{a} \quad (3.2)$$

where,

h = lag distance,

C_o = nugget variance ≥ 0,

W = slope at origin,

a = real number

The power model is called linear model when "a" equals to one. Fig. 3.3 shows the example of power model.

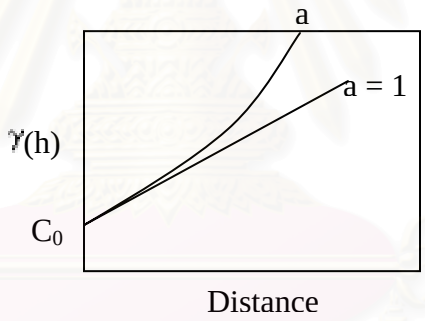

Figure 3.3: Example of Power Model.

(ii) Spherical Model

Based on the behavior at the origin and the presence of sill in the increasing of variogram values, the spherical model is called transitional model. Some other models that are defined as transitional model are exponential model and Gaussian model. This model is described by the following formula:

$$\gamma(h) = \begin{cases} C_0 + C_1\left[1.5(\frac{h}{a}) - 0.5(\frac{h}{a})^3\right] & when \quad h \le a \\ C_0 + C_1 & when \quad h > a \end{cases} \qquad (3.3)$$

where,

h = the lag distance,

C_o = nugget variance ≥ 0,

C_1 = structural variance $\geq C_o$, and

a = range

Fig. 3.4 shows the example of Spherical model.

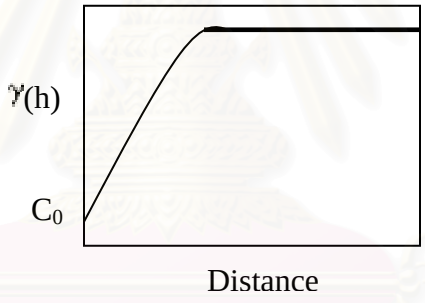

Figure 3.4: Example of Spherical Model.

(iii) Exponential model

Exponential model is a transitional model where the transition of the variogram value takes a longer distance comparing to other models. The equation and definitions of the exponential model is as follows:

$$\gamma(h) = \begin{cases} C_0 + C_1\left[1 - \exp(-\frac{h}{a})\right] & when \quad h \le a \\ C_0 + C_1 & when \quad h > a \end{cases} \tag{3.4}$$

where,

C_0 = nugget value,

C_1 = sill value,

a = range,

h = distance

Fig. 3.5 shows the example of Exponential model.

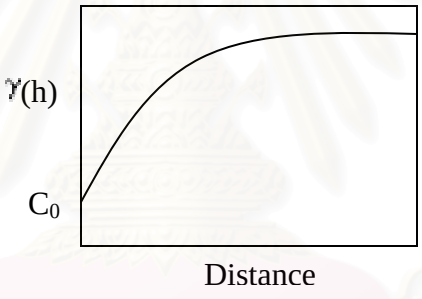

Figure 3.5: Example of Exponential Model.

(iv) Gaussian model

Gaussian model is a transitional model with the S-curve behavior at the origin. The equation and definition of Gaussian model is:

$$\gamma(h) = \begin{cases} C_0 + C_1\left[1 - \exp(-\frac{h^2}{a^2})\right] & when \quad h \le a \\ C_0 + C_1 & when \quad h > a \end{cases} \tag{3.5}$$

where,

C_0 = nugget value,

C_1 = sill value,

a = range,

h = distance

Fig. 3.6 shows the example of Gaussian model

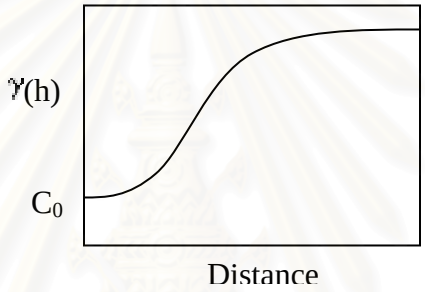

Figure 3.6: Example of Gaussian Model.

3.1.3 Krigging estimation

Kriging is a geostatistical technique for estimating attribute values at a point, over an area, or within a volume. It is a linear-regression technique, normally used to interpolate rock properties between known points. There is no bias and its error variance is minimized. In the oil field, known points are the properties obtained from wells such as seismic and outcrop data. However, the smooth interpolation produced by kriging often fails to incorporate small-scale heterogeneity and/or extreme values in the properties being distributed, which are important factors in modeling. Fig. 3.7 shows the example of krigging estimation.

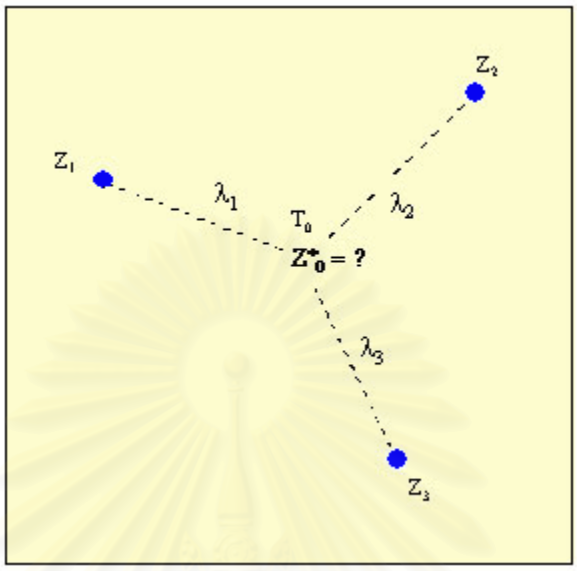

Figure 3.7: Example of krigging estimation.

From Fig. 3.7, given samples located at (Z_α), where α = 1, 2, 3 and λ_α is the weight of the sample 1, 2, 3. The estimates (Z_0) have to be found using krigging estimation.

Consider Z_0 as a linear combination of the data Z_α

$$Z_0 = \sum \lambda_\alpha Z_\alpha$$

Where: $\sum \lambda_\alpha = 1$ and $E (Z_0 - Z_\alpha)^2$ is minimum

Although, krigging estimation is very robust as it is a linear-regression technique and it is an exact interpolator if the control point matches with a grid node, it tends to produce smooth images of reality (like all interpolation techniques). In doing so, short scale variability is poorly reproduced, while it underestimates extremes (high or low values).

3.1.4 Geostatistical Simulation

Stochastic modeling, also known as conditional simulation, is a variation of conventional kriging or cokrigging. An important advantage of the geostatistical approach to mapping is the ability to model the spatial covariance before interpolation. Unlike krigging estimation, conditional simulation aims to simulate the real condition of the data. In geostatistical simulation, the study starts with the finding of spatial variability structure of variable. And, this structure is used as conditional information together with available samples to construct the conditional probability distribution function (*pdf*) at every location. Then, the simulated values are uniformly drawn from these estimated *pdf*. Finally, many realization maps are then generated. Each realization map is different from the other and conditioned to the available samples and the previously simulated data. Fig. 3.8 shows examples of porosity realizations, made from *pdf* at different locations.

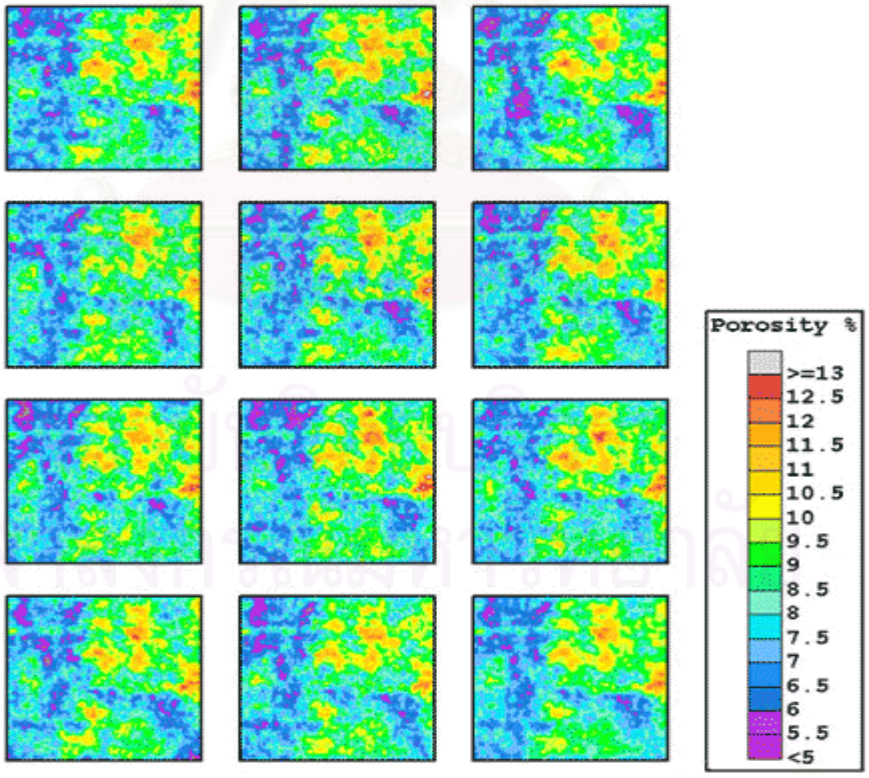

Figure 3.8: Geostatistical Simulation of Porosity realization.

3.1.4.1 Gaussian Simulation

Consider the distribution over a field A of one or more attribute(s) $z(u), u \in A$. Geostatistical simulation makes the alternatives, which are equally probable and high-resolution models of the spatial distribution of $z(u)$. To implement Sequential Gaussian Simulation, some related algorithms, which are normal score transform, checking for bivariate normality, and Simple Kriging (Deutsch and Journel, 1992), need to be explained.

(i) Normal Score Transform

The assumption of Gaussian Simulation states that the study variable has to follow standard normal distribution with zero mean and unit variance. The process of transforming original data to standard normal data is carried out using normal score transform function.

Let Z and Y be the two data sets and their *cdf* (Cumulative Distribution Function) are $F_Z(z)$ and $F_Y(y)$, respectively. The transform $Y = \varphi(Z)$ identifies the cumulative probabilities, which correspond to the Z and Y p-quantiles:

$$F_Y(y_P) = F_Z(z_p) = p, \forall p \in [0,1] \tag{3.6}$$

Thus,

$$y = F_Y^{-1}(F_Z(z)) \tag{3.7}$$

with $F_Y^{-1}(\cdot)$ being the inverse *cdf*, or quantile function, of Y data set:

$$y_p = F_Y^{-1}(p), \forall p \in [0,1] \tag{3.8}$$

In case that Y is standard normal with *cdf* $F_Y(y) = G(y)$, the transform $G^{-1}(F_Z(\cdot))$ is the normal score transform.

(ii) Checking for Bivariate Normality

To perform the simulation, the bivariate *cdf* of any pair of values $Y(u), Y(u+h)$, $\forall h$, has to be normal. In fact, there are several ways to check the bivariate normality of a normal score data set but the famous method is comparing the experimental bivariate *cdf* of any set of data pairs $\{y(U_\alpha), y(U_\alpha + h), \alpha = 1, ..., N(h)\}$ with covariance function $C_Y(h)$, which is shown as follows:

$$\text{Prob}\{Y(u) \le y_p, Y(u+h) \le y_p\} = p^2 + \frac{1}{2\pi}\int_0^{\arcsin C_Y(h)} \exp\left(-\frac{y_p^2}{1+\sin\theta}\right) d\theta \tag{3.9}$$

Where $y_p = G^{-1}(p)$ is the standard normal p-quantile and $C_Y(h)$ is the covariance function of the standard normal random function of $Y(u)$.

However, the bivariate probability of the above equation is the non-centered indicator covariance for the threshold y_p:

$$\text{Prob}\{Y(u) \le y_p, Y(u+h) \le y_p\} = E\{I(u;p) \cdot I(u+h;p)\} = p - \gamma_I(h;p) \tag{3.10}$$

Where

$I(u;p)$ = 1; if $Y(u) \le y_p$,
= 0; otherwise.

$\gamma_I(h;p)$ = the indicator variogram for the p-quantile threshold y_p.

(iii) Simple Kriging

Simple Kriging uses the basic linear regression algorithm and corresponding estimator:

$$\left[Z^*_{SK}(u) - m(u) \right] = \sum_{\alpha=1}^{n} \lambda_\alpha(u) \left[Z(u_\alpha) - m(u_\alpha) \right] \tag{3.11}$$

where

$Z(u)$ = the random variable model at location u.

u_α = the n data locations.

$m(u) = E\{Z(u)\}$ = the location-dependent expected value of random variable $Z(u)$.

$Z^*_{SK}(u)$ = the linear regression estimator, which is called Simple Kriging.

The Simple Kriging weights $\lambda_\alpha(u)$ are calculated from the following Simple Kriging system:

$$\sum_{\beta=1}^{n} \lambda_\beta(u) C(u_\beta, u_\alpha) = C(u, u_\alpha), \alpha = 1, ..., n \tag{3.12}$$

In the Simple Kriging system, it is required that the means of $m(u)$ and $m(u_\alpha), \alpha = 1, ..., n$ must be known. In addition, the $(n+1)$ by $(n+1)$ covariance matrix $\left[C(u_\alpha, u_\beta), \alpha, \beta = 0, 1, ..., n \right]$ with $u_0 = u$ are required in conducting the Simple Kriging. However, when the random function of $Z(u)$ is stationary with constant mean m, and covariance function $C(h) = C(u, u+h), \forall u$, Eq. 3.11 can be reduced to:

$$Z^*_{SK}(u) = \sum_{\alpha=1}^{n} \lambda_\alpha(u) Z(u_\alpha) + \left[1 - \sum_{\alpha=1}^{n} \lambda_\alpha(u) \right] m \tag{3.13}$$

with the Simple Kriging variance:

$$\sigma^2_{SK}(u) = C(0) - \sum_{\alpha=1}^{n} \lambda_\alpha(u) C(u - u_\alpha) \tag{3.14}$$

where $\sigma^2_{SK}(u)$ is Simple Kriging variance.

In a nutshell, the mean and variance of conditional probability distribution are calculated using Simple Kriging system by which the kriged estimated values represent the means and the Kriging variances represent the variances.

3.1.4.2 Sequential Gaussian Simulation Procedure

Sequential Gaussian Simulation is an estimation model defined under multigaussian assumption. The conditional probability distribution functions are fully characterized by their means and variances given by Simple Kriging System. The estimated means and variances honor both available data and simulated data. The procedure to execute the simulation is presented as follows:

1. Transform the data set into a standard normal score data.
2. Check for Bivariate Normality of the normal score data. The data must meet the condition, if not, other simulation should be considered.
3. Construct variogram analysis to fit with a proper model.
4. Select at random grid node.
5. Krigging estimate is performed at selected visited node to estimate the mean and variance.
6. Represent a simulated data from that distribution, and add the simulated data to the data set.
7. Select another grid node at random and repeat the procedure for Simple Kriging until all grid nodes are simulated.
8. Back transform the simulated data to the original space, and the realization map is created.
9. Provide different random number sequences for random visited nodes and repeat the same procedure for additional realization maps.

In summary, Sequential Gaussian Simulation is a high performance tool to estimate fine-scale properties distribution. Fig. 3.9 shows the flowchart of Sequential Gaussian Simulation procedure.

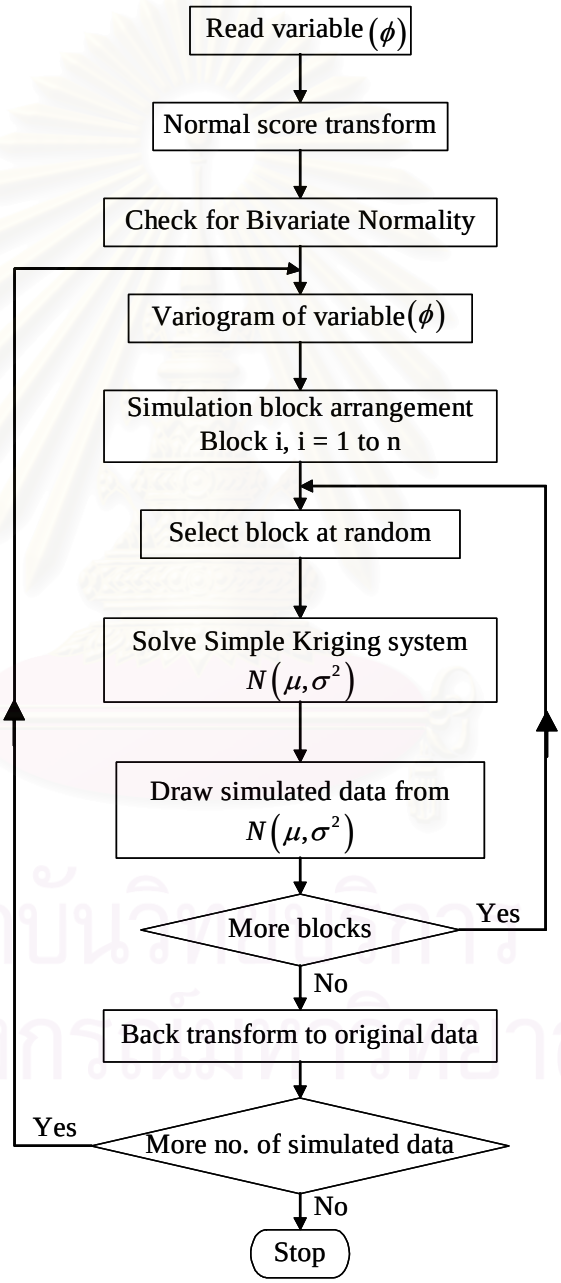

Figure 3.9: Sequential Gaussian Simulation process.

Geostatistical method is an effective way to estimate reservoir parameters such as permeability, net oil thickness, and porosity. In practice, the procedure of geostatistical estimation or simulation involves these steps of work: (1) preparing the raw data; (2) finding variogram model; (3) generating fine-scale property distribution based on kriging estimation or stochastic simulation.

3.2 Upscaling

Generally, geologic models created using geostatistical techniques are very huge models. There are typically millions of cells that make up the model comprising of many detailed features of reservoir. Moreover, studying a fine-scale reservoir model requires a great deal of time and file management. To simulate a reservoir at a very fine resolution is unreasonable and financially unacceptable. Thus, to reduce simulation time and cost, the reservoir engineer coarsens the fine grid of the original geological model and assigns new reservoir properties for the coarse grid blocks. This process is called upscaling.

Upscaling methods are expected to reduce the size of the original geological model with minimum lost of accuracy. The values are assigned for the properties of coarse grid blocks in such a way that the coarse grid blocks would reproduce almost the same behavior as the fine grid blocks. Upscaling techniques can be divided into two main techniques: analytical and numerical.

3.2.1 Analytical Techniques

Analytical techniques are the simple and easy way for averaging compared with numerical techniques. In this study, we will describe three types of averaging: simple averaging, composite 1-D solutions, and renormalization technique.

3.2.1.1 Simple Averaging

In a simple averaging method, the averaging formula is not justified by reference to an approximate flow solution. The examples of simple averaging are arithmetic and harmonic averaging. Fig. 3.10 shows an example of finding average permeability (kIi) in one direction using arithmetic and harmonic averaging.

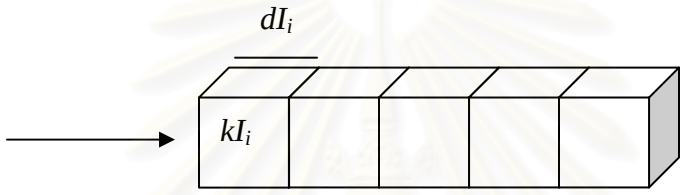

Figure 3.10: An example of simple averaging.

kI_i represents the absolute permeability of the microcell in the I-direction and dI_i represents estimate of the length of the microcell in the I-direction for microcell *i*.

(i) Arithmetic averaging

Arithmetic averaging is equivalent to assuming that all the microcells are in series. The Arithmetic averaging equation is shown below:

$$KI \sum \frac{V_i}{dI_i^2} = \sum \frac{V_i kI_i}{dI_i^2} \qquad (3.15)$$

where

KI = Upscaled absolute permeability in the I-direction

V_i = Estimated volume of the cell *i*

(ii) Harmonic averaging

Harmonic averaging is equivalent to assuming that all the microcells are in parallel. The Harmonic averaging equation is shown below:

$$\frac{1}{KI}\sum\frac{dI_i^{\,2}}{V_i}=\sum\frac{dI_i^{\,2}}{V_i kI_i} \tag{3.16}$$

3.2.1.2 Composite 1-D Solutions

This averaging technique is a combination between arithmetic and harmonic averaging. There are two types of combination which are harmonic-arithmetic and arithmetic-harmonic averaging. Fig. 3.11 shows an example of the flow direction and microcells.

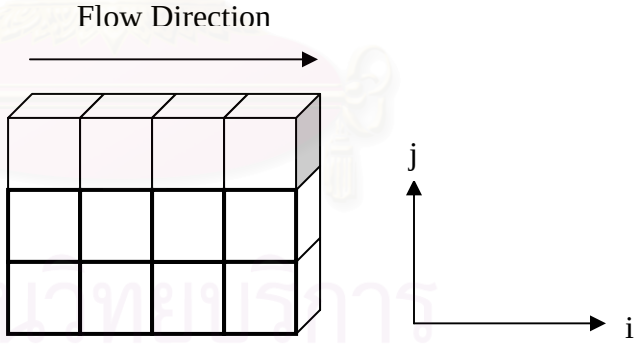

Figure 3.11: Flow direction and microcells.

(i) Harmonic-arithmetic averaging

In this method, microcells are averaged using Harmonic averaging first in the i-direction and then arithmetic averaging is performed in the j-direction as shown in Fig. 3.12. The equation of harmonic-arithmetic is shown below.

$$\sum_j \frac{1}{\sum_i \frac{dI_{ij}^2}{V_{ij} kI_{ij}}} = KI \sum_j \frac{1}{\sum_i \frac{dI_{ij}^2}{V_{ij}}} \tag{3.17}$$

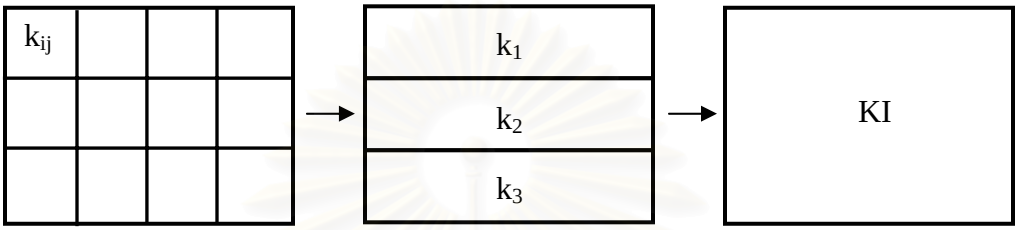

Figure 3.12: Harmonic-arithmetic averaging.

(ii) Arithmetic-harmonic averaging

In this method, microcells are averaged using arithmetic averaging first in the j-direction and then harmonic averaging is performed in the i-direction as shown in Fig. 3.13. The equation of arithmetic-harmonic is shown below.

$$KI = \frac{\sum_i \frac{1}{\sum_j \frac{V_{ij}}{dI_{ij}^2}}}{\sum_i \frac{1}{\sum_j \frac{V_{ij} kI_{ij}}{dI_{ij}^2}}} \tag{3.18}$$

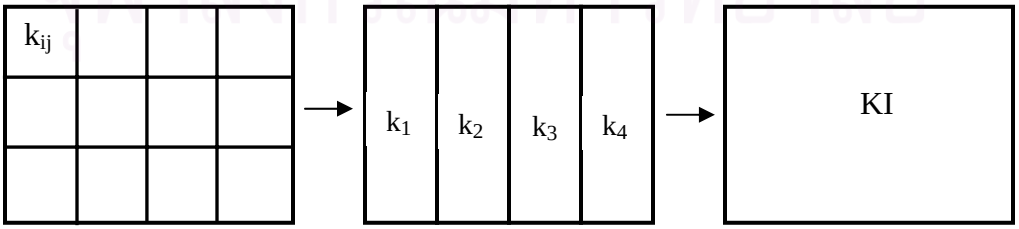

Figure 3.13: Arithmetic-harmonic averaging.

3.2.1.3 Renormalization

The renormalization[3] method considers adjacent blocks as an equivalent resistor network assuming that pressure along the boundaries perpendicular to the flow direction are constant. Then, the equivalent resistor between the midpoints of the edges is equal to 1/K for a block of permeability K. This is equivalent to two resistors in series of 1/ (2K) as shown in Fig. 3.14.

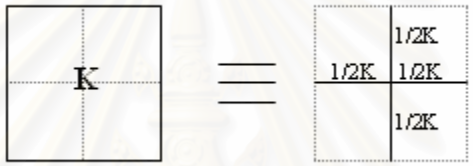

Figure 3.14: Permeability in resistor network.

Effective permeability is calculated in only one direction. Therefore, we can set the end edges to uniform pressures. Fig. 3.15 shows the transformation from permeability type to resistor type.

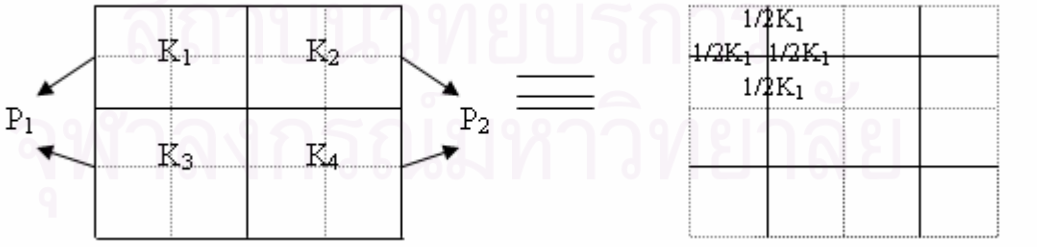

P_1 and P_2 are constant.

Figure 3.15: Permeability in resistor network.

The dead end branches are trimmed off and joined together. Fig 3.16 shows a sketch of an equivalent resistor network.

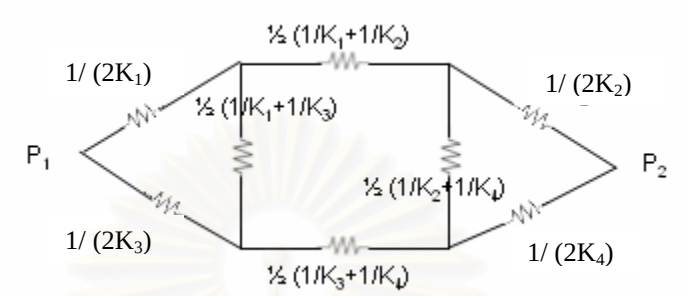

Figure 3.16: New equivalent resistor network.

From Fig. 3.16, this network may be simplified by use of the star-triangle transformation to give a circuit of resistors in series and parallel as depicted in Fig. 3.17.

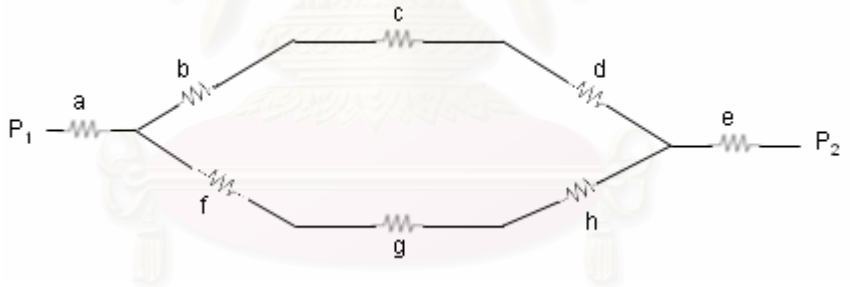

Figure 3.17: Star-triangle transformed equivalent resistor network.

where

$a = 1/[4(K_1+K_3)]$, $b = 1/(4K_1)$, $c = ½(1/K_1+1/K_2)$, $d = 1/(4K_2)$
$e = 1/[4(K_2+K_4)]$, $f = 1/(4K_3)$, $g = ½(1/K_3+1/K_4)$, $h = 1/(4K_4)$

This circuit is equivalent to Fig 3.18.

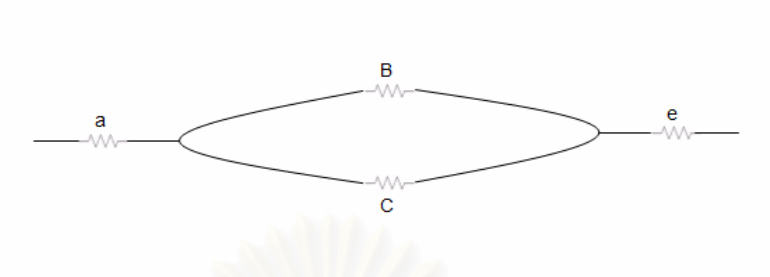

Figure 3.18: Transformed equivalent resistor network.

where

$B=3/4[(K_1+K_2)/K_1K_2]$, $C=3/4[(K_3+K_4)/K_3K_4]$

The effective permeability of the four permeabilities is then

$$f(K) = 4(K_1+K_3)(K_2+K_4)[K_2K_4(K_1+K_3)+K_1K_3(K_2+K_4)]X \{[K_2K_4(K_1+K_3)+K_1K_3(K_2+K_4)][K_1+K_2+K_3+K_4]+ 3(K_1+K_2)(K_3+K_4)(K_1+K_3)(K_2+K_4)\}^{-1} \quad (3.19)$$

3.2.2 Numerical techniques

A myriad of numerical methods has been introduced by various researchers. Most of these methods are able to provide higher accuracy than the analytical procedures; however, they require solving flow equations at the fine scale which is time consuming. Numerical upscaling is usually used for complex modeling in situations where accuracy is the most important factor. The principle is that the detailed, stochastic description is divided into a number of sectors easy to accommodate in a flow simulator. In each of this sector, the flow equation is solved under stationary conditions; average pressures and inter-region flows are computed for regions.

The pressure-solver method is the most accurate technique to calculate the permeability of a large coarse block containing many fine grid blocks. The upscaled

permeability is determined by solving flow equations with constant pressure and no-flow boundary conditions. This approach solves the fine-grid pressure distribution first and then calculates the permeability using the pressure drop and the calculated flux. The pressure-solver technique is generally limited by the size and complexity of a geologic model.

3.3 Coarse-scale Permeability Distribution

Upscaling approaches in this study are divided into two main categories, which are upscaling of global fine-scale geostatistical estimates (conventional upscaling) and upscaling of local fine-scale geostatistical estimates (upscaling only at certain location to reduce the upscaling time).

3.3.1 Coarse-scale Permeability Distribution Based on Upscaling of Global Fine-scale Geostatistical Estimates

This is a conventional approach used to upscale reservoir properties by first applying Geostatistics to determine fine-scale geostatistical estimate for every block and then upscaling reservoir properties for the entire area of interest.

The process of the global upscaling can be divided into three stages. The first step is collecting data at well locations. Fig. 3.19 sketches well locations at which permeability is sampled. Second, we use Geostatistics to expand the sampled data to fine-scale field estimates. Fig. 3.20 displays scale of permeability distribution obtained from Geostatistics. Third, global upscaling of the fine-scale estimates to coarser field estimates is performed. Fig. 3.21 shows scale of distribution after global upscaling.

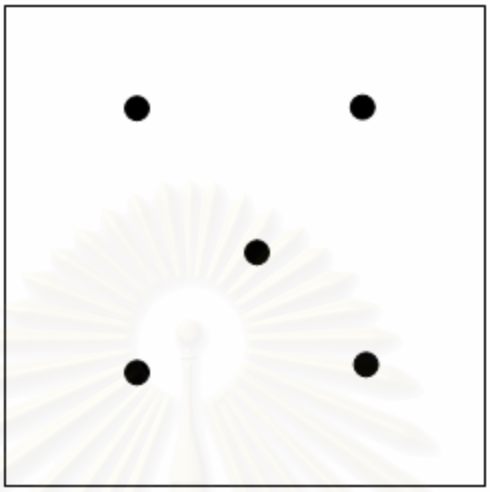

Figure 3.19: Permeabilities sampled at well locations.

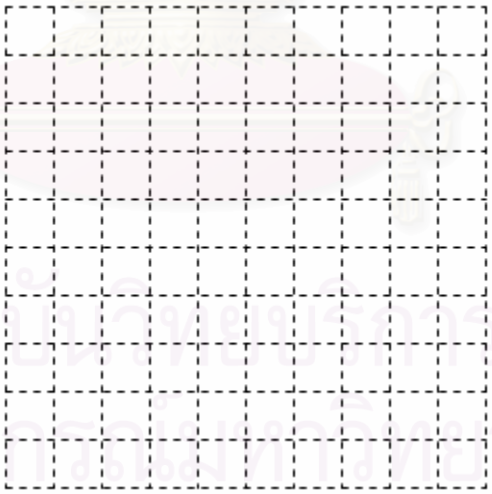

Figure 3.20: Scale of permeability distribution obtained from Geostatistics.

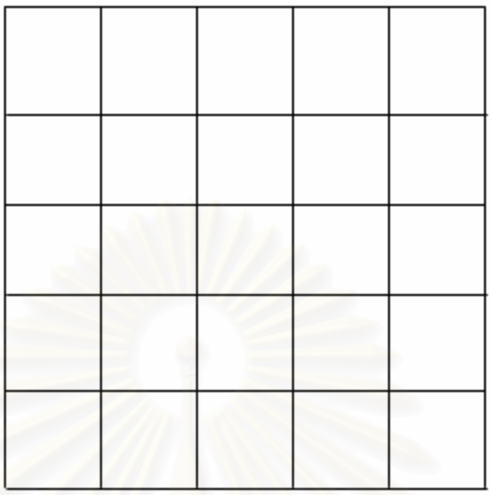

Figure 3.21: Scale of permeability distribution after global upscaling.

3.3.2 Coarse-scale Permeability Distribution Based on Upscaling of Local Fine-scale Geostatistical Estimates

In this approach, Geostatistics is applied to obtain the fine-scale geostatistical estimate for every block. Then, we upscale the local fine-scale geostatistical estimates, i.e., upscaling is performed only in the blocks where the wells are located. After that, Geostatistics is applied again to determine the distribution of reservoir properties at coarse scale.

There are four steps involved in this approach. The first step is to collect data at well locations. Fig. 3.22 shows permeability sampled at well locations. Second, Geostatistics is applied to expand the sampled data to fine-scale field estimates. Fig. 3.23 displays scale of permeability distribution obtained from Geostatistics. Third, local upscaling of fine-scale estimates is performed, i.e., upscaling only the blocks at which the wells are located. Fig. 3.24 shows local upscaling. Finally, Geostatistics is used to expand

the local upscaled estimates to full field upscaled estimates. Fig. 3.25 displays scale of permeability obtained from Geostatistics.

Figure 3.22: Permeabilities sampled at well locations.

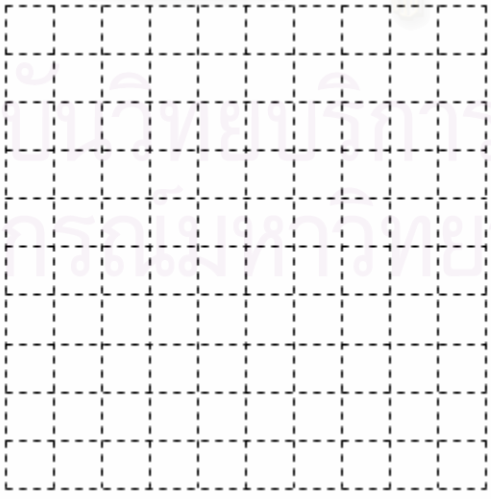

Figure 3.23: Scale of permeability distribution obtained from Geostatistics.

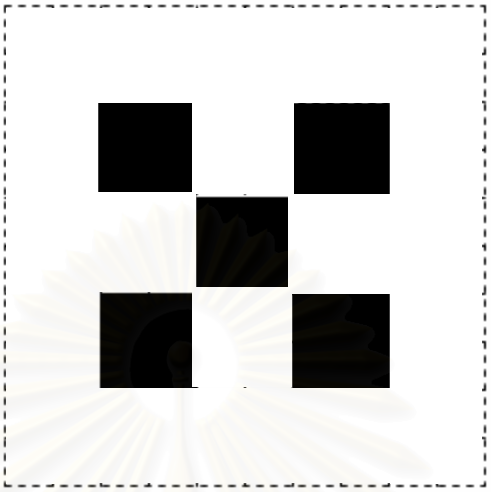

Figure 3.24: Local upscaling.

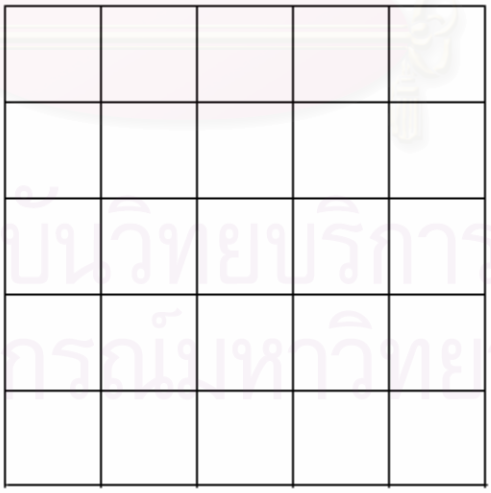

Figure 3.25: Scale of permeability obtained from Geostatistics.

CHAPTER IV

RESULTS AND DISCUSSION

This chapter composes of four sections, which are generating raw data, creating realizations, upscaling, and discussion of results. Three synthetic reservoir models were used in this study. The first and second reservoirs were constructed based on Krigging estimation (Reservoir I and II). The third reservoir was constructed using stochastic simulation (Reservoir III). These three reservoirs were upscaled using two different approaches, local and global upscaling. Then, the results of both local and global upscaling were compared based on two methods which are values of permeability and results of reservoir simulation.

4.1 Generating raw data

In order to compare the performance of local and global upscaling techniques, artificial data sets were generated. There are two points to consider in generating the data, which are well spacing and value of variable of interest, which is permeability. Well spacing in this study is approximately about 1640 feet. The permeability value is between 30 and 220 md. There are 14 permeability values sampled from 14 vertical wells in Reservoir I and II, located in the study area of 4,020 × 4,010 ft^2 which can be divided into 400 × 400 blocks with the size 10 × 10 ft^2. For Reservoir III, 28 permeability data were taken from 16 vertical wells and 3 horizontal wells, located in reservoir with an area of 2,000 × 2,000 ft^2 which can be divided into 200 × 200 blocks with the size 10 × 10 ft^2.

Table 4.1: Permeability values at sampled locations for Reservoir I.

X-coordinate (feet)	Y-coordinate (feet)	Permeability (md)
840	3590	70
1840	3590	30
3340	3590	130
640	2730	40
1840	2750	190
2840	3090	170
1340	1980	90
2840	1990	100
840	1380	140
1840	1070	120
3340	1340	220
840	590	80
2840	590	150
3340	1050	200

Table 4.2: Permeability values at sampled locations for Reservoir II.

X-coordinate (feet)	Y-coordinate (feet)	Permeability (md)
840	3590	40
1840	3590	100
3340	3590	180
640	2730	190
1840	2750	50
2840	3090	60
1340	1980	120
2840	1990	100
840	1380	190
1840	1070	30
3340	1340	160
840	590	110
2840	590	130
3340	1050	170

Table 4.3: Permeability values at sampled locations for Reservoir III.

X-coordinate (feet)	Y-coordinate (feet)	Permeability (md)
160	250	112
270	720	128
330	1260	115
340	1260	118
350	1260	121
360	1260	124
230	1780	83
480	320	118
490	330	120
500	340	122
510	350	124
540	1640	102
760	720	138
740	1280	142
860	180	96
990	1100	150
960	1650	108
1230	430	106
1300	900	132
1310	1520	126
1440	1290	136
1690	320	78
1620	900	106
1620	920	108
1620	940	110
1620	960	112
1780	1780	100
1940	1250	95

Tables 4.1, 4.2, and 4.3 show permeability values at sampled locations for Reservoir I, II, and III respectively. Fig. 4.1 shows the location map of the permeability data for Reservoir I and II while Fig. 4.2 shows the location map of the permeability data for Reservoir III.

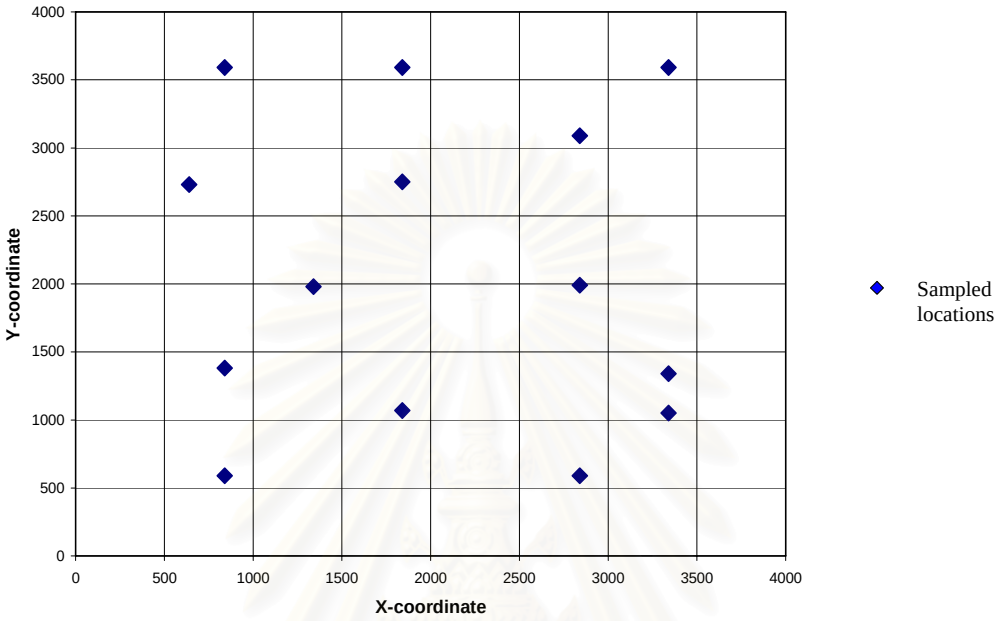

Figure 4.1: Location map of permeability data for Reservoir I and II.

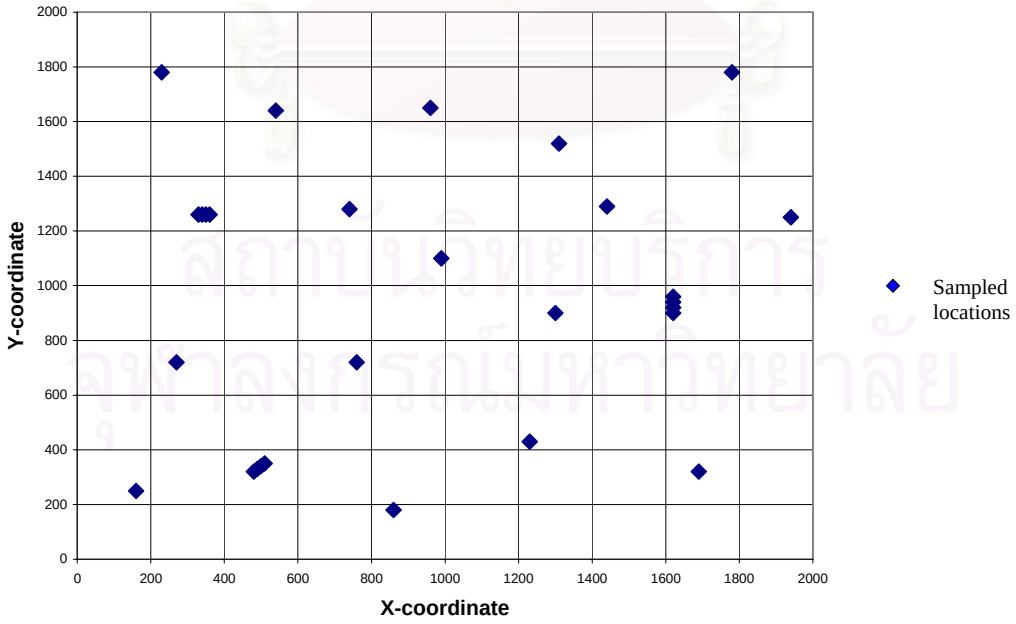

Figure 4.2: Location map of permeability data for Reservoir III.

As shown in Fig. 4.2, Reservoir III has 16 vertical wells and three horizontal wells scatter around the study area. Horizontal wells can be recognized from close data locations.

Table 4.4 shows a statistical analysis of the permeability data for Reservoir I. The mean of the data is 123.57, and variance and standard deviation are 3455.49 and 58.78, respectively. The minimum and maximum values of the data are 30 and 220, respectively. The first, second, and third quartiles are 75, 125, and 160, respectively. Coefficient of variation, skewness, and kurtosis are 47.57, 0.03, and 1.97, respectively. The statistics of Reservoir I show that values of the data spread from 30 to 220. The coefficient of variation is very high indicates there are high variation in the sample. The small skewness (0.03) close to zero and the small difference between the median (125) and the mean (123.57) indicate that the histogram of the data is approximately symmetric.

Table 4.5 shows a statistical analysis of the permeability data for Reservoir II. The mean of the data is 116.43, and variance and standard deviation are 3178.57 and 56.38, respectively. The minimum and maximum values of the data are 30 and 190, respectively. The first, second, and third quartiles are 55, 115, and 165, respectively. Coefficient of variation, skewness, and kurtosis are 48.42, -0.13, and 1.69, respectively. The statistics of Reservoir II show that values of the data spread from 30 to 190. The coefficient of variation is very high indicates there are high variation in the sample. The small skewness (-0.13) close to zero and the small difference between the median (115) and the mean (116.43) indicate that the histogram of the data is approximately symmetric.

Table 4.6 shows a statistical analysis of the permeability data for Reservoir III. The mean of the data is 115.35, and variance and standard deviation are 282.98 and 16.82, respectively. The minimum and maximum values of the data are 78 and 150, respectively. The first, second, and third quartiles are 106, 116, and 124, respectively. Coefficient of variation, skewness, and kurtosis are 14.58, -0.16, and 2.87, respectively.

The statistics of Reservoir III show that values of the data spread from 78 to 150. The coefficient of variation is very high indicates there are high variation in the sample. The small skewness (-0.16) close to zero and the small difference between the median (116.5) and the mean (115.35) indicate that the histogram of the data is approximately symmetric.

Table 4.4: Statistics of permeability data for Reservoir I.

Parameters	Values
Mean	123.57
Variance	3455.49
Std. Dev.	58.78
Minimum	30.00
25th%	75.00
Median	125.00
75th%	160.00
Maximum	220.00
Coefficient of variation	47.57
Skewness	0.03
Kurtosis	1.97

Table 4.5: Statistics of permeability data for Reservoir II.

Parameters	Values
Mean	116.43
Variance	3178.57
Std. Dev.	56.38
Minimum	30.00
25th%	55.00
Median	115.00
75th%	165.00
Maximum	190.00
Coefficient of variation	48.42
Skewness	-0.13
Kurtosis	1.69

Table 4.6: Statistics of permeability data for Reservoir III.

Parameters	Values
Mean	115.35
Variance	282.98
Std. Dev.	16.82
Minimum	78.00
25th%	106.00
Median	116.50
75th%	124.00
Maximum	150.00
Coefficient of variation	14.58
Skewness	-0.16
Kurtosis	2.87

4.2 Creating the realizations

This part presents the procedure for generating geological model of the permeability. In this section, there are two different methodologies based on estimation process in Geostatistics which are Krigging estimation for Reservoir I and II and Sequential Gaussian Simulation estimation for Reservoir III.

4.2.1 Krigging estimation for Reservoir I and II

For Reservoir I and II, geological models based on Krigging estimation were constructed using a program called PETREL[12].

Variogram calculations of these data and variogram modeling were also constructed using PETREL program. Since there are a few points, directional variogram is difficult if not impossible to determine. Therefore, this study used omnidirectional variogram which can represent variogram in all directions.

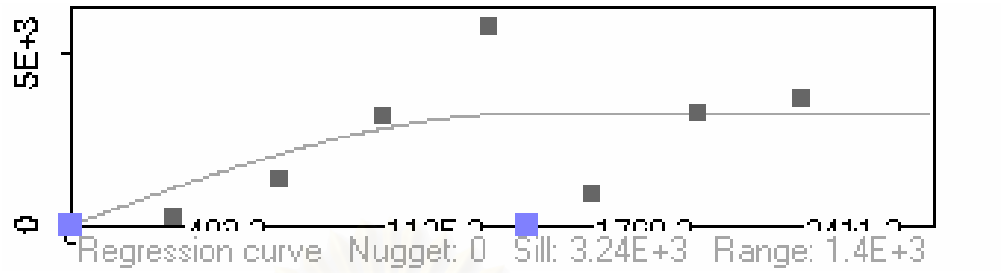

Figure 4.3: Omnidirectional variogram for Reservoir I.

Fig. 4.3 shows the variogram values and its model for Reservoir I. The parameters used to calculate this variogram are 321.5 feet of lag distance, 160.75 feet of lag tolerance, 8 lags, 0 degree of direction, 90 degree of angular tolerance, and no limits of maximum bandwidth. The solid line shown in the figure is the variogram model. Table 4.7 shows the model parameters of variogram for Reservoir I which is spherical model with nugget of 0.00, range of 1,400 feet, and sill of 3,240.

Table 4.7: Variogram model parameters for Reservoir I.

Parameters	Values
Model	Spherical
Nugget	0.00
Range	1,400 feet
Sill	3,240

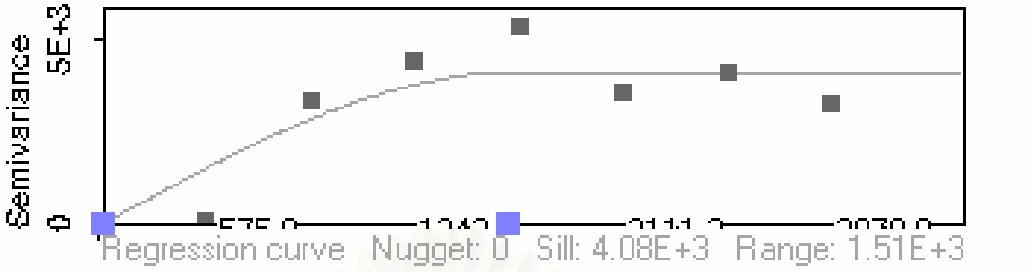

Figure 4.4: Omnidirectional variogram for Reservoir II.

Fig. 4.4 shows the variogram values and its model for Reservoir II. The parameters used to calculate this variogram are 383.9 feet of lag distance, 191.95 feet of lag tolerance, 8 lags, 0 degree of direction, 90 degree of angular tolerance, and no limits of maximum bandwidth. The solid line shown in the figure is the variogram model. Table 4.8 shows the model parameters of variogram for Reservoir II, which is spherical model with nugget of 0.00, range of 1,510 feet, and sill of 4,080.

Table 4.8: Variogram model parameters for Reservoir II.

Parameters	Values
Model	Spherical
Nugget	0.00
Range	1,510 feet
Sill	4,080

After the variogram model parameters were found, these parameters were used to create fine-scale geostatistical model based on Krigging estimation method. Figs. 4.5 and 4.6 show the picture of geological model for Reservoir I and II, respectively. The red color represents high values of permeability while the blue color represents low value of permeability. Table 4.9 and 4.10 show statistics of permeability data based on Krigging estimation for Reservoir I and II, respectively.

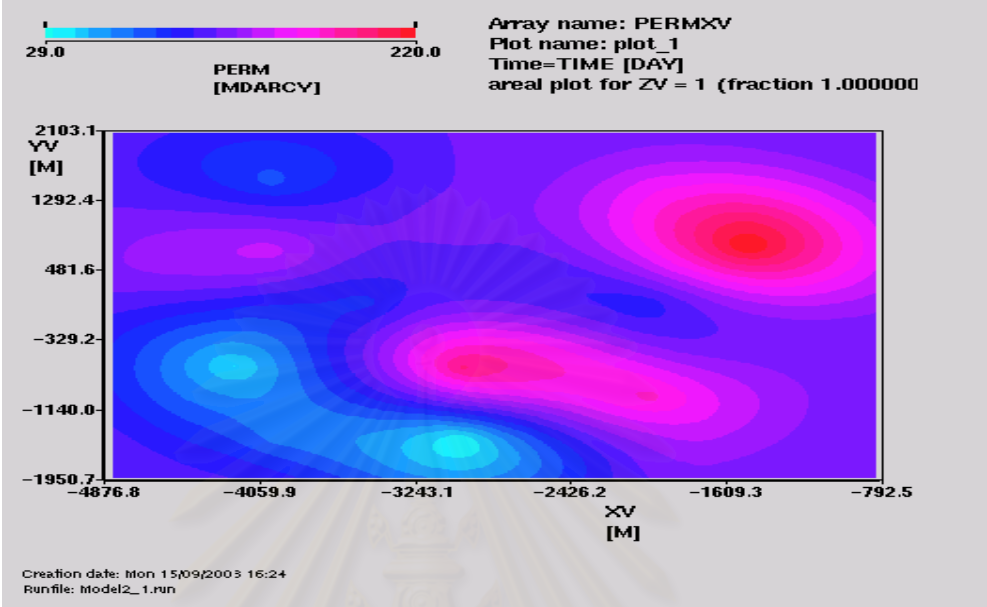

Figure 4.5: Geological model using Krigging estimation for Reservoir I.

Table 4.9: Statistics of permeability data based on Krigging estimation for Reservoir I.

Parameters	Values
Mean	117.14
Variance	944.48
Std. Dev.	30.73
Minimum	31.21
25th%	100.04
Median	117.40
75th%	132.71
Maximum	217.52
Coefficient of variation	26.24
Skewness	0.15
Kurtosis	3.30

The statistics of permeability data based on Krigging estimation show that the data was smoothed by Krigging estimation. The variance reduces from 3455.49 down to 944.48 and Standard deviation from 58.78 to 30.73.

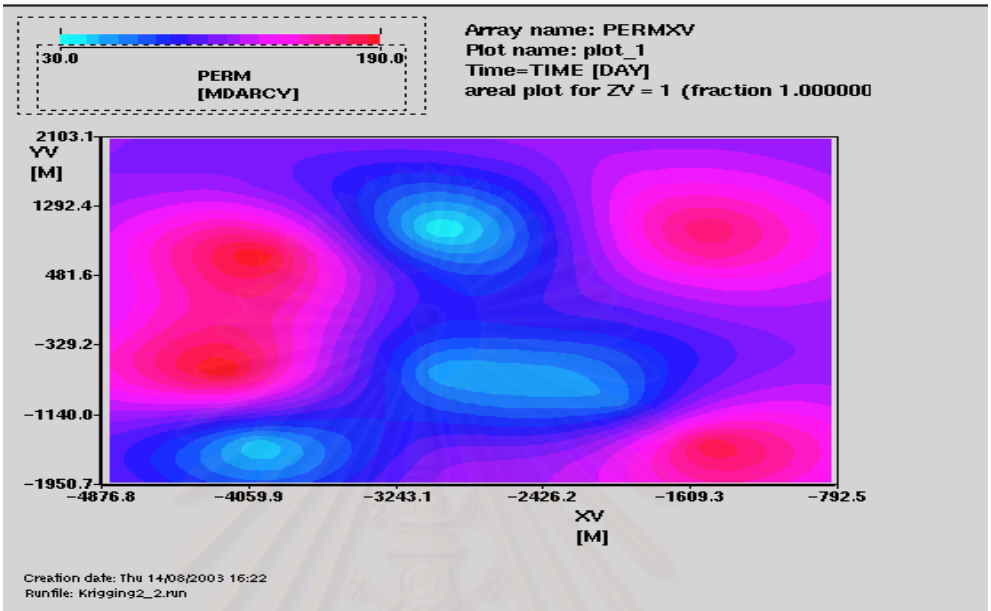

Figure 4.6: Geological model using Krigging estimation for Reservoir II.

Table 4.10: Statistics of permeability data based on Krigging estimation for Reservoir II.

Parameters	Values
Mean	111.54
Variance	1032.04
Std. Dev.	32.13
Minimum	32.09
25th%	86.87
Median	110.69
75th%	136.12
Maximum	188.71
Coefficient of variation	28.80
Skewness	0.04
Kurtosis	2.23

The statistics of permeability data based on Krigging estimation show that the data was smoothed by Krigging estimation. The variance reduces from 3178.57 down to 1032.04 and Standard deviation from 56.38 to 32.13.

4.2.2 Sequential Gaussian Simulation estimation for Reservoir III

The simulation process can be divided into 2 steps, which are finding the spatial variability structure of permeability variable (known as variogram model) and conducting the simulation. The first step, constructing the variogram model, is executed by Variowin computer program, which is a good graphic display computer program that can show analysts how fit of a model in comparison with the calculated variogram values. The second step which is performing the Sequential Gaussian Simulation is implemented by GSLIB program.

4.2.2.1 Constructing the variogram model

To perform the Sequential Gaussian Simulation, the sample values have to be transformed to normal score data before further analysis due to its assumption of multigaussian distribution. In this study, the data were transformed using GSLIB program. The normal score data are presented in Table 4.11.

Table 4.11: Permeability values at sampled locations and normal score values.

X coordinate (Feet)	Y coordinate (Feet)	Permeability values	Normal score values
160	250	112	-0.1347
270	720	128	0.8544
330	1260	115	-0.0448
340	1260	118	0.1347
350	1260	121	0.3186
360	1260	124	0.5142
230	1780	83	-1.6112
480	320	118	0.0448
490	330	120	0.2257
500	340	122	0.4144
510	350	124	0.6193
540	1640	102	-0.8544
760	720	138	1.3452
740	1280	142	1.6112
860	180	96	-1.1503
990	1100	150	2.1002
960	1650	108	-0.4144
1230	430	106	-0.6193
1300	900	132	0.9915
1310	1520	126	0.7318
1440	1290	136	1.1503
1690	320	78	-2.1002
1620	900	106	-0.7318
1620	920	108	-0.5142
1620	940	110	-0.3186
1620	960	112	-0.2257
1780	1780	100	-0.9915
1940	1250	95	-1.3452

Table 4.12 shows the statistics of the normal score data, which were transformed from the original permeability data. The new data have a mean of zero and variance and standard deviation of one, which are the characteristics of standard normal distribution. The minimum and maximum values are -2.1 and 2.1, respectively. The first, second, and third quartiles are -0.732, 0.000, and 0.619, respectively. Coefficient of variation, skewness, and kurtosis are 0, 0, and 2.601, respectively.

Table 4.12: Statistical analysis of the normal score data.

Parameters	Values
Mean	0.00
Variance	1.00
Std. Dev.	1.00
Minimum	-2.10
25th%	-0.73
Median	0.00
75th%	0.62
Maximum	2.10
Coefficient of variation	0.00
Skewness	0.00
Kurtosis	2.60

After the normal score data were prepared, variogram calculations of these data and a variogram modeling were performed using the Variowin program. Fig. 4.7 illustrates the plot of the experimental variogram values at difference distances and its model.

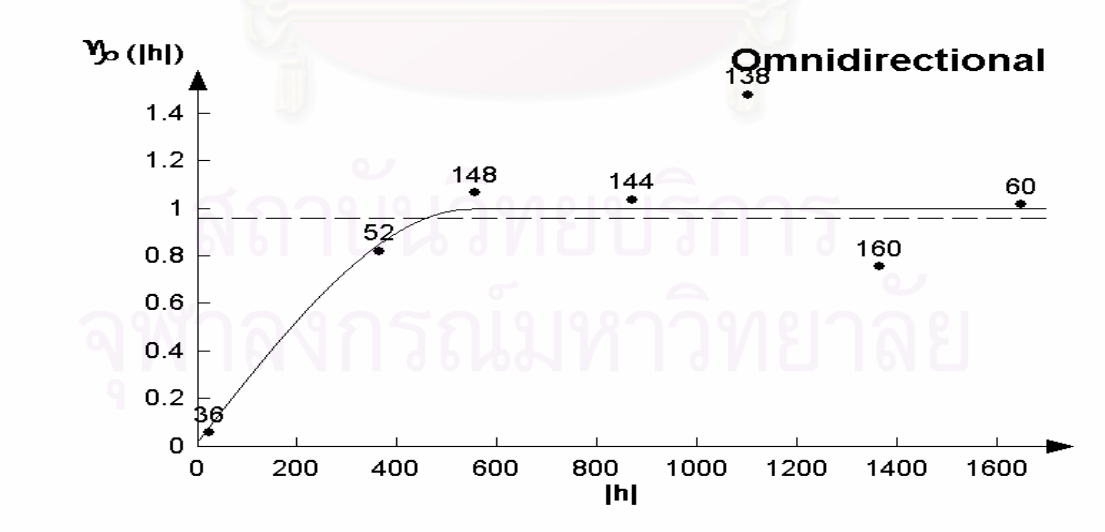

Figure 4.7: Omnidirectional variogram and its variogram model for normal score data.

The parameters used to calculate this variogram plot are 400 feet of lag spacing, 200 feet of lag tolerance, 6 lags, 0 degree of direction, 90 degree of angular tolerance, and no limits of maximum bandwidth. The numbers shown near the black dots are the number of pairs that were used in the calculation for each lag distance and the black solid line is the variogram model. Table 4.13 shows the model parameters of variogram, which are spherical model with nugget of 0.02, range of 548 feet, and sill of 0.98. Sequential Gaussian Simulation technique was used to generate 60 realizations using variogram model obtained previously.

Table 4.13: Variogram model parameters of normal score data.

Parameters	Values
Model	Spherical
Nugget	0.02
Range	548 feet
Sill	0.98

The variogram model for Reservoir III exhibits a small nugget effect, with the nugget value of 0.02 which is approximately 2 percent of the sill value. The normal score permeability data yields a correlation distance of 548 feet, defined within the range distance and representing all directions. The sill value (0.98) almost equals to the normal score permeability data variance (1.00). In overall, this variogram model represents the spatial variability structure of the transformed permeability data, and it will be used as conditioning information in the simulation process.

Variogram calculation is an important step because the accuracy of the estimated values or realizations mostly depends on the variogram model. Hence, many variogram models were tried when fitting the variogram plot to find the best fit model. After a

variogram model is found, there is a condition that the data set has to meet the bivariate normal distribution before conducting Sequential Gaussian Simulation.

4.2.2.2 Checking for Bivariate Normality

The check for bivariate normality can be carried out by comparing the theoretical variogram of Bivariate Gaussian model with experimental indicator variogram at several cut-off values, such as second quartile, median, and third quartile. In this study, the median was chosen to be the cut-off value to examine the Bivariate Normality around the average of data set. In the checking process, the experimental indicator variogram corresponding to a specific cut-off, median cut-off in this case was compared to the theoretical variogram calculated from Eq. 3.9. The procedure for this check can be elaborated as follows:

1. Calculating an experimental indicator variogram at median cut-off, which is 116.5 for this study.
2. Calculating the theoretical indicator variogram of Bivariate Gaussian model at median cut-off using Eq. 3.9.
3. Comparison of the two indicator variograms that are obtained from step 1 and step 2.

In the comparison of these two variograms, some parameters for variogram calculation were specified as shown in Table 4.14. These parameters were set to be the same for both experimental and Gaussian model indicator variograms. The cut-off porosity value is equal to median, which is 116.5.

Table 4.14: Variogram parameters used to check for Bivariate Normality.

Parameters	Values
Number of lag	40
Lag spacing	100
Median cut-off	116.5

Fig. 4.8 shows the experimental and Gaussian model indicator variograms corresponding to the second quartile, which is the median. As seen in the figure, there is a good correspondence between experimental indicator variogram at median cut-off and theoretical indicator variogram of Bivariate Gaussian model. This means that Sequential Gaussian Simulation can be used for this data set.

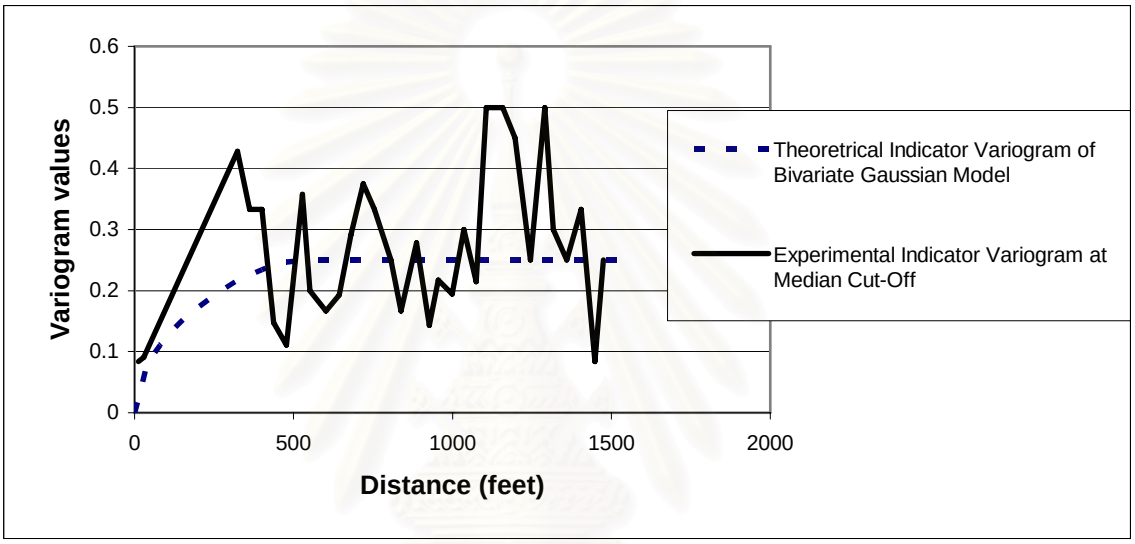

Figure 4.8: Experimental Indicator variogram and Gaussian model-derived indicator variogram at median cut-off.

4.2.2.3 Sequential Gaussian Simulation

Sequential Gaussian Simulation can generate many realizations at equal probability from the same data set. The probability distribution (*ccdf*) of the randomly visited node is constructed by Simple Kriging process, conditioned to the original data and previously simulated data. Then, the realization at the visited node is generated using the random number generator and the constructed *ccdf*. In practice, several realizations are generated to examine the spatial variability structure of a data set. The number of realizations generated in this study is sixty. In this study, these realization maps were generated by Sequential Gaussian Simulation available in GSLIB program. Fig. 4.9 to 4.16 shows the 60 realization maps of permeability data for Reservoir III.

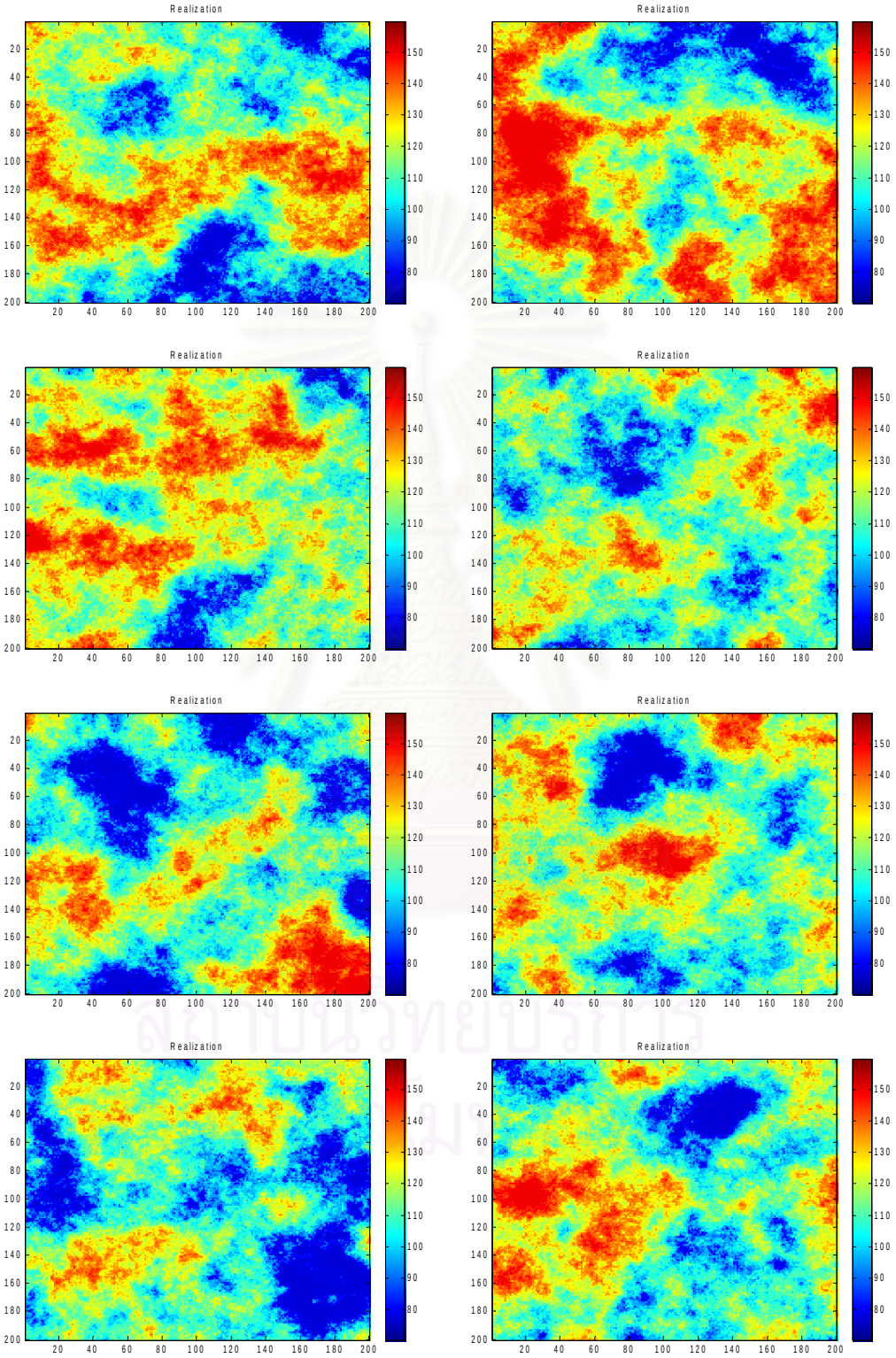

Figure 4.9: Permeability distribution for realizations 1-8.

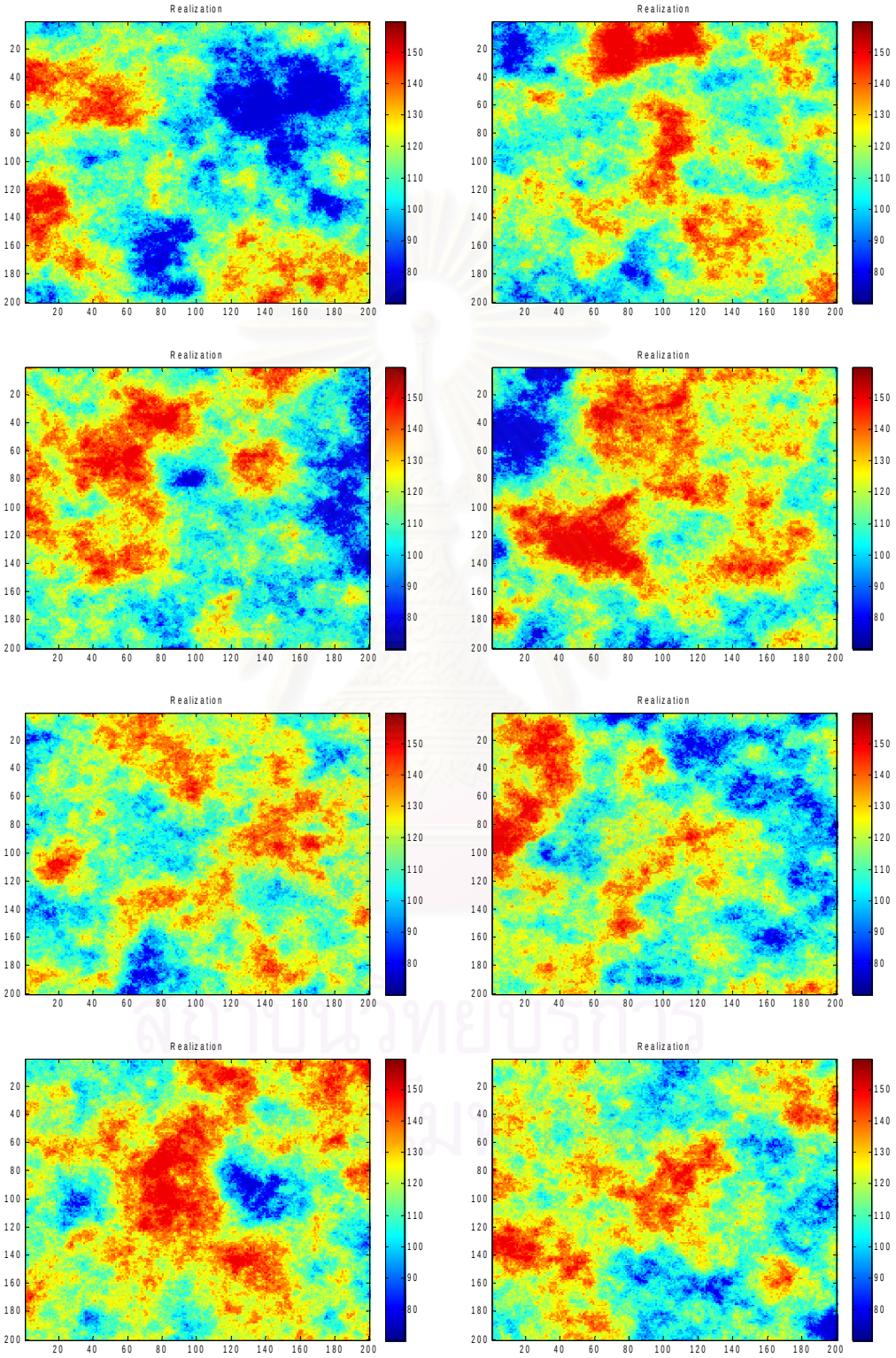

Figure 4.10: Permeability distribution for realizations 9-16.

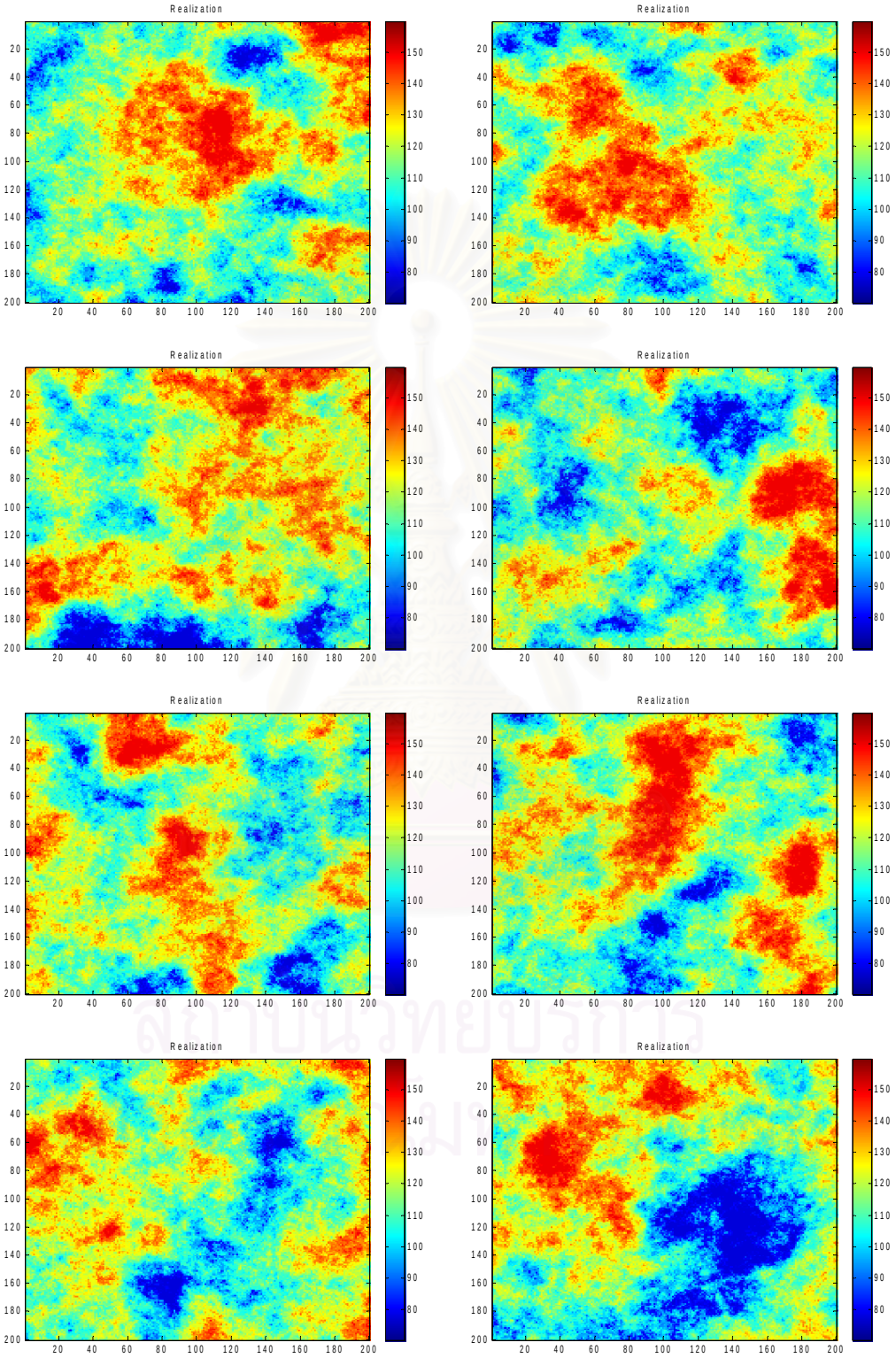

Figure 4.11: Permeability distribution for realizations 17-24.

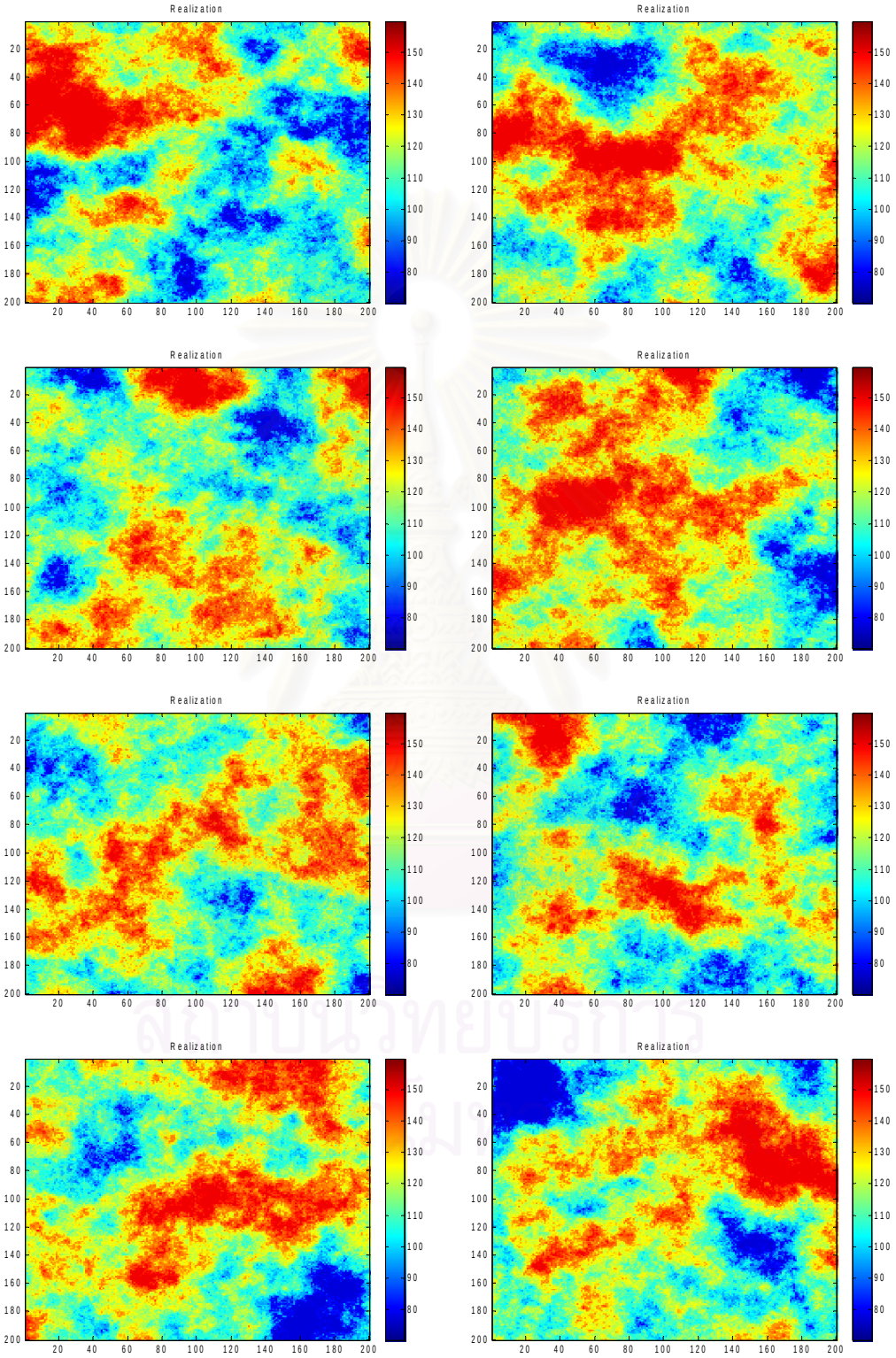

Figure 4.12: Permeability distribution for realizations 25-32.

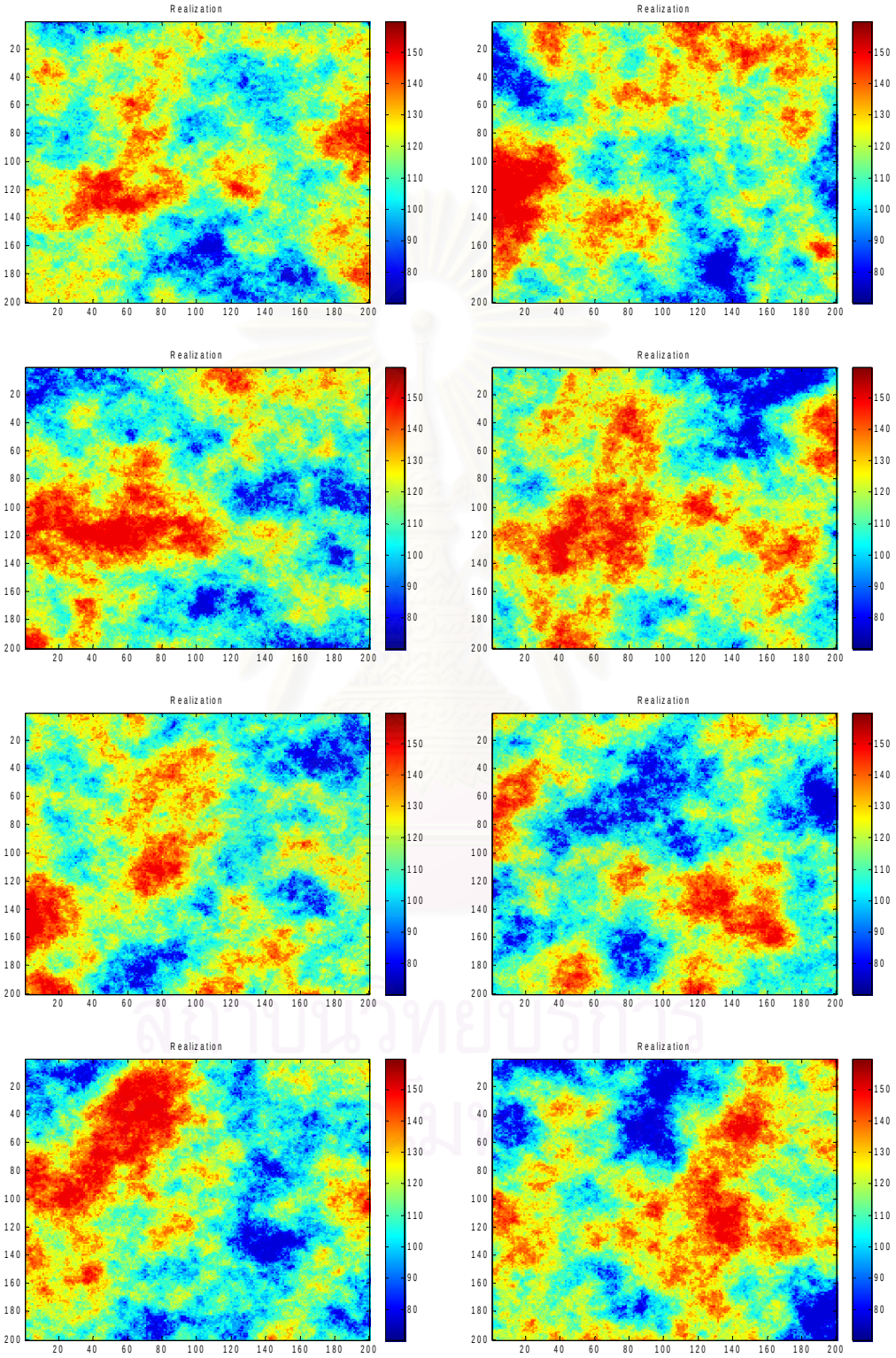

Figure 4.13: Permeability distribution for realizations 33-40.

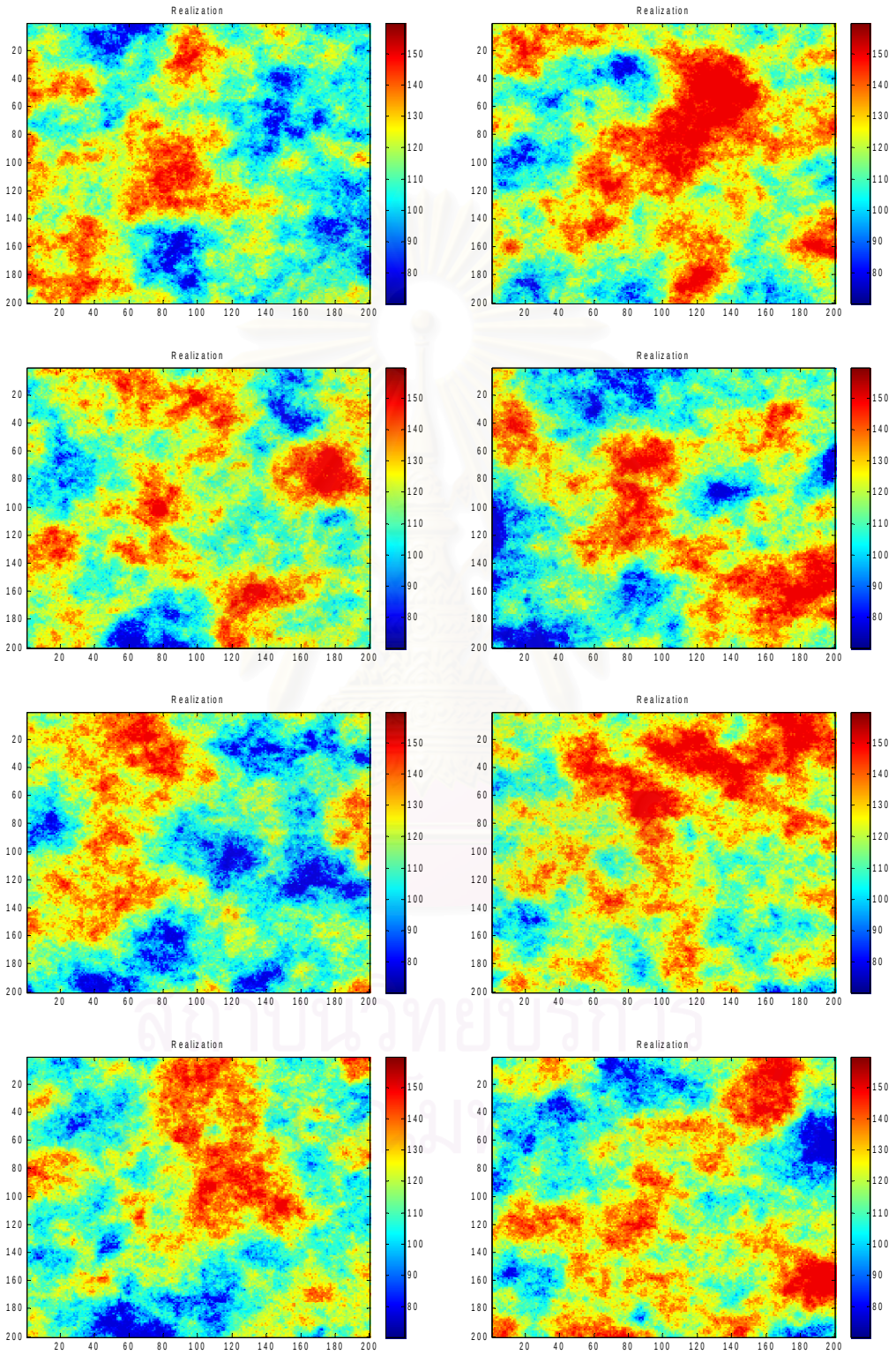

Figure 4.14: Permeability distribution for realizations 41-48.

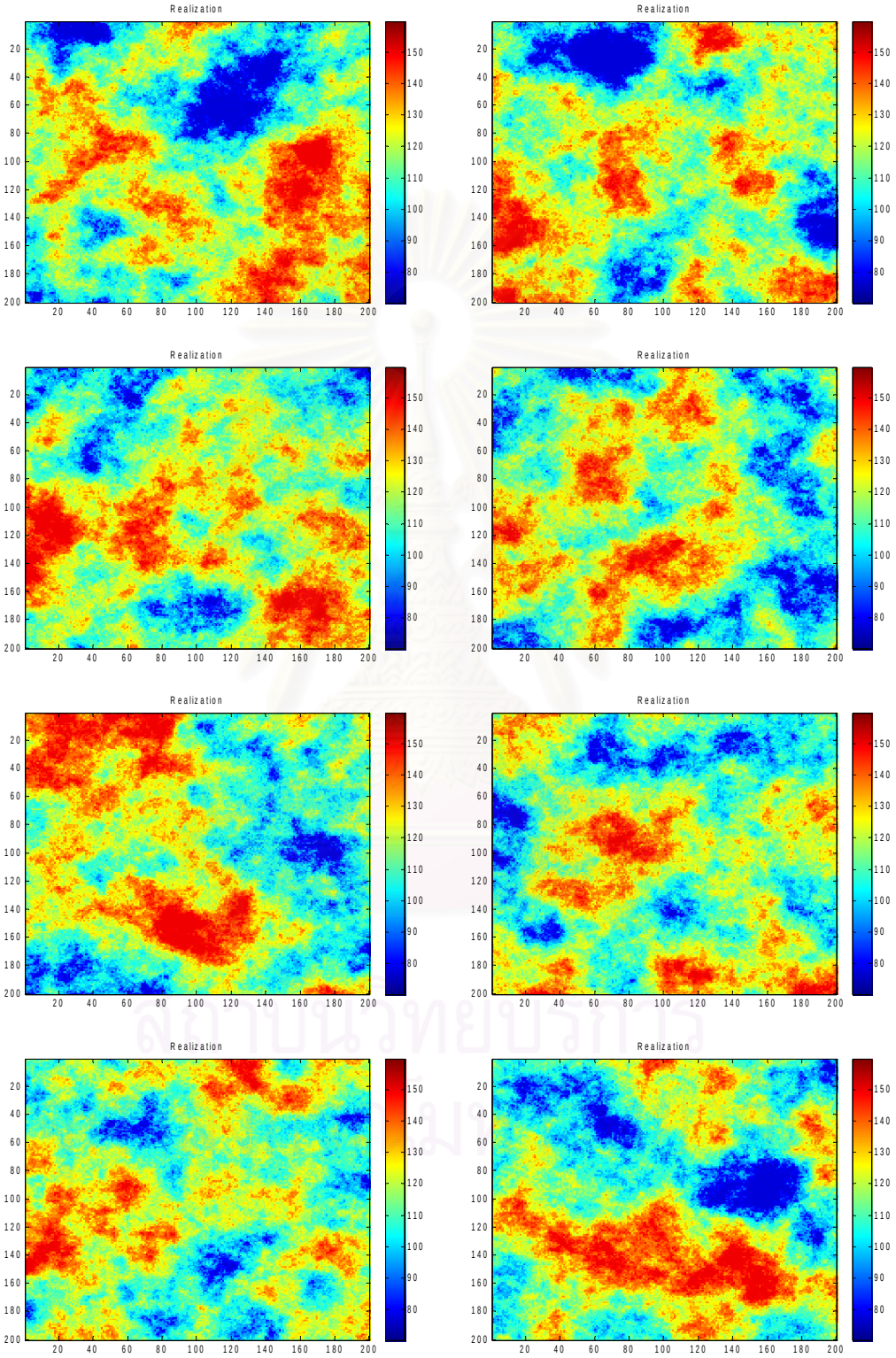

Figure 4.15: Permeability distribution for realizations 49-56.

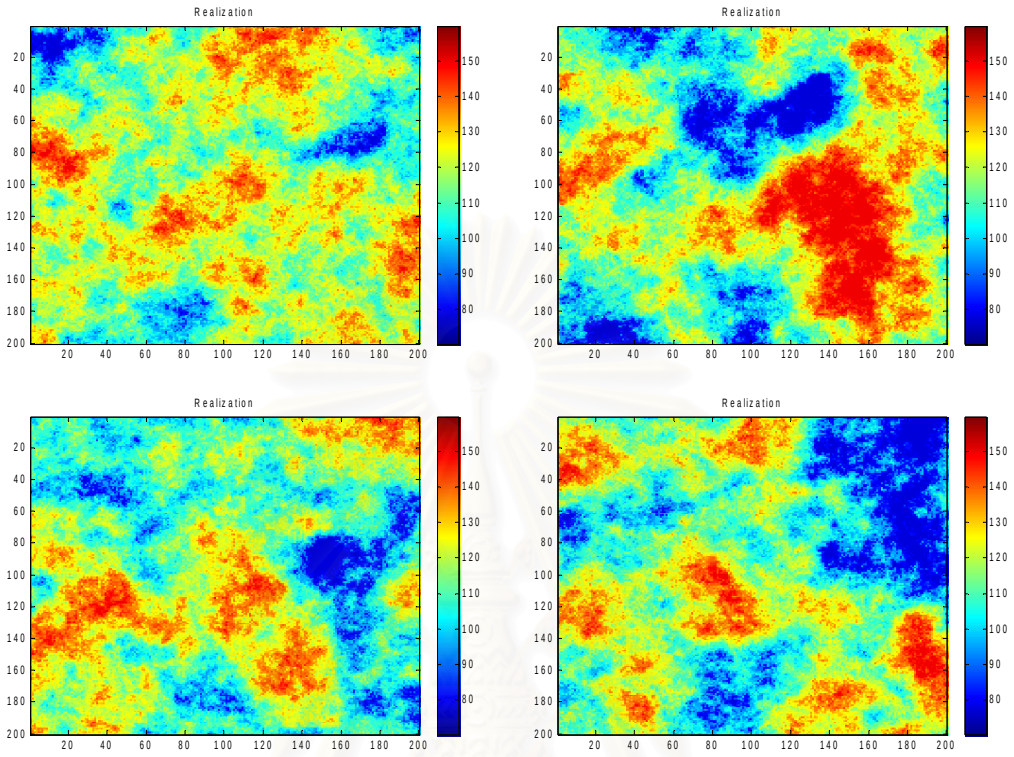

Figure 4.16: Permeability distribution for realizations 57-60.

4.3 Creating Coarse-Scale Permeability Distribution

Based on the previous study of Tang[8] which shows that Harmonic-Arithmetic averaging is better than Arithmetic-Harmonic averaging, all realizations in this study were upscaled using Harmonic-Arithmetic average. Moreover, upscaling was performed only in the horizontal direction called aerial upscaling. There are two different upscaling approaches in this work: global and local upscaling. Global upscaling is a conventional method to upscale fine-scale property while local upscaling is introduced in this study to speed up the computation time. To check the effectiveness of the new procedure, three reservoir models (Reservoir I, II, and III) were used.

4.3.1 Coarse-Scale Permeability Distribution Based on Global Upscaling

This upscaling approach is conventionally used to upscale fine-scale geological model because it is simple and straight forward. However, it is time consuming because all the data in fine-scale geological model have to be upscaled. In this approach, upscaling is performed for all fine-scale grid blocks of which permeabilities are generated by geostatistical methods. In this study, permeability distribution was generated using Krigging and Sequential Gaussian Simulation.

4.3.1.1 Based on Global upscaling and Krigging

Global upscaling was conducted for fine-scale permeability distributions of Reservoir I and II, which were generated by Krigging. Figs. 4.17 and 4.18 show the distribution of coarse-scale permeabilities that were globally upscaled for Reservoir I and II, respectively. The upscaling was performed at the ratio of 4:1, meaning that the upscaling was performed from the original dimension of 400 × 400 to 100 × 100.

Comparing the coarse-scale permeability shown in Fig. 4.17 and Fig. 4.18 with the fine-scale permeability distribution shown in Fig 4.5 and Fig. 4.6 for Reservoir I and II, respectively, we can see that there are the similarities of permeability distribution before and after global upscaling.

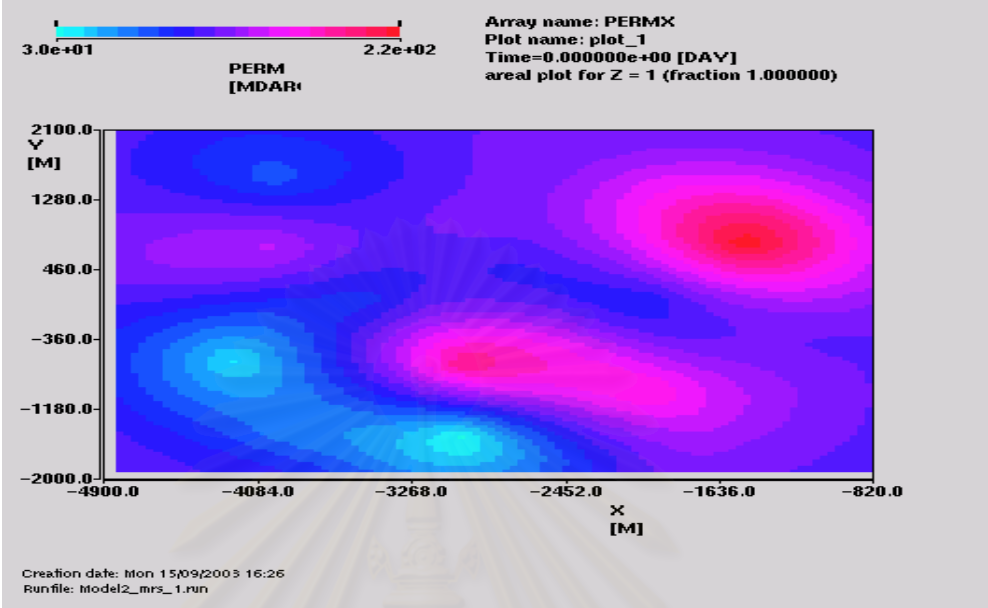

Figure 4.17: Permeability distribution for Reservoir I based on global upscaling.

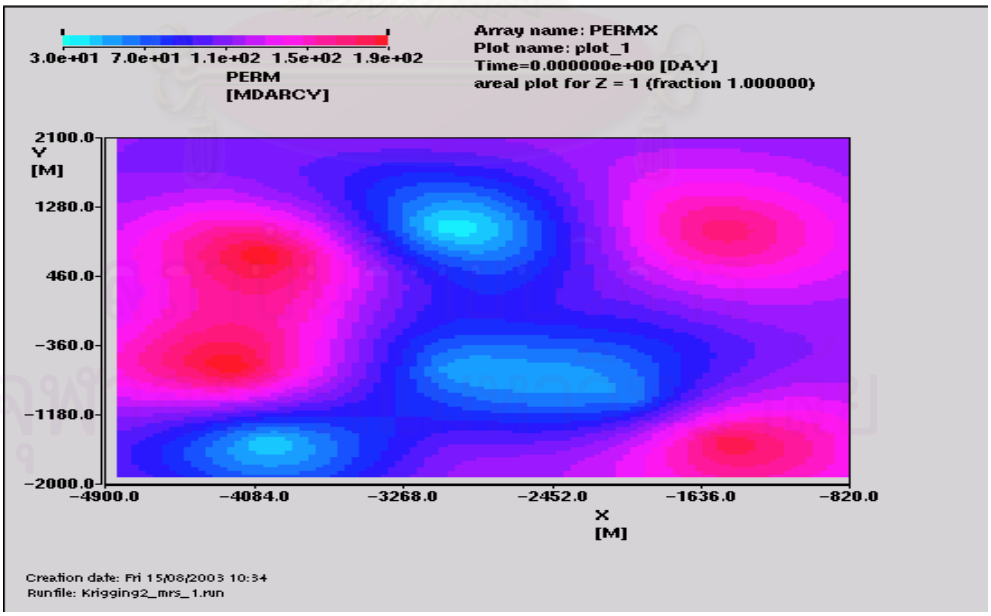

Figure 4.18: Permeability distribution for Reservoir II based on global upscaling.

4.3.1.2 Based on Global upscaling and Sequential Gaussian Simulation

Global upscaling was also applied to fine-scale permeability distribution of Reservoir III which was generated by Sequential Gaussian Simulation. Figs. 4.19 to 4.26 show the 60 globally upscaled realization maps of permeability data for Reservoir III. The upscaling was performed at the ratio of 2:1, meaning that the upscaling was performed from the original dimension of 200 × 200 to 100 × 100.

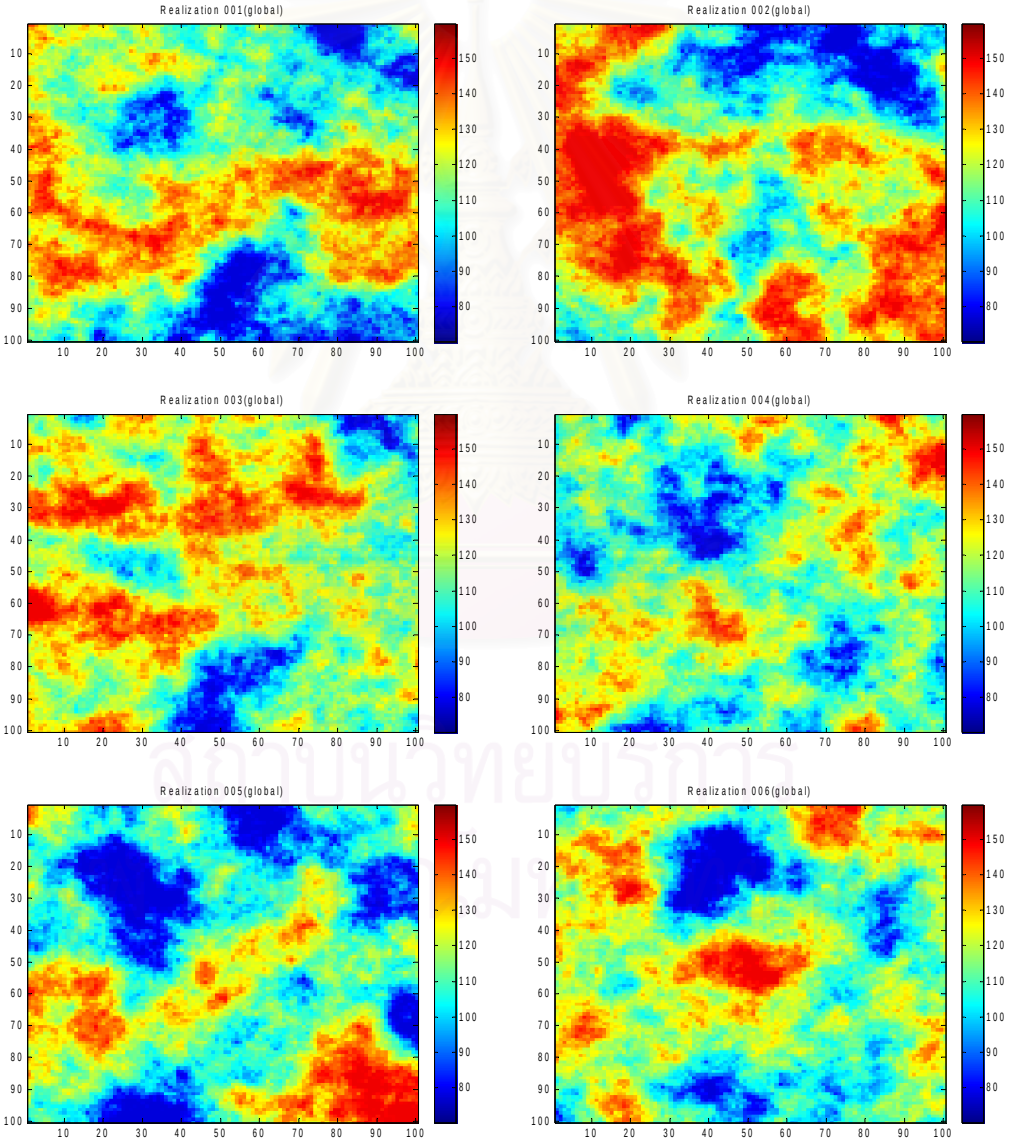

Figure 4.19: Permeability distribution for realizations 1-6 based on global upscaling.

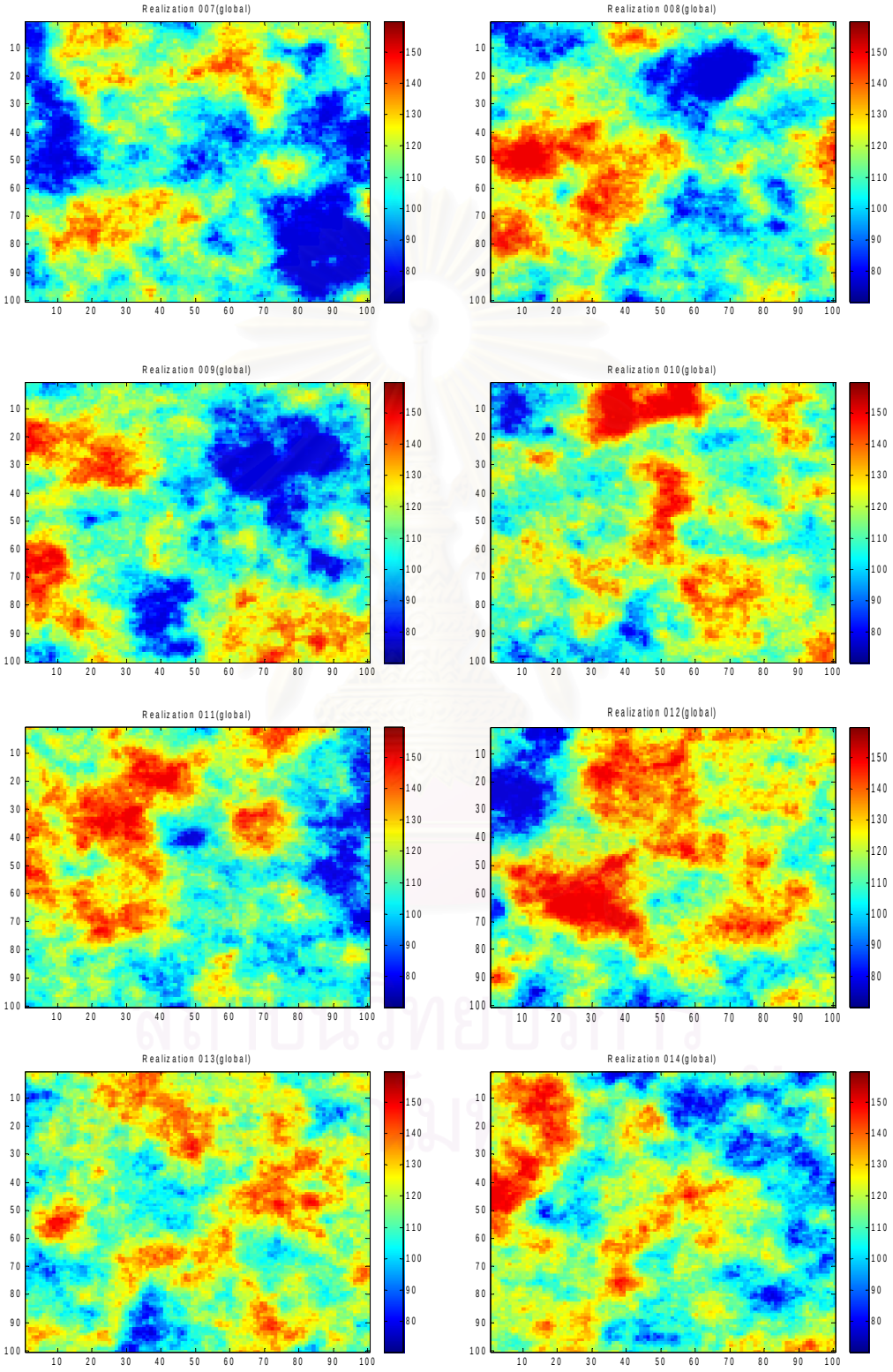

Figure 4.20: Permeability distribution for realizations 7-14 based on global upscaling.

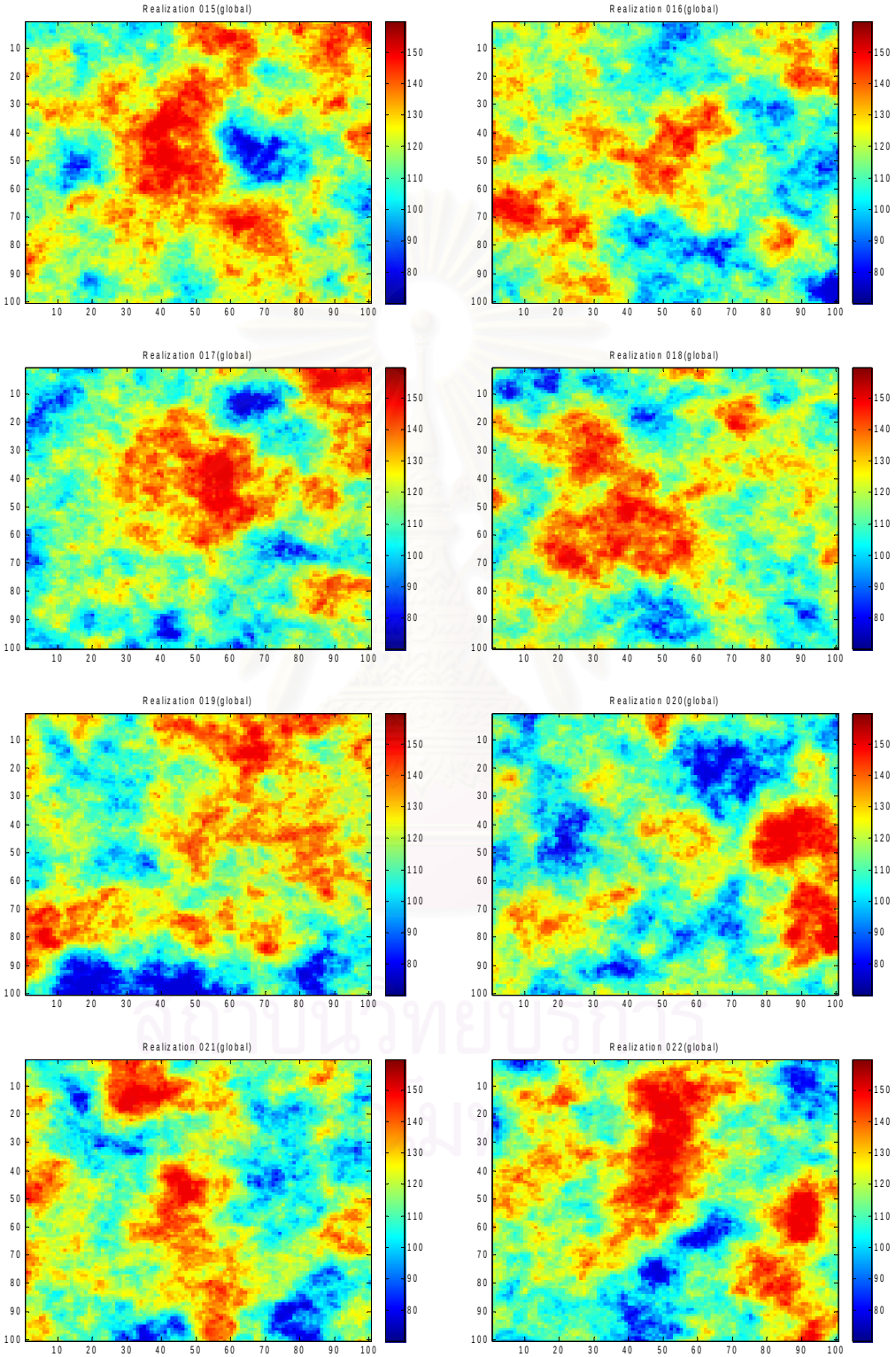

Figure 4.21: Permeability distribution for realizations 15-22 based on global upscaling.

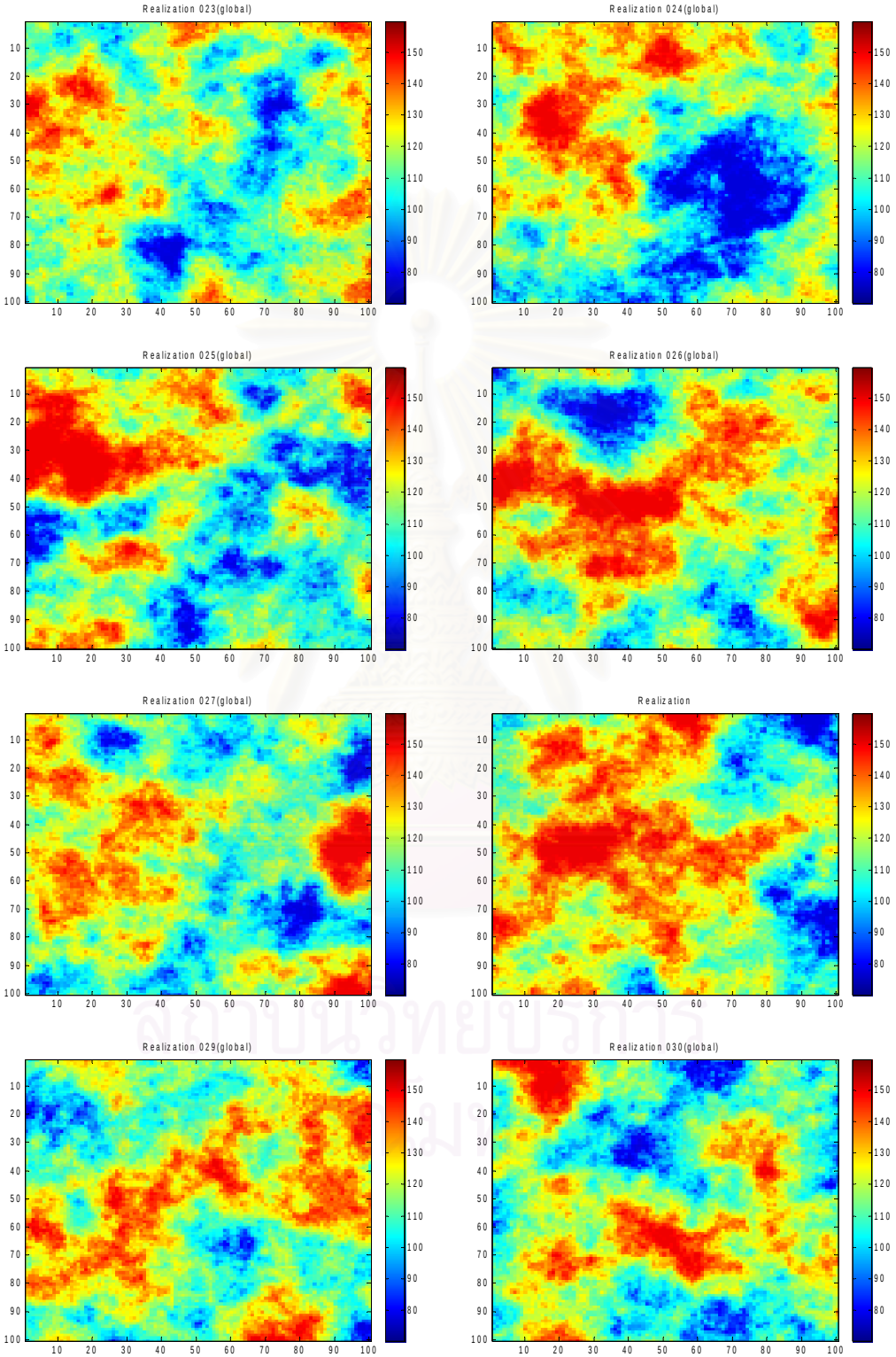

Figure 4.22: Permeability distribution for realizations 23-30 based on global upscaling.

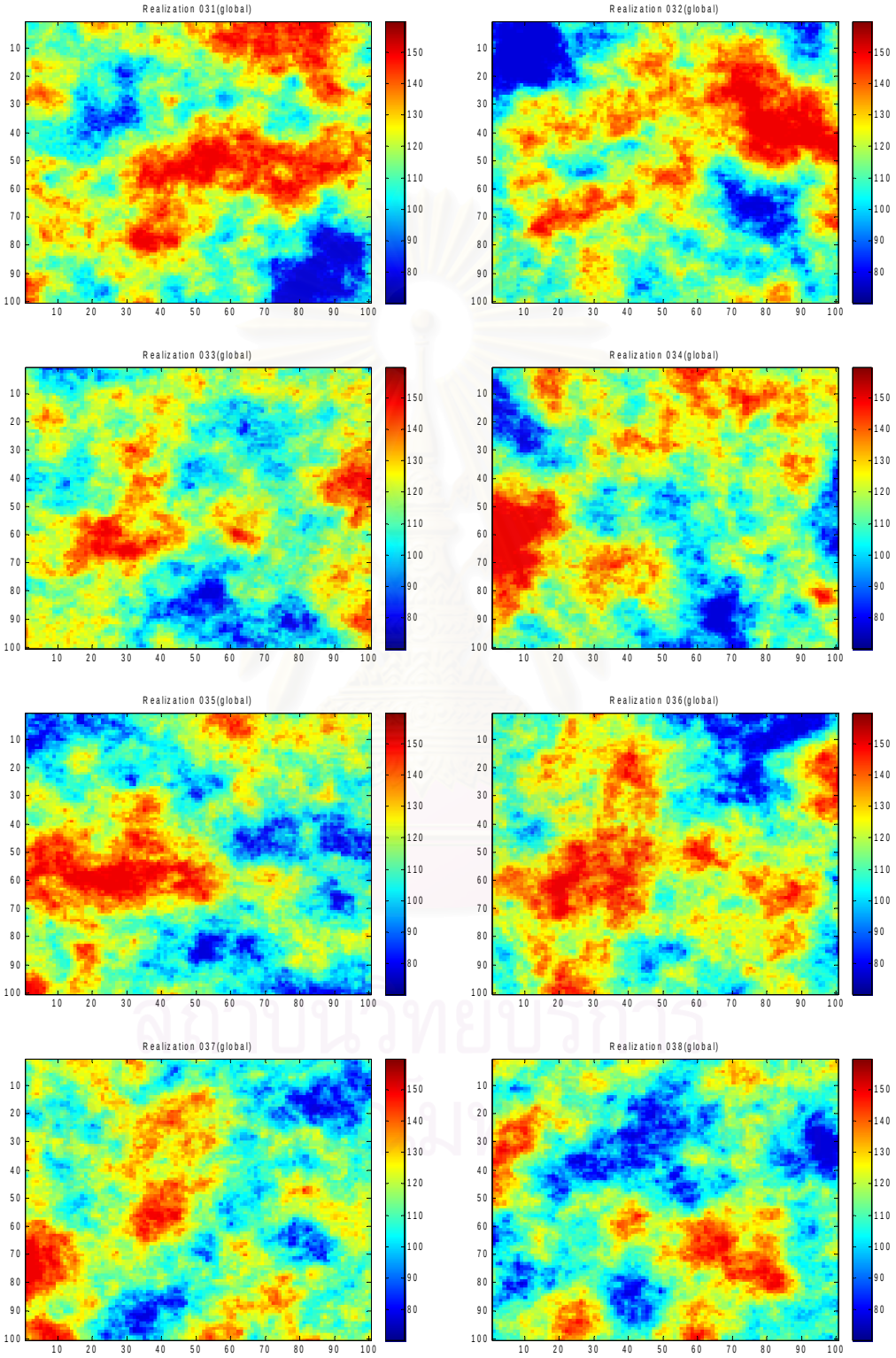

Figure 4.23: Permeability distribution for realizations 31-38 based on global upscaling.

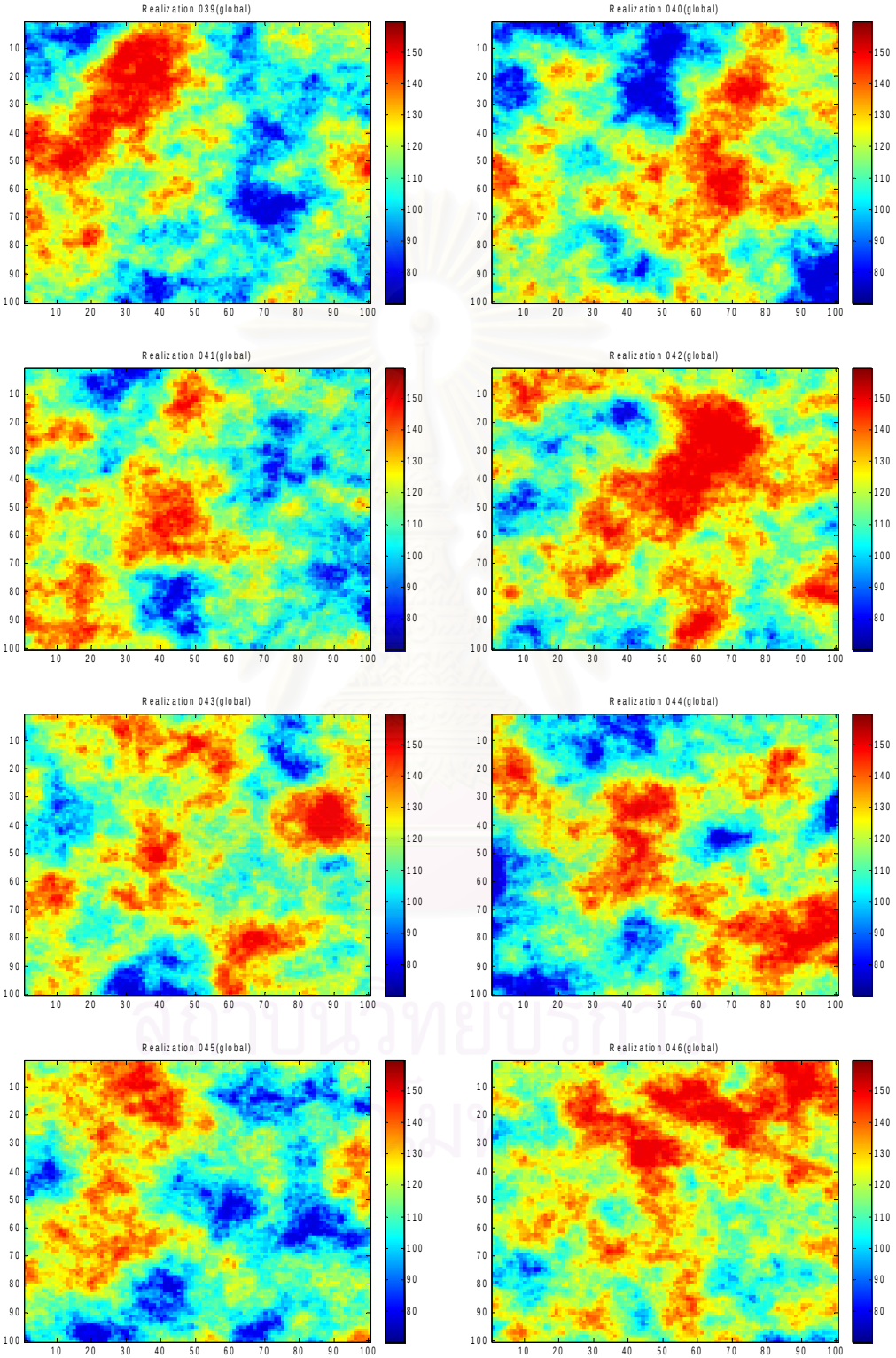

Figure 4.24: Permeability distribution for realizations 39-46 based on global upscaling.

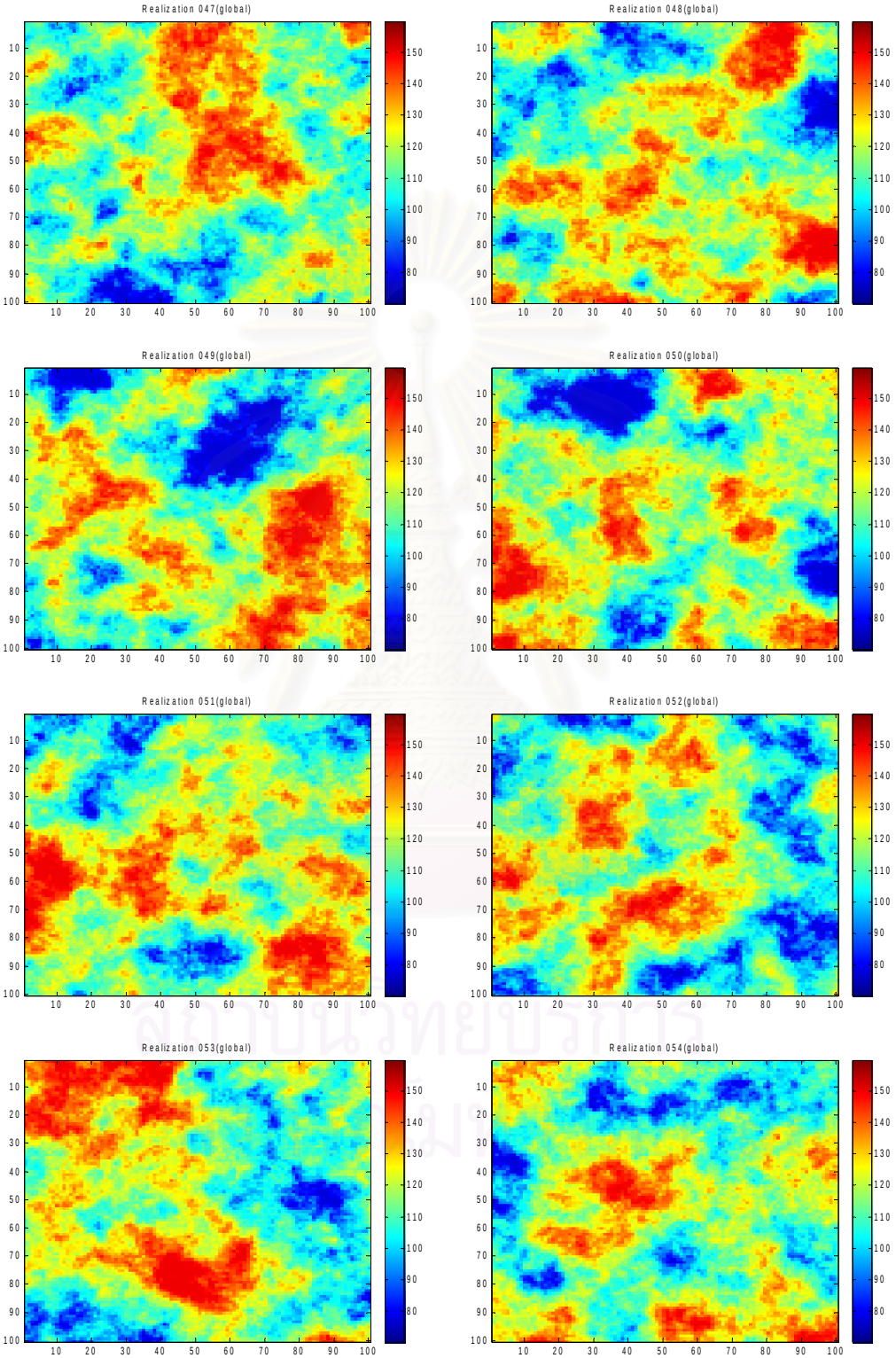

Figure 4.25: Permeability distribution for realizations 47-54 based on global upscaling.

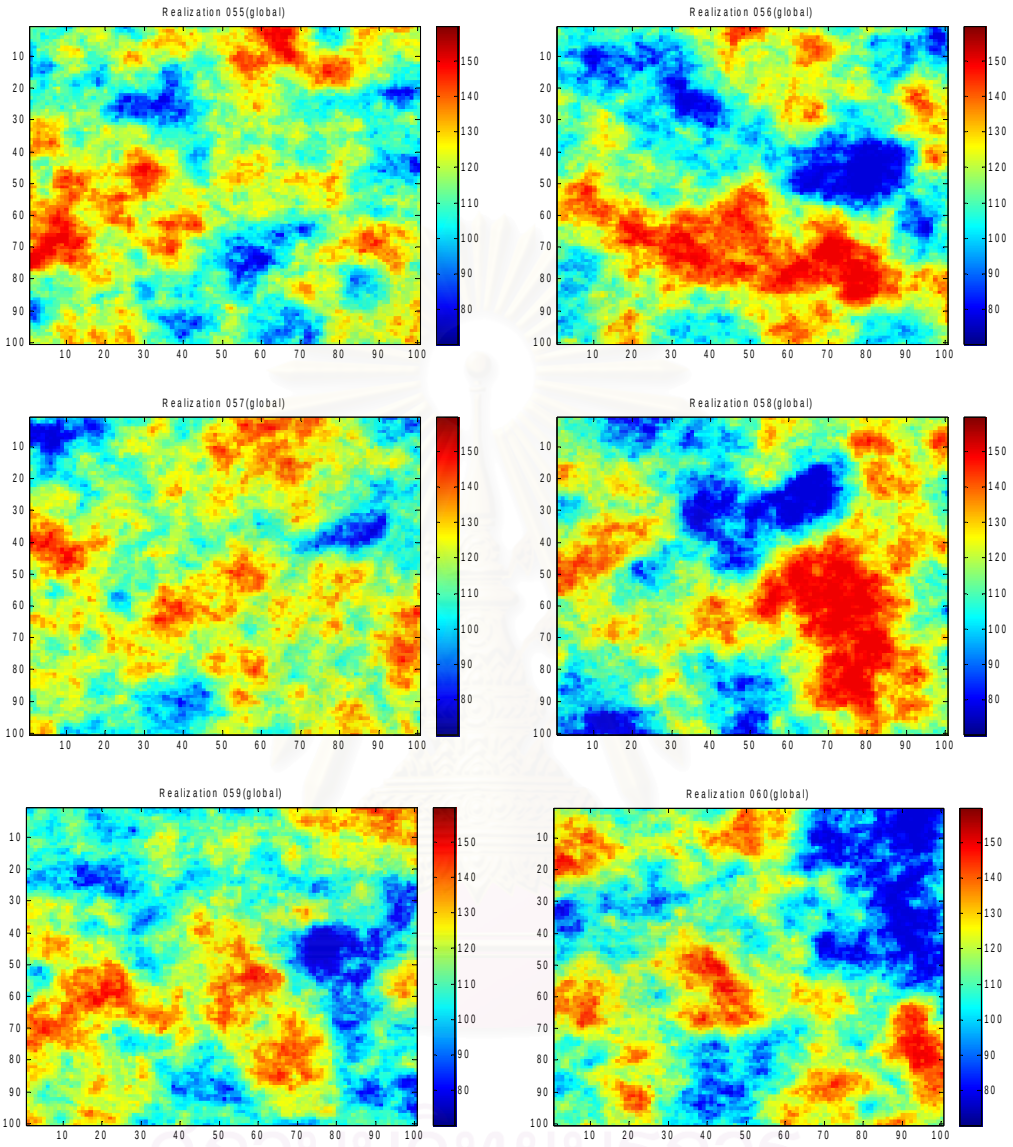

Figure 4.26: Permeability distribution for realizations 55-60 based on global upscaling.

There are many differences among these 60 globally upscaled realizations because Sequential Gaussian Simulation generates the probability distribution at randomly visited node. However, all realizations are equally probable in representing the actual permeability distribution.

4.3.2 Coarse Scale Permeability Distribution Based on Local Upscaling

The procedure of determining coarse scale permeability distribution based on local upscaling is introduced in order to reduce computational time. The first step is the same as global upscaling, that is, to determine the spatial distribution of permeability using Krigging. The next step is to determine the permeabilities for the coarse blocks at data locations.

4.3.2.1 Based on Local Upscaling and Krigging

Local upscaling was performed for Reservoir I and II, of which fine-scale permeability distributions were generated by Krigging method. Upscaling was performed to upscale 4 fine-scale blocks to 1 coarse block. Tables 4.15 and 4.16 show the upscaled estimates of local upscaling for Reservoir I and II, respectively.

Table 4.15: Value of locally upscaled permeability for Reservoir I.

Well number	Permeability (md)	Locally upscaled permeability (md)
1	70	69.966
2	30	32.358
3	130	130.020
4	40	41.282
5	190	188.710
6	170	169.040
7	90	91.022
8	100	101.040
9	140	139.090
10	120	119.960
11	220	218.510
12	80	80.646
13	150	149.660
14	200	199.240

Table 4.16: Value of locally upscaled permeability for Reservoir II.

Well number	Permeability (md)	Locally upscaled permeability (md)
1	40	41.798
2	100	99.666
3	180	178.38
4	190	188.48
5	50	50.76
6	60	61.29
7	120	119.52
8	100	100.64
9	190	188.34
10	30	31.349
11	160	159.95
12	110	109.85
13	130	130.1
14	170	169.16

Fig. 4.27 shows the variogram values and its model of the locally upscaled permeabilities for Reservoir I. The parameter used to calculate this variogram are 332.2 feet of lag distance, 166.1 feet of lag tolerance, 8 lags, 0 degree of direction, 90 degree of angular tolerance, and no limits of maximum bandwidth. Table 4.17 shows the model parameters of variogram for Reservoir I which is spherical model with nugget of 0.00, range of 1,600 feet, and sill of 2,820.

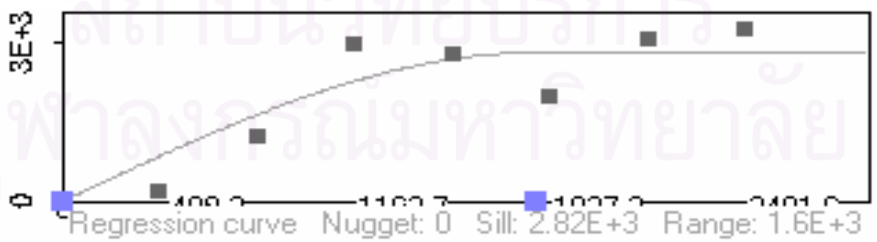

Figure 4.27: Omnidirectional variogram of locally upscaled permeabilities for Reservoir I.

Table 4.17: Variogram model parameters of Reservoir I based on local upscaling.

Parameters	Values
Model	Spherical
Nugget	0.00
Range	1,600 feet
Sill	2,820

Fig. 4.28 shows the variogram values and its model of locally upscaled permeabilities for Reservoir II. The parameter used to calculate this variogram are 340.9 feet of lag distance, 170.45 feet of lag tolerance, 8 lags, 0 degree of direction, 90 degree of angular tolerance, and no limits of maximum bandwidth. Table 4.18 shows the model parameters of variogram for Reservoir II which is spherical model with nugget of 0.00, range of 1,530 feet, and sill of 4,230.

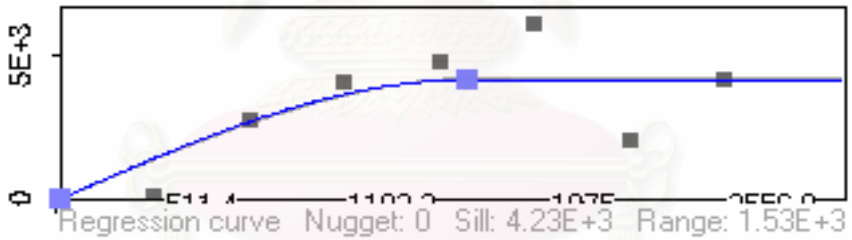

Figure 4.28: Omnidirectional variogram of locally upscaled permeabilities for Reservoir II.

Table 4.18: Variogram model parameters of Reservoir II based on local upscaling.

Parameters	Values
Model	Spherical
Nugget	0.00
Range	1,530 feet
Sill	4,230

After the variogram model of the upscaled permeabilities was created, Krigging estimation was performed to determine coarse-scale permeability distribution. Figs 4.29 and 4.30 show distribution of coarse-scale permeabilities constructed from locally upscaled permeabilities for Reservoir I and II, respectively.

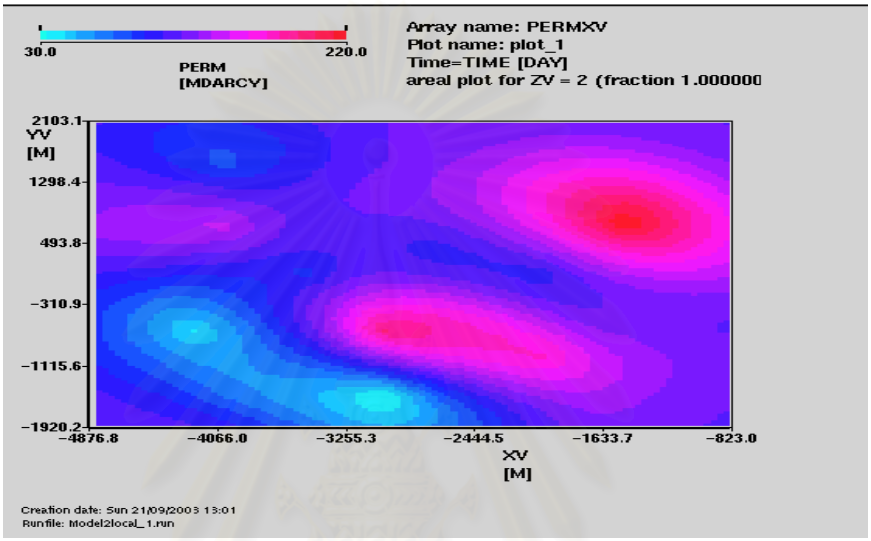

Figure 4.29: Coarse-scale permeability distribution for Reservoir I based on local upscaling and Krigging estimation.

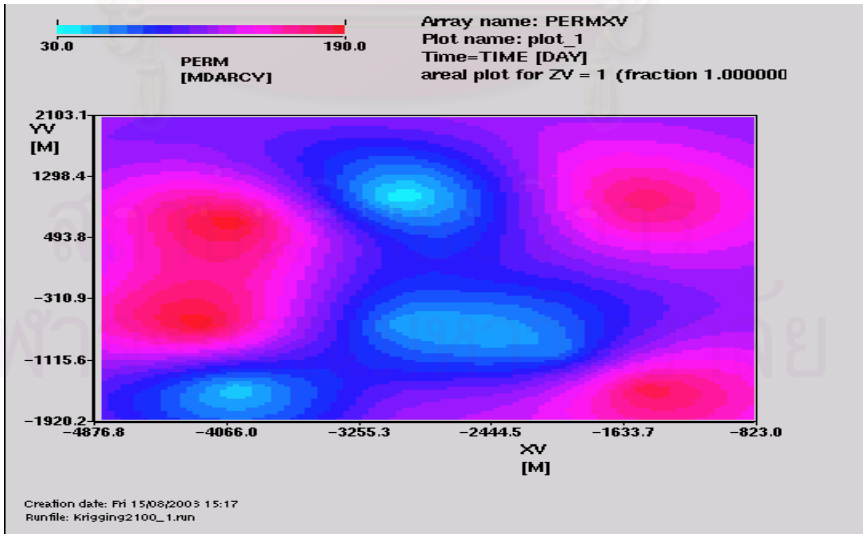

Figure 4.30: Coarse-scale permeability distribution for Reservoir II based on local upscaling and Krigging estimation.

4.3.2.2 Based on Local Upscaling and Sequential Gaussian Simulation

Local Upscaling was performed for Reservoir III, of which fine-scale permeability distribution was determined by Krigging. Krigging estimation had to be performed to find the estimated data around data locations to do local upscaling. The 60 fine-scale geological realizations cannot be used as a reference because each one is random. Thus, we used Krigging estimates as a reference. Fig. 4.31 represents the variogram of permeability raw data. The parameters, used to calculate this variogram plot are 420 feet of lag distance, 210 feet of lag tolerance, 4 lags, 0 degree of direction, 90 degree of angular tolerance, and no limits of maximum bandwidth.

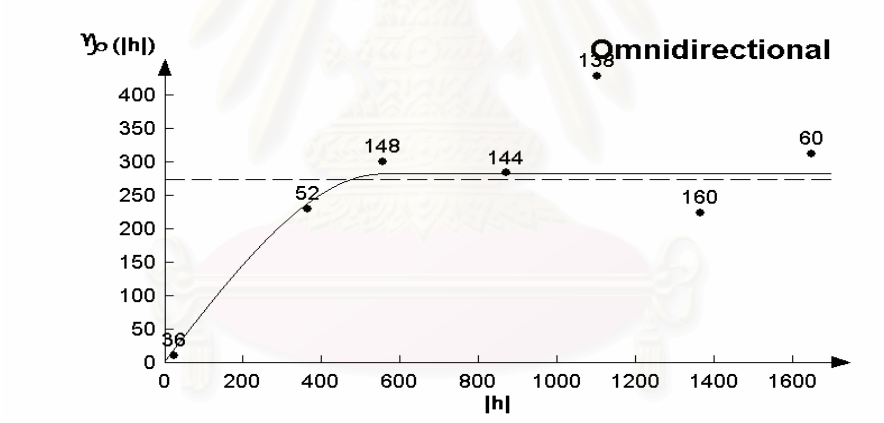

Figure 4.31: Omnidirectional variogram for Reservoir III.

In Fig. 4.31, the line is the variogram model. The result of fitting the variogram model is shown in the Table 4.19.

Table 4.19: Variogram model parameters for Reservoir III.

Parameters	Values
Model	Spherical
Nugget	2.9
Range	554 feet
Sill	280

After the variogram model parameters were found, these parameters were used to create and estimate fine-scale geostatistic model based using Krigging estimation method. Then, the Harmonic-Arithmetic averaging method was used to determine permeabilities of coarse blocks at original data locations. Table 4.20 shows the upscaled estimates of local upscaling for Reservoir III.

Table 4.20: Value of locally upscaled permeability for Reservoir III.

X coordinate (Feet)	Y coordinate (Feet)	Permeability values	Locally Upscaled
160	250	112	100
270	720	128	128
330	1260	115	118
340	1260	118	118
350	1260	121	120
360	1260	124	120
230	1780	83	84
480	320	118	119
490	330	120	119
500	340	122	122
510	350	124	122
540	1640	102	101
760	720	138	138
740	1280	142	140
860	180	96	97
990	1100	150	149
960	1650	108	98
1230	430	106	119
1300	900	132	133
1310	1520	126	126
1440	1290	136	124
1690	320	78	79
1620	900	106	108
1620	920	108	110
1620	940	110	111
1620	960	112	113
1780	1780	100	101
1940	1250	95	100

These locally upscaled permeabilities would be used as the new raw data to generate 60 realizations based on Sequential Gaussian Simulation at the scale of 100 × 100 blocks with an area of 20 × 20 ft per block.

Table 4.21 gives a statistical analysis of the locally upscaled permeability values for Reservoir III. The mean of the data is 116.39, and variance and standard deviation are

276.84 and 16.64, respectively. The minimum and maximum values of the data set are 79 and 149, respectively. The first, second, and third quartiles are 101, 119, and 124, respectively. Coefficient of variation, skewness, and kurtosis are 14.29, -0.25, and 2.86, respectively.

Table 4.21: Statistics of locally upscaled permeability data for Reservoir III.

Parameters	Values
Mean	116.39
Variance	276.84
Std. Dev.	16.64
Minimum	79.00
25th%	101.00
Median	119.00
75th%	124.00
Maximum	149.00
Coefficient of variation	14.29
Skewness	-0.25
Kurtosis	2.86

4.3.2.2.1 Constructing the variogram model

To perform the Sequential Gaussian Simulation, the sample values have to be transformed to normal score data before further analysis due to its assumption of multigaussian distribution. In this study, the data were transformed using GSLIB program. The normal score data are shown in Table 4.22.

Table 4.22: Value of normal score transforms of permeability values for Reservoir III.

X coordinate (Feet)	Y coordinate (Feet)	Permeability values	Normal score values
160	250	100	-2.1002
270	720	128	-1.6112
330	1260	118	-1.3452
340	1260	118	-1.1503
350	1260	120	-0.9915
360	1260	120	-0.8544
230	1780	84	-0.7318
480	320	119	-0.6193
490	330	119	-0.5142
500	340	122	-0.4144
510	350	122	-0.3186
540	1640	101	-0.2257
760	720	138	-0.1347
740	1280	140	-0.0448
860	180	97	0.0448
990	1100	149	0.1347
960	1650	98	0.2257
1230	430	119	0.3186
1300	900	133	0.4144
1310	1520	126	0.5142
1440	1290	124	0.6193
1690	320	79	0.7318
1620	900	108	0.8544
1620	920	110	0.9915
1620	940	111	1.1503
1620	960	113	1.3452
1780	1780	101	1.6112
1940	1250	142	2.1002

Table 4.23 shows the statistics of the normal score data, which were transformed from the original permeability data. The new data have a mean of zero and variance and standard deviation of one, which are the characteristics of standard normal distribution. The minimum and maximum values are -2.1 and 2.1, respectively. The first, second, and third quartiles are -0.732, 0.000, and 0.619, respectively. Coefficient of variation, skewness, and kurtosis are 0, 0, and 2.601, respectively.

Table 4.23: Statistical analysis of the normal score data.

Parameters	Values
Mean	0.000
Variance	1.000
Std. Dev.	1.000
Minimum	-2.100
25th%	-0.732
Median	0.000
75th%	0.619
Maximum	2.100
Coefficient of variation	0.000
Skewness	0.000
Kurtosis	2.601

After the normal score data were prepared, variogram calculations of these data and variogram modeling were performed using the Variowin program. Fig. 4.32 illustrates the plot of the experimental variogram values at difference distances and its model.

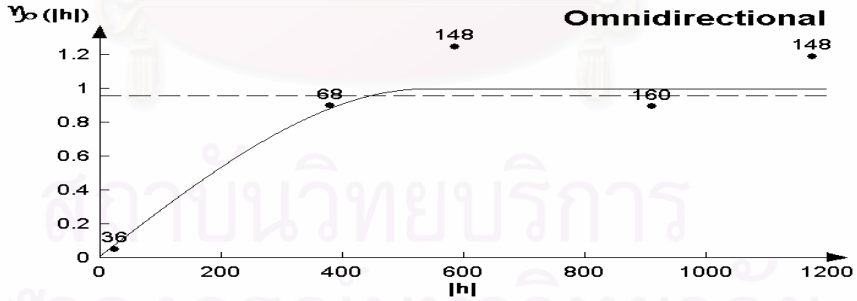

Figure 4.32: Omnidirectional variogram plot and its variogram model for normal score data.

The parameters used to calculate this variogram plot are 420 feet of lag spacing, 210 feet of lag tolerance, 6 lags, 0 degree of direction, 90 degree of angular tolerance, and no limits of maximum bandwidth. In Fig. 4.32, the numbers shown near the black dots

are the number of pairs that were used in the calculation for each lag distance, and the black solid line is the variogram model. The result of fitting the variogram model is shown in Table 4.24.

Table 4.24: Variogram model parameters of normal score data.

Parameters	Values
Model	Spherical
Nugget	0.01
Range	538 feet
Sill	0.99

The variogram model exhibits a small nugget effect, with the nugget value of 0.01 which is approximately 1 percent of the sill value. The normal score permeability data yields a correlation distance of 538 feet defined within the range distance and representing all directions. The sill value (0.99) almost equals to the normal score permeability data variance (1.00). In overall, this variogram model represents the spatial variability structure of the transformed permeability data, and it would be used as the conditioning information in the simulation process.

4.3.2.2.2 Checking for Bivariate Normality

In the comparison of the theoretical variogram of Bivariate Gaussian model with experimental indicator variogram, some parameters for variogram calculation are specified as shown in Table 4.25.

Table 4.25: Variogram parameters used to check for Bivariate Normality.

Parameters	Values
Number of lag	40
Lag spacing	100
Cut-off	119

The parameters used in variogram calculation were set to be the same for both experimental and Gaussian model indicator variograms. The cut-off permeability value is equal to median, which is 119.

Fig. 4.33 shows the experimental and Gaussian model indicator variograms corresponding to the second quartile which is the median. As seen in the figure, there is a good correspondence between experimental indicator variogram at median cut-off and theoretical indicator variogram of Bivariate Gaussian model. That means Sequential Gaussian Simulation can be used for this data set.

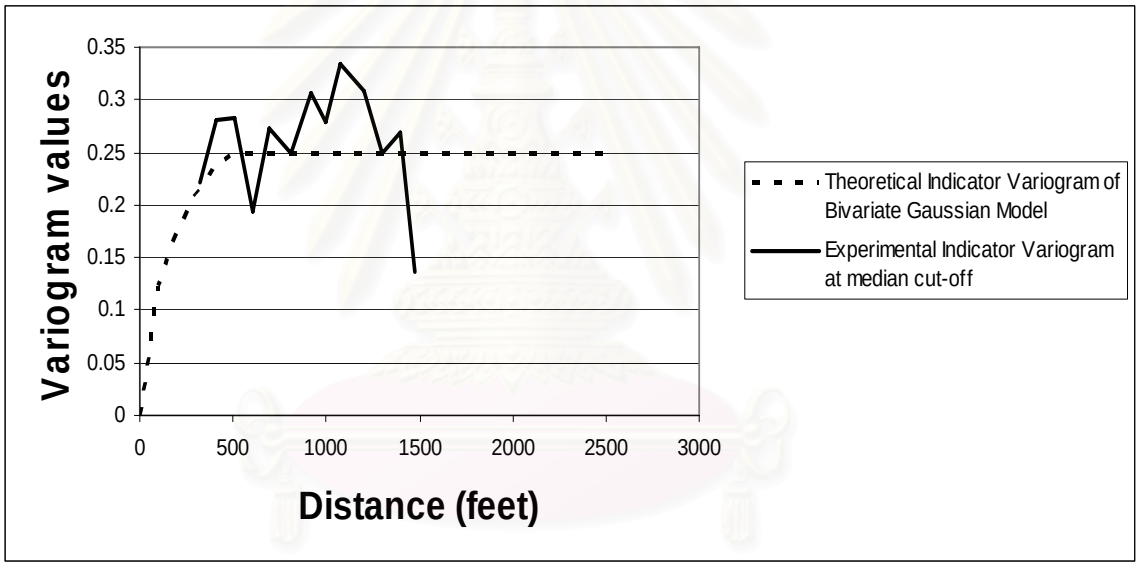

Figure 4.33: Experimental Indicator variogram and Gaussian model-derived indicator variogram at median cut-off.

4.2.2.2.3 Sequential Gaussian Simulation

After constructing the variogram, the next step is to generate permeability distributions using Sequential Gaussian Simulation. The results of 60 realization maps of permeability data at the scale of 100 × 100 grid blocks are shown in Figs. 4.34 through 4.41.

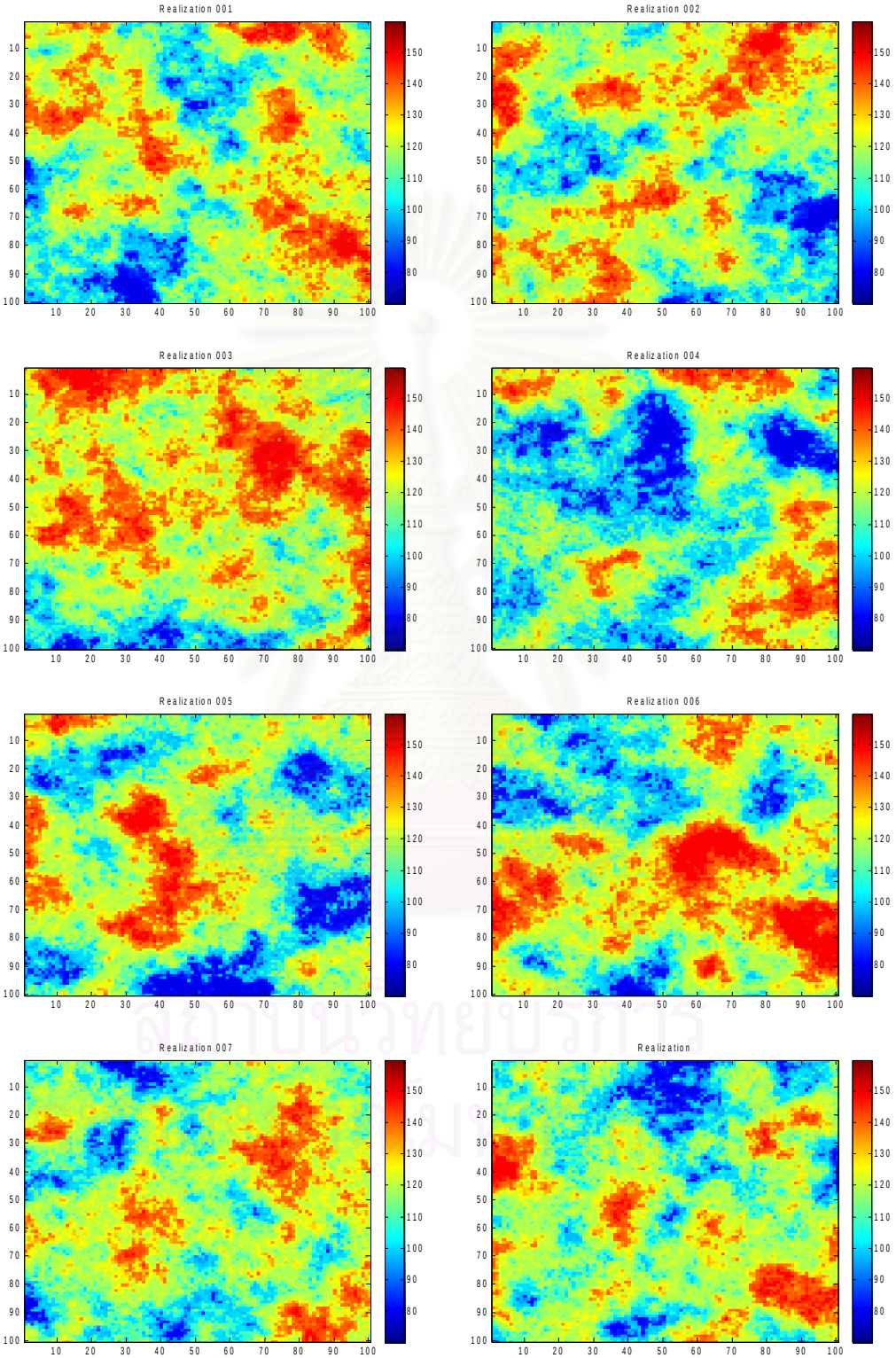

Figure 4.34: Permeability distribution for realizations 1-8 based on local upscaling.

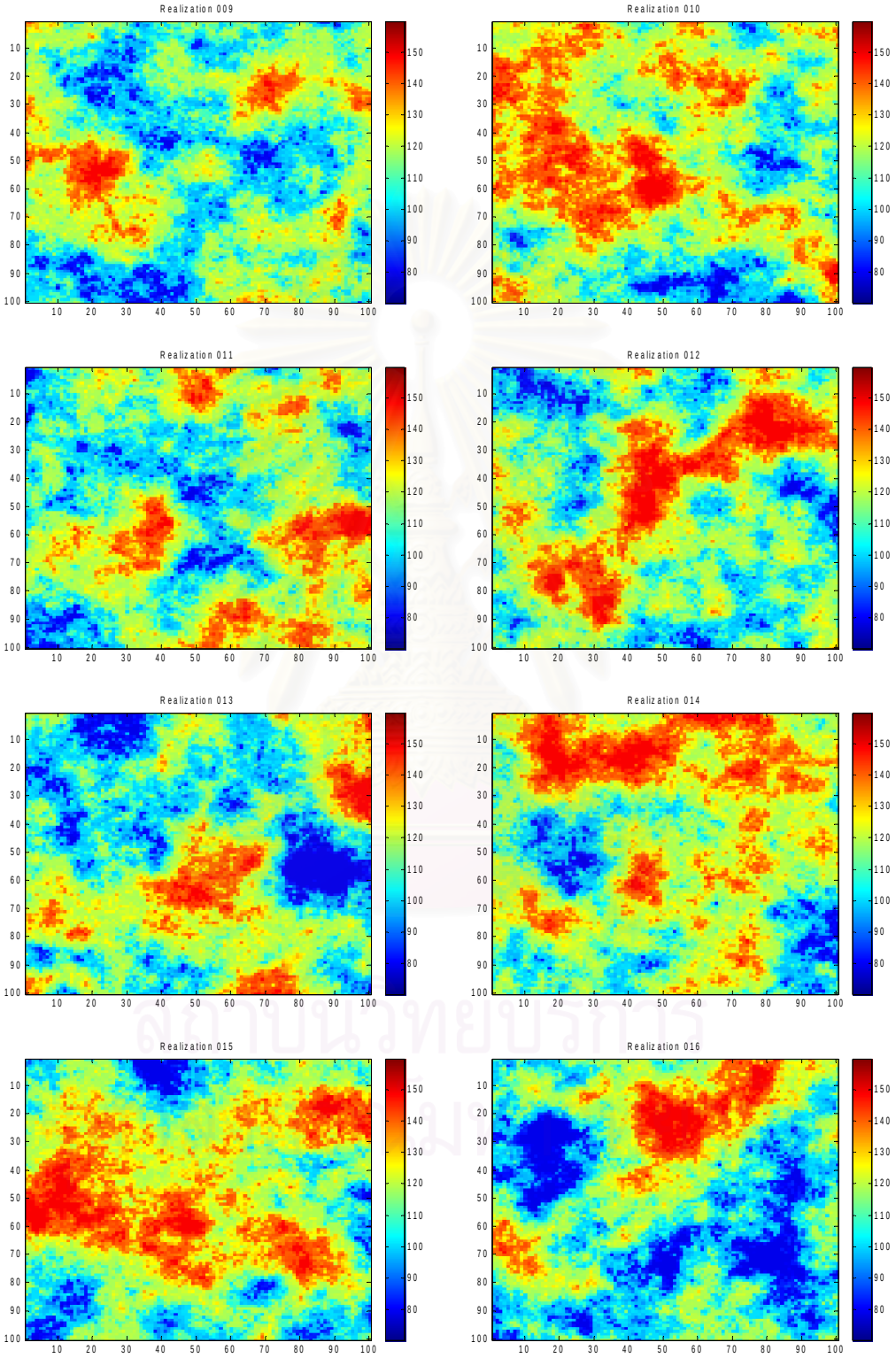

Figure 4.35: Permeability distribution for realizations 9-16 based on local upscaling.

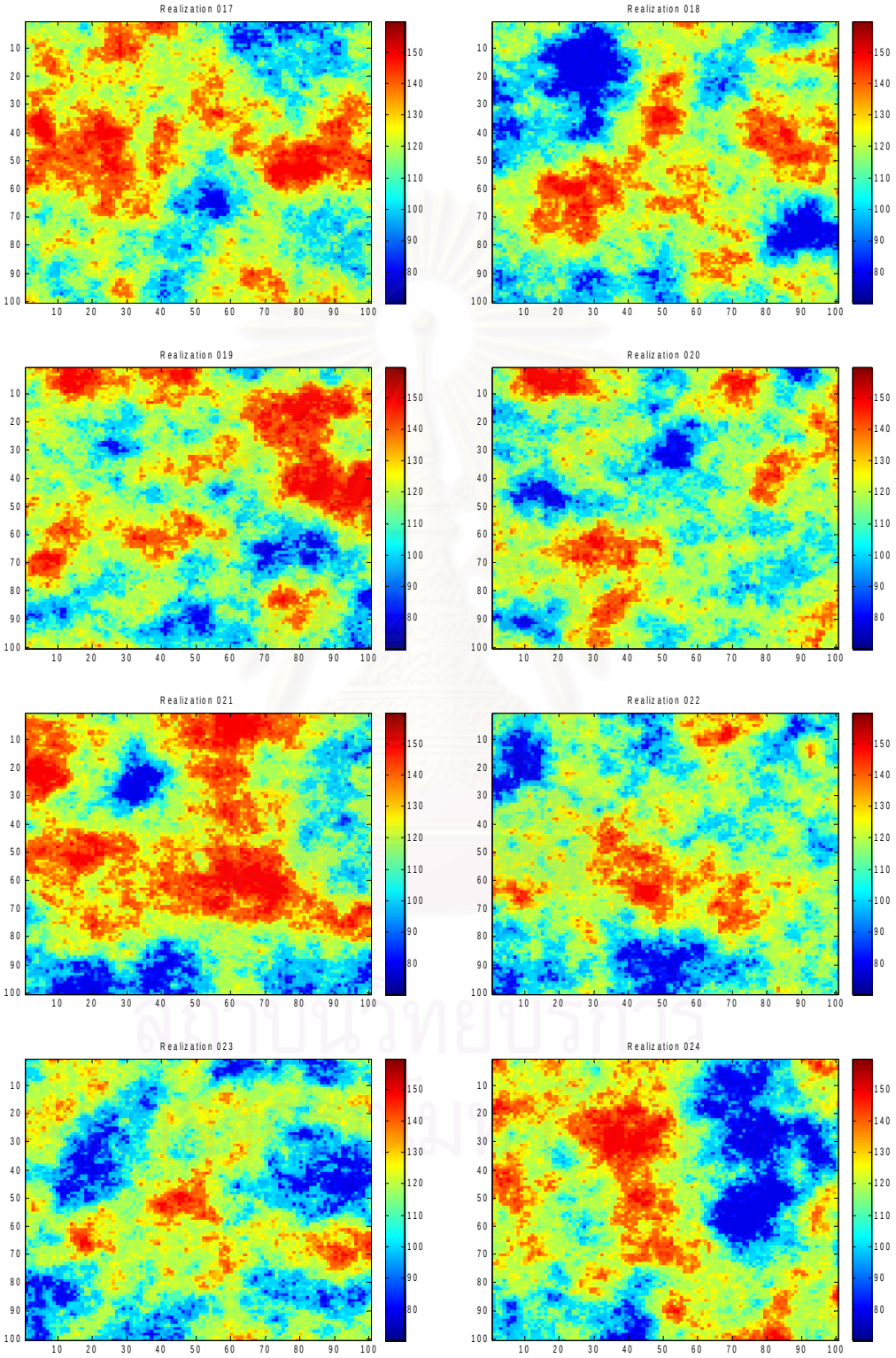

Figure 4.36: Permeability distribution for realizations 17-24 based on local upscaling.

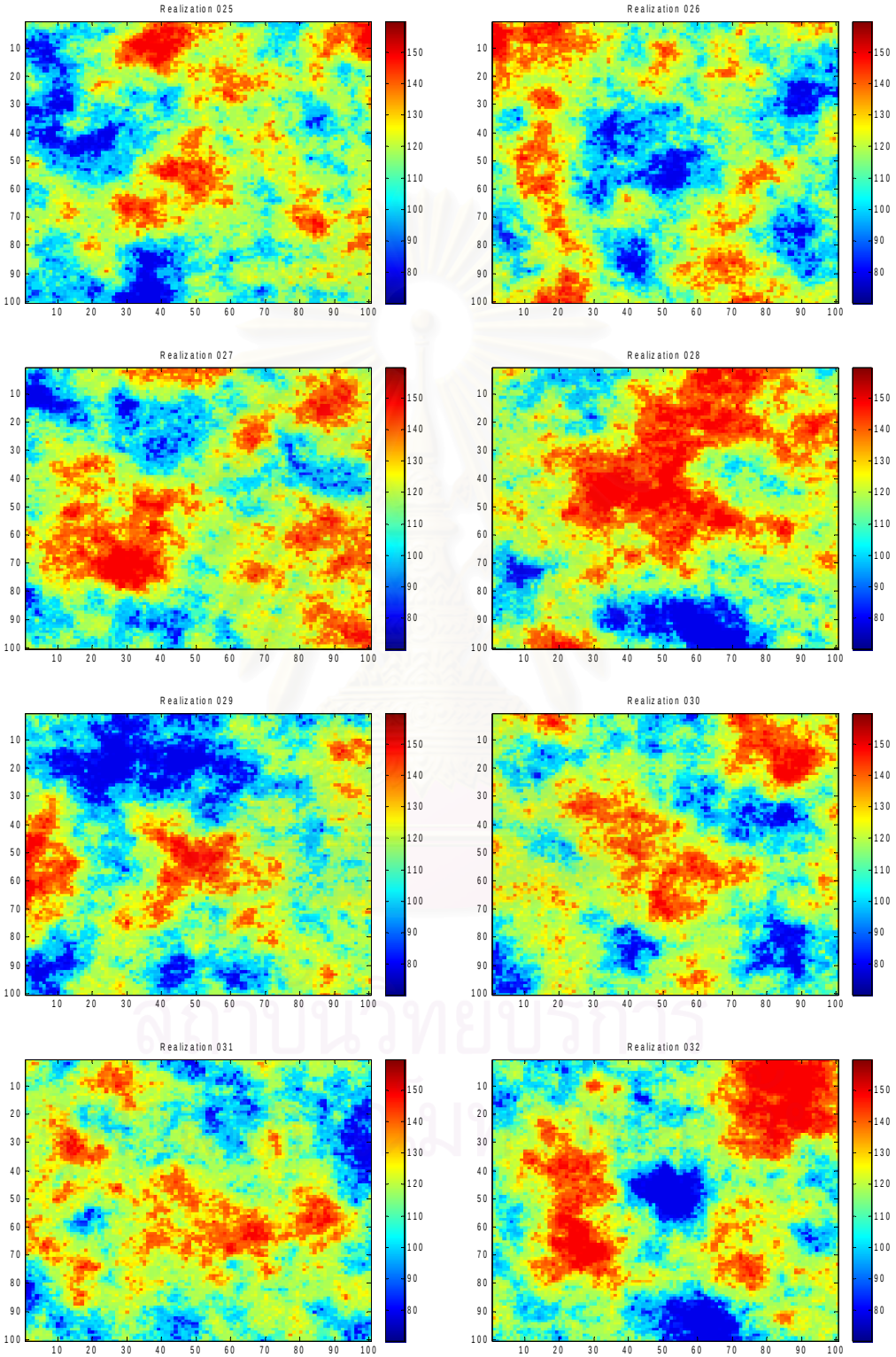

Figure 4.37: Permeability distribution for realizations 25-32 based on local upscaling.

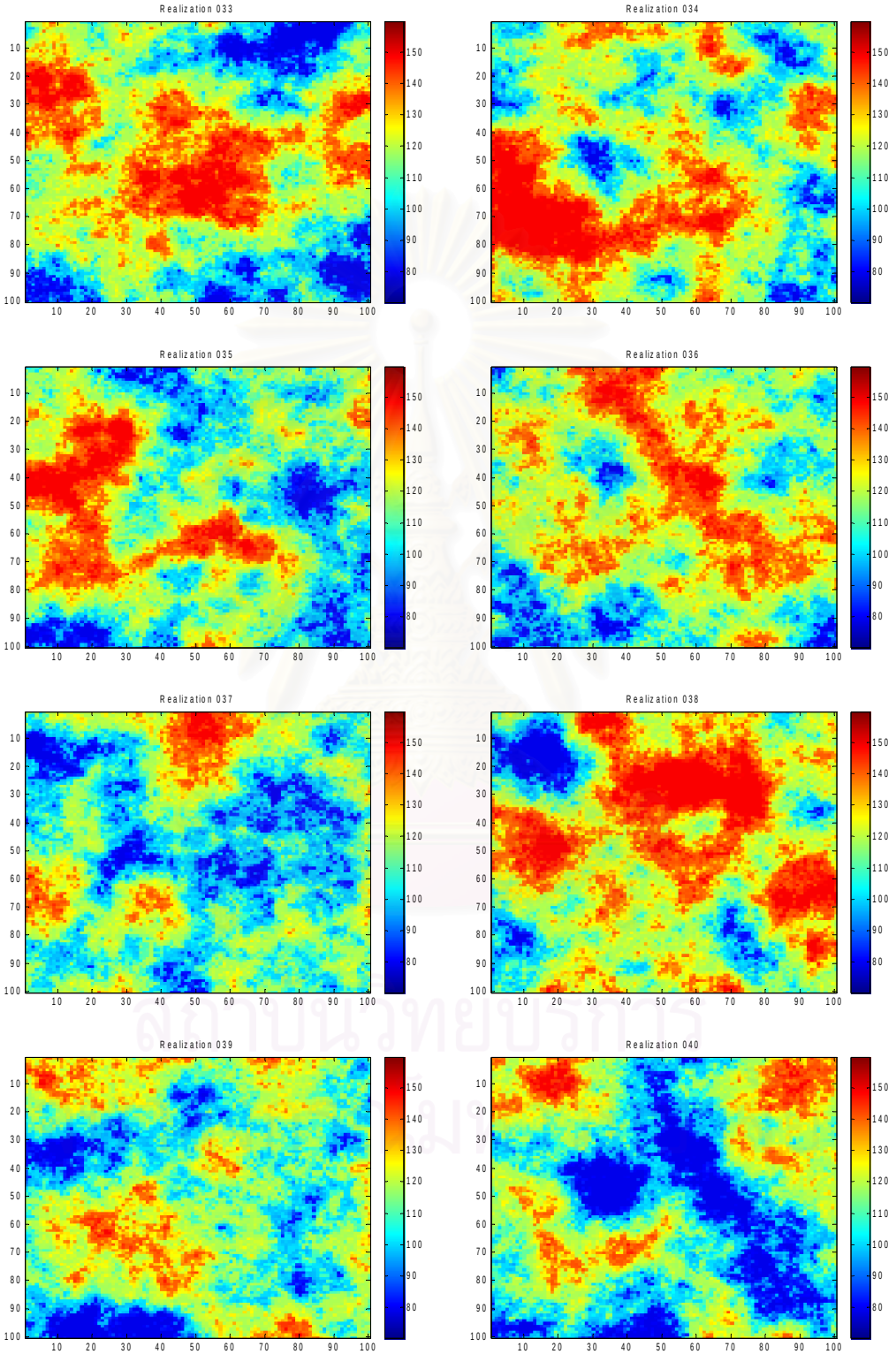

Figure 4.38: Permeability distribution for realizations 33-40 based on local upscaling.

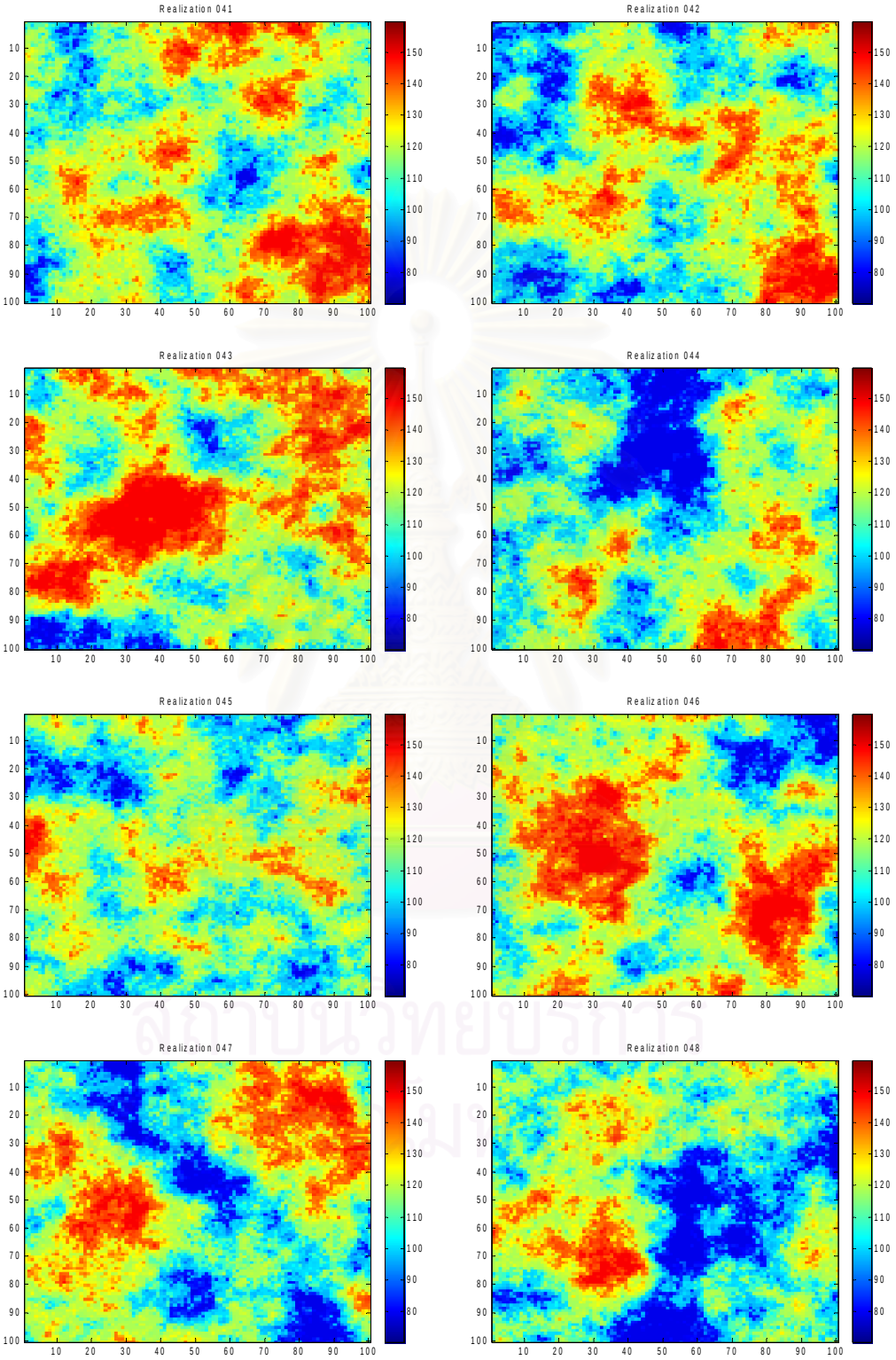

Figure 4.39: Permeability distribution for realizations 41-48 based on local upscaling.

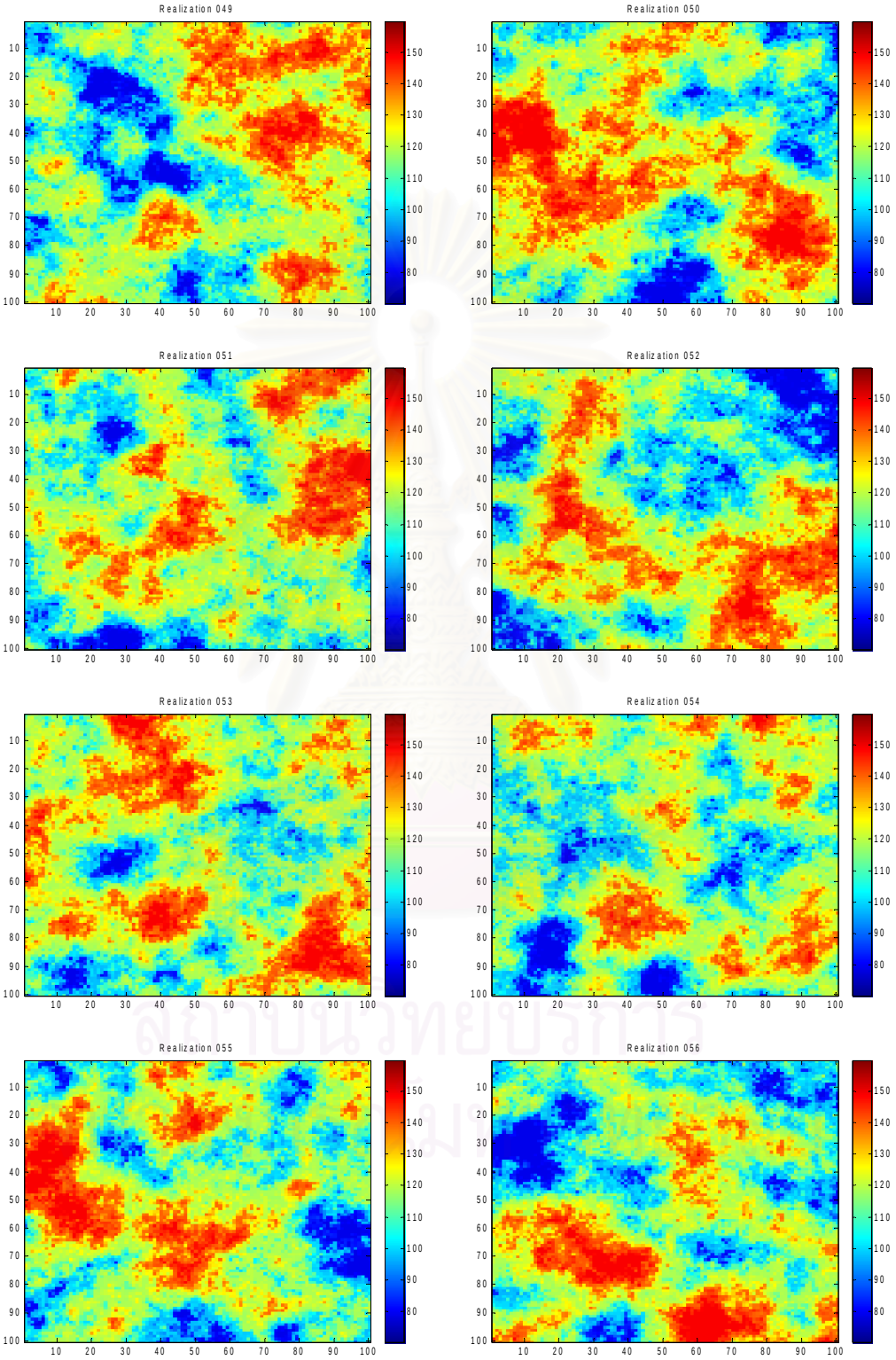

Figure 4.40: Permeability distribution for realizations 49-56 based on local upscaling.

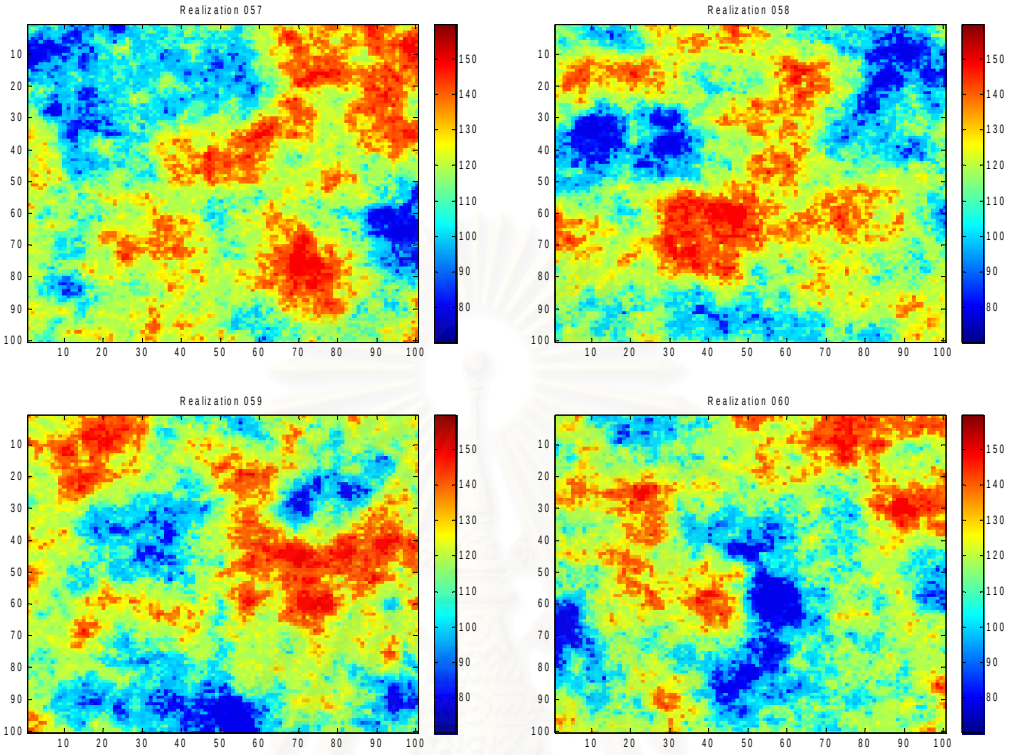

Figure 4.41: Permeability distribution for realizations 57-60 based on local upscaling.

4.4 Comparing the results

There are two different approaches to determine the coarse-scale permeability distribution which are based on global and local upscaling. The results obtained from the two methods for these three reservoirs were compared based on their values and results of reservoir simulation.

4.4.1 Comparison based on values of permeability

Fig. 4.42 shows coarse-scale permeability distributions based on global and local upscaling for Reservoir I. Fig. 4.43 shows coarse-scale permeability distributions based on global and local upscaling for Reservoir II. Figs 4.44 and 4.45 show the relationship between coarse scale estimates of permeability based on global and local upscaling for

Reservoir I and II, respectively. For Reservoir III, there are 60 realizations for coarse scale permeability based on both global and local upscaling. In order to make a comparison, all 60 realizations have to be averaged. Fig. 4.46 shows averaged permeability values at the scale of 100 × 100 grid blocks based on global and local upscaling. Fig. 4.47 shows the relationship between coarse-scale permeabilities based on global and local upscaling for Reservoir III.

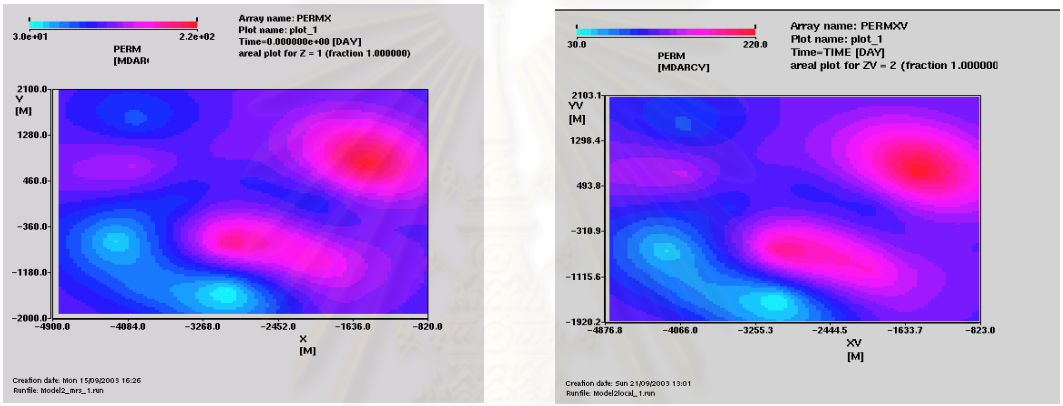

Global Upscaling Local Upscaling

Figure 4.42: Permeability distributions based on global and local upscaling for Reservoir I.

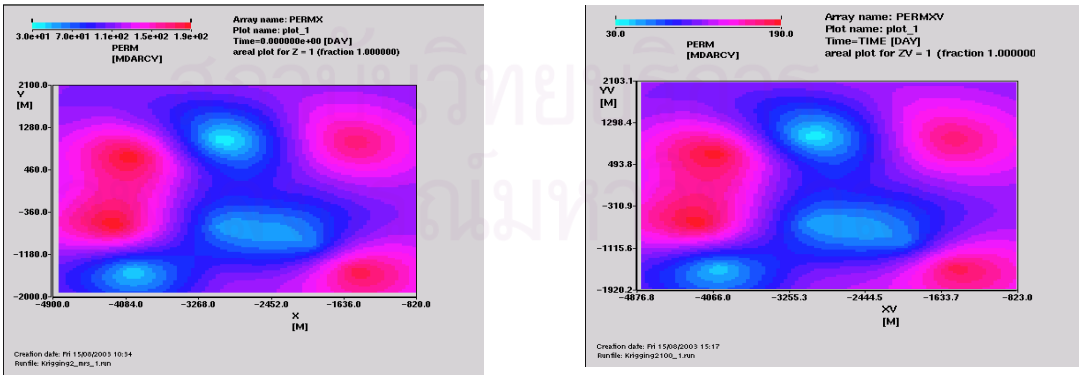

Global Upscaling Local Upscaling

Figure 4.43: Permeability distributions based on global and local upscaling for Reservoir II.

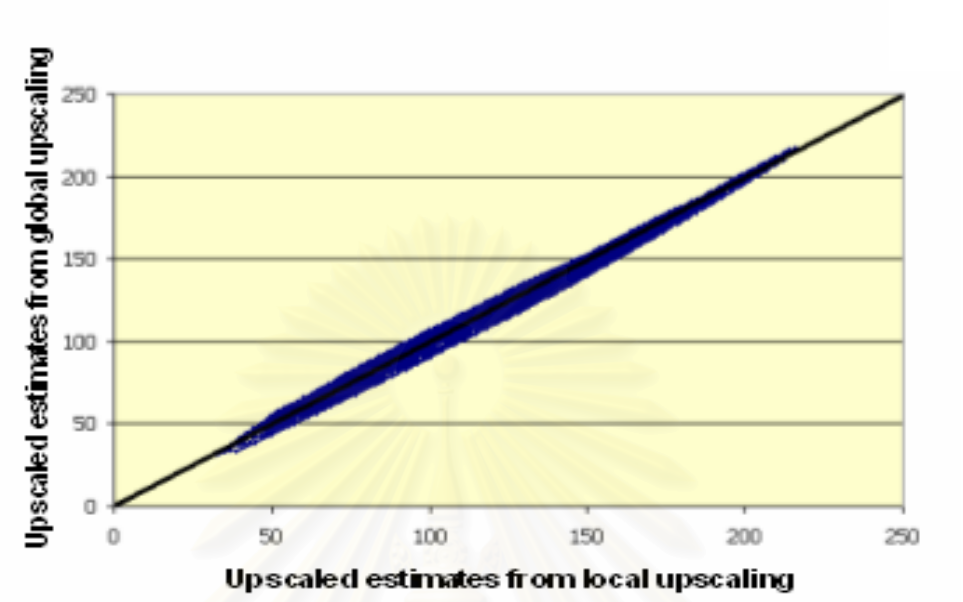

Figure 4.44: The correlation between upscaled permeability values from global and local upscaling for Reservoir I.

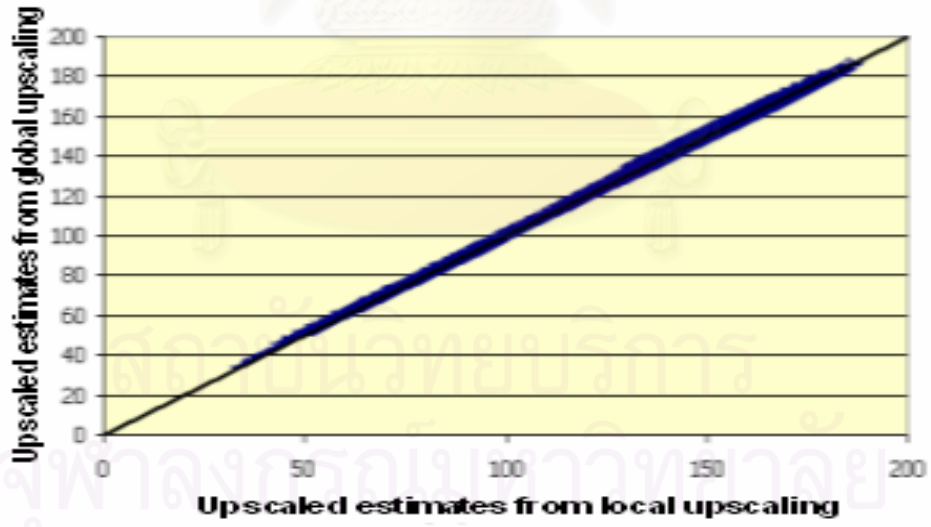

Figure 4.45: The correlation between upscaled permeability values from global and local upscaling for Reservoir II.

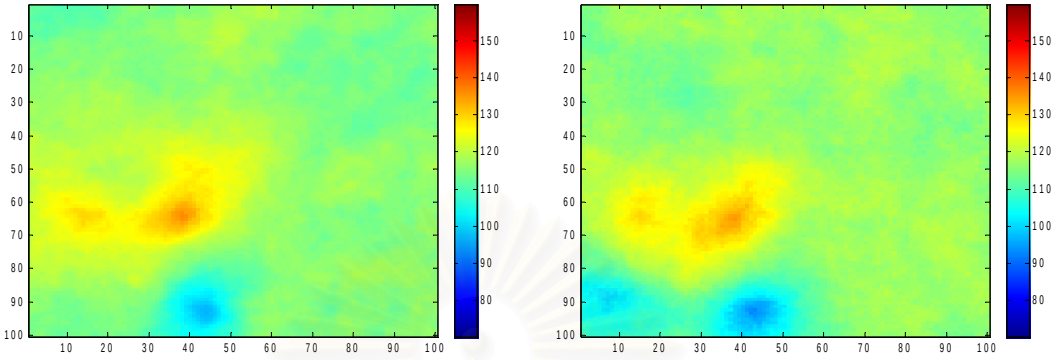

Average upscaled permeabilities from global upscaling

Average upscaled permeabilities from local upscaling

Figure 4.46: Picture of average upscaled permeability values from global and local upscaling for Reservoir III.

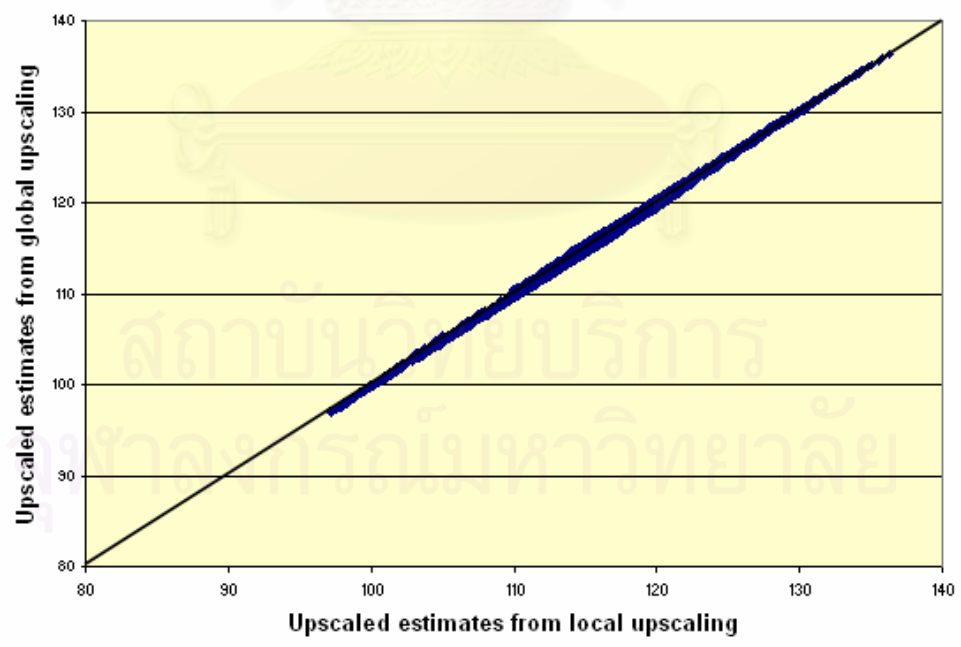

Figure 4.47: The correlation between upscaled permeability values from global and local upscaling for Reservoir III.

As seen in Figs. 4.44, 4.45, and 4.47, a strong linear correlation between upscaled permeability values from global and local upscaling and the correlation values are 0.996, 0.999, and 0.998 for Reservoir I, II and III, respectively. They indicate a good match between the two approaches. Moreover, the similarity between upscaled permeability values from global and local upscaling for Reservoir I, II and III can be seen on Figs. 4.42, 4.43 and 4.46, respectively.

4.4.2 Comparison based on results of reservoir simulation

Only Reservoir I and II, for which permeability distributions were obtained via Krigging estimation, were compared using reservoir simulation. The simulation was not performed for Reservoir III because there are too many realizations generated by Sequential Gaussian Simulation. This study used a simulation program called Spider[14]. All properties except permeabilities, minimum bottom hole pressure, and skin factor were assumed to be the same for both reservoir models. The simulation assumed that the thickness of the model is 1 ft and porosity is 0.25 throughout the reservoir. The properties that need to be entered into the reservoir simulation are:

4.4.2.1 PVT data

Table 4.26: PVT data.

P (psia)	**B_0** (rb/stb)	**R_s** (mcf/stb)	**Oil viscosity** (cp)	**B_g** (rb/mcf)	**Gas viscosity** (cp)
500	1.1152	0.1201	0.8962298	6.23746	0.01649
1000	1.19498	0.2827	0.6452354	3.02018	0.01772
1500	1.29073	0.4665	0.5124182	1.95571	0.01899
2000	1.39964	0.6655	0.4300265	1.43099	0.02031
2359	1.485	0.816	0.3876277	1.19611	0.02127

4.4.2.2 Relative Permeability

Table 4.27 shows relative permeability used in simulation program for these two reservoirs.

Table 4.27: Relative permeability.

	Saturation		End Point		Corey Exponent
S_{orw}	0.12	$K_{row}(S_{wc})$	0.6	N_{ow}	3
S_{org}	0.06	$K_{rg}(S_{wc})$	0.93	N_{og}	3
S_{gc}	0.037	$K_{rw}(S_{orw})$	0.35	N_g	2.8
S_{wc}	0.27			N_w	3

4.2.2.3 Well data and locations

Six production wells were used in this study. Tables 4.28 and 4.29 show well data and locations for Reservoir I and II, respectively. Fig. 4.48 shows the location of these production wells.

Table 4.28: Well data and locations for Reservoir I.

Well name	Well completion	X direction (ft)	Y direction (ft)	Pressure constraint (minBHP) (psia)	Maximum Rate (bbl/d)	Radius (ft)	Skin Factor
Pw1	Vertical	1,000	1,000	500	10,000	0.3	1
Pw2	Vertical	2,000	1,520	500	10,000	0.3	1
Pw3	Vertical	3,000	1,000	500	10,000	0.3	1
Pw4	Vertical	1,000	3,000	500	10,000	0.3	1
Pw5	Vertical	2,000	2,520	500	10,000	0.3	1
Pw6	Vertical	3,000	3,000	500	10,000	0.3	1

Table 4.29: Well data and locations for Reservoir II.

Well name	Well completion	X direction (10 ft)	Y direction (10 ft)	Pressure constraint (minBHP) (psia)	Maximum Rate (bbl/d)	Radius (ft)	Skin Factor
Pw1	Vertical	1,000	1,000	700	10,000	0.3	0
Pw2	Vertical	2,000	1,520	700	10,000	0.3	0
Pw3	Vertical	3,000	1,000	700	10,000	0.3	0
Pw4	Vertical	1,000	3,000	700	10,000	0.3	0
Pw5	Vertical	2,000	2,520	700	10,000	0.3	0
Pw6	Vertical	3,000	3,000	700	10,000	0.3	0

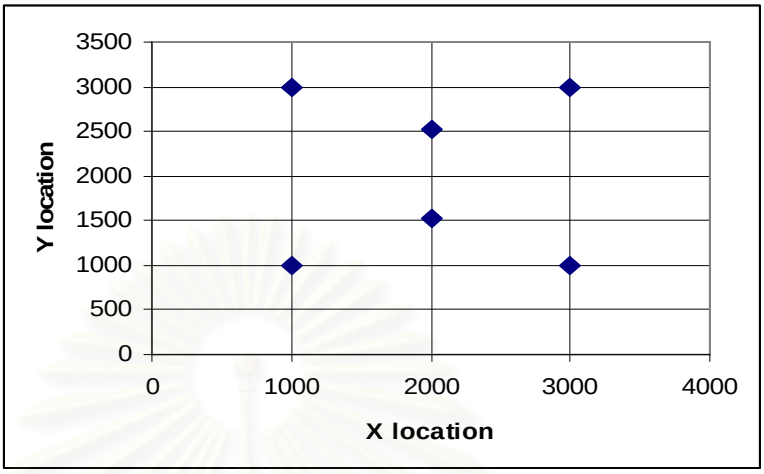

Figure 4.48: Locations of six production wells.

4.2.2.4 Simulation results

Reservoir simulation results on these two models can be divided into three scenarios: fine-scale simulation, simulation based on coarse-scale permeability distribution obtained from global upscaling, and simulation based on coarse-scale permeability distribution obtained from local upscaling. Figs. 4.49 and 4.50 show a comparison of oil rate for Reservoir I and II, respectively. Figs. 4.51 and 4.52 present a comparison of gas rate for Reservoir I and II, respectively. Figs. 4.53 and 4.54 display a comparison of bottom hole pressure for Reservoir I and II, respectively. These figures show that coarse-scale permeability obtained from local upscaling provide similar results with the coarse-scale permeability distribution obtained from global upscaling and the fine-scale permeability distribution.

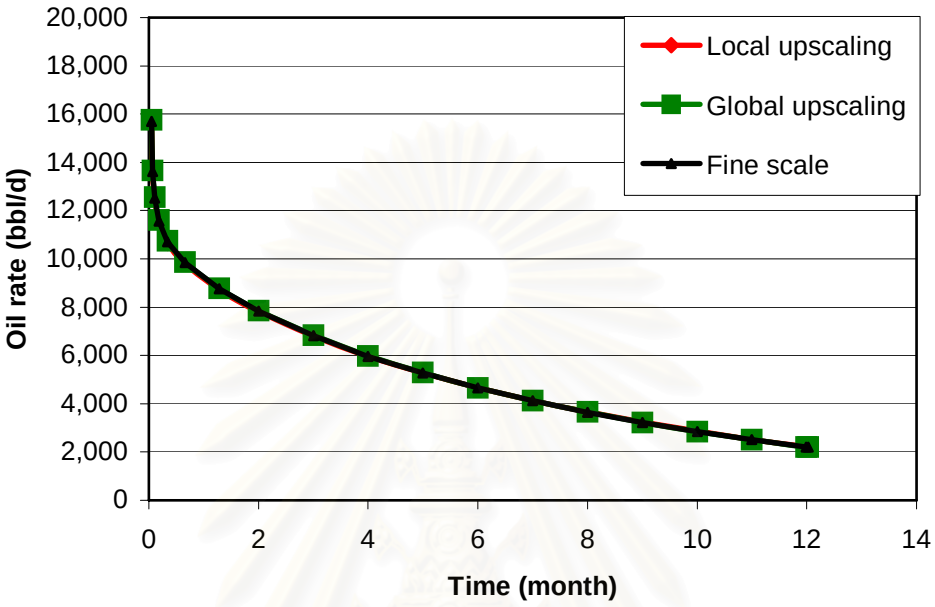

Figure 4.49: Oil rate obtained from simulation for Reservoir I.

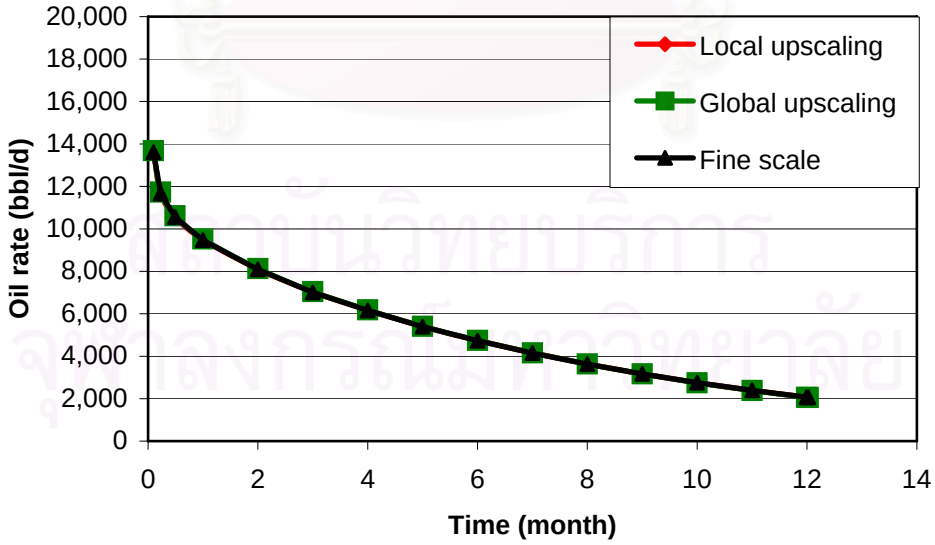

Figure 4.50: Oil rate obtained from simulation for Reservoir II.

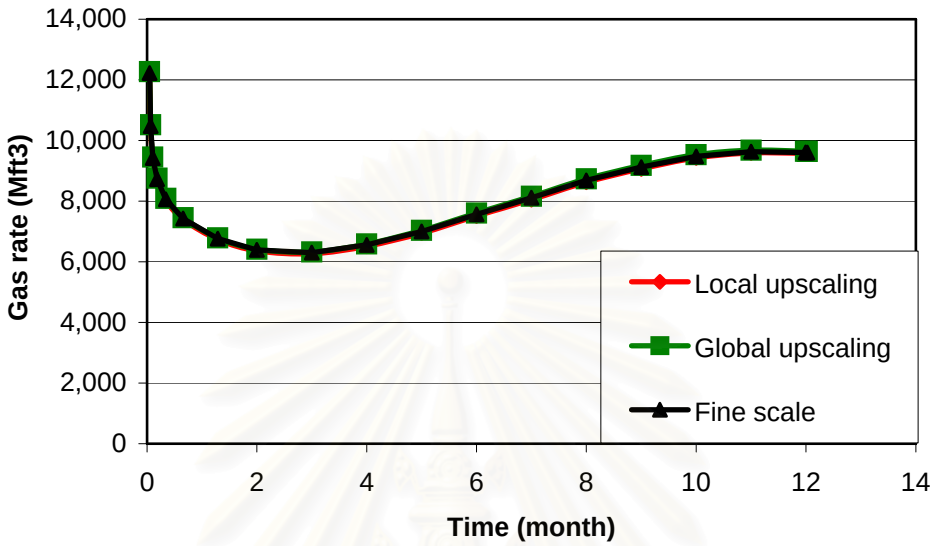

Figure 4.51: Gas rate obtained from simulation for Reservoir I.

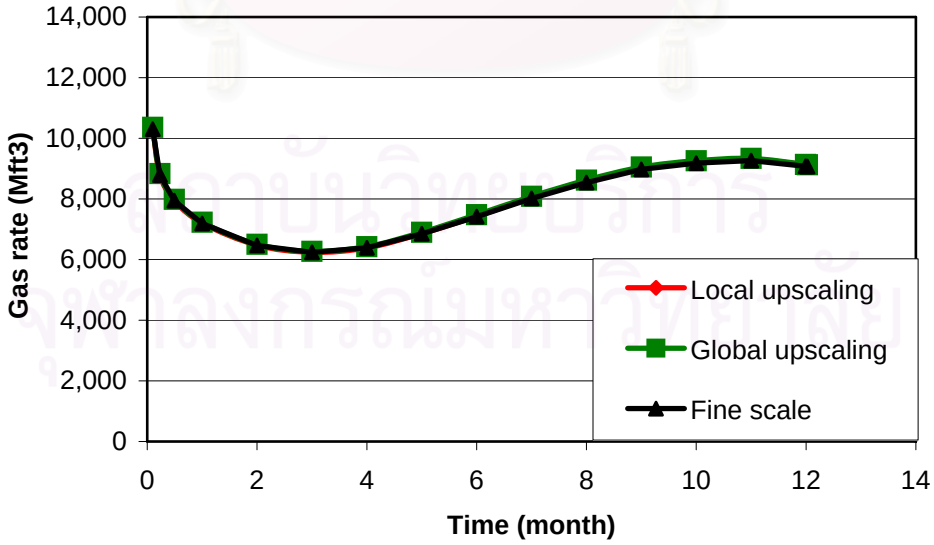

Figure 4.52: Gas rate obtained from simulation for Reservoir II.

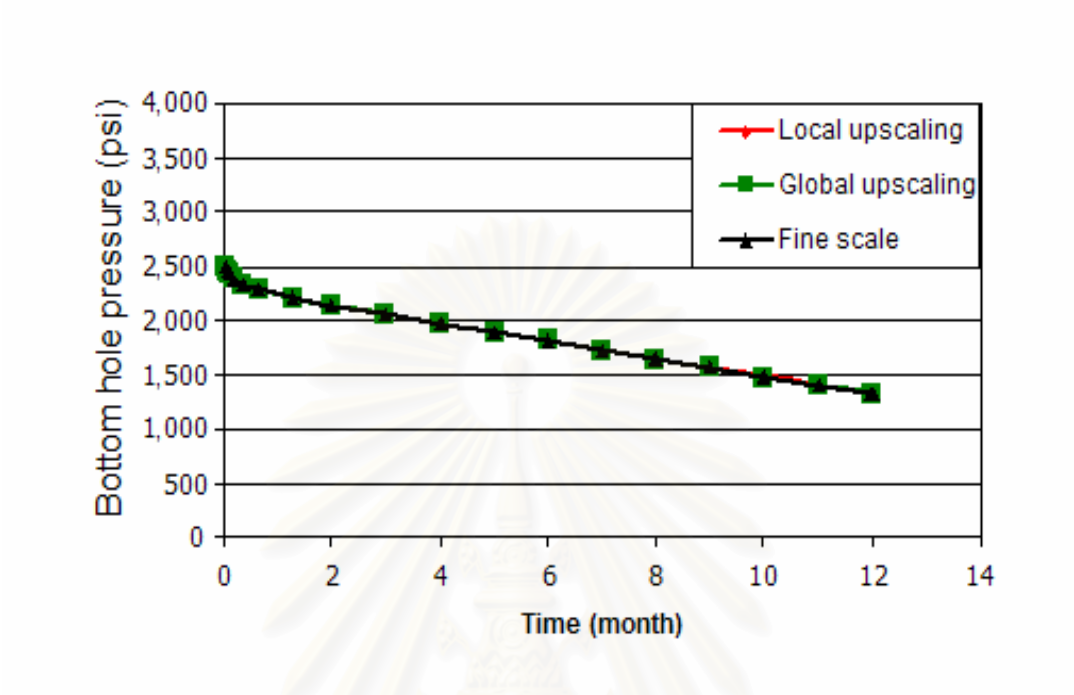

Figure 4.53: Bottom hole pressure obtained from simulation for Reservoir I.

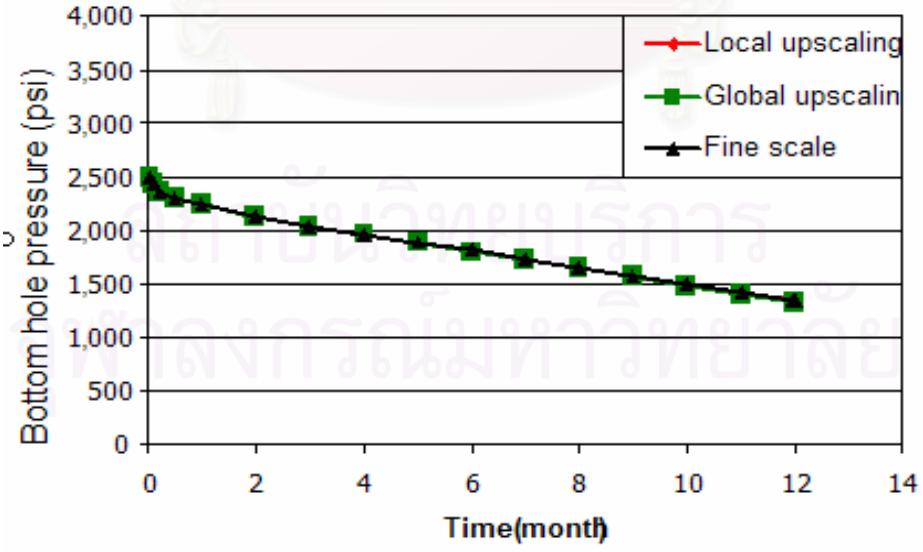

Figure 4.54: Bottom hole pressure obtained from simulation for Reservoir II.

In addition, the pressure distributions after one year of production of fine-scale permeability distribution, coarse-scale permeability distribution based on global upscaling, and coarse-scale permeability distribution based on local upscaling for Reservoir I are shown in Figs. 4.55, 4.56, and 4.57, respectively. These figures show that coarse-scale permeability distribution based on local upscaling provide similar results with coarse-scale permeability distribution based on global upscaling and the fine-scale permeability distribution.

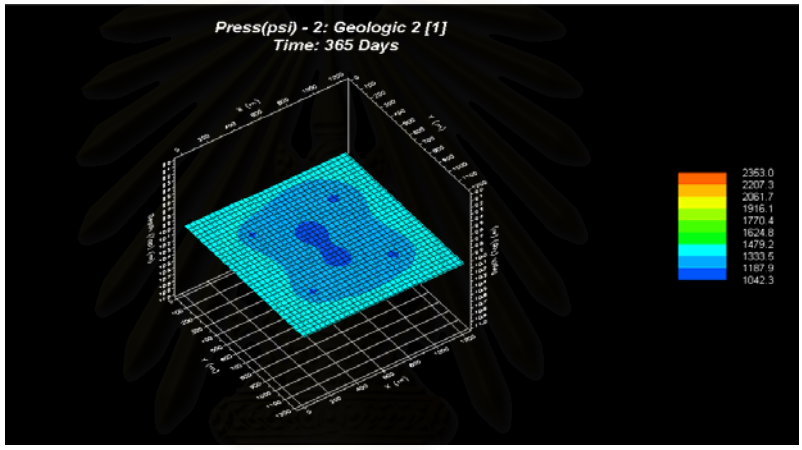

Figure 4.55: Pressure distribution after one year of production for fine-scale simulation for Reservoir I.

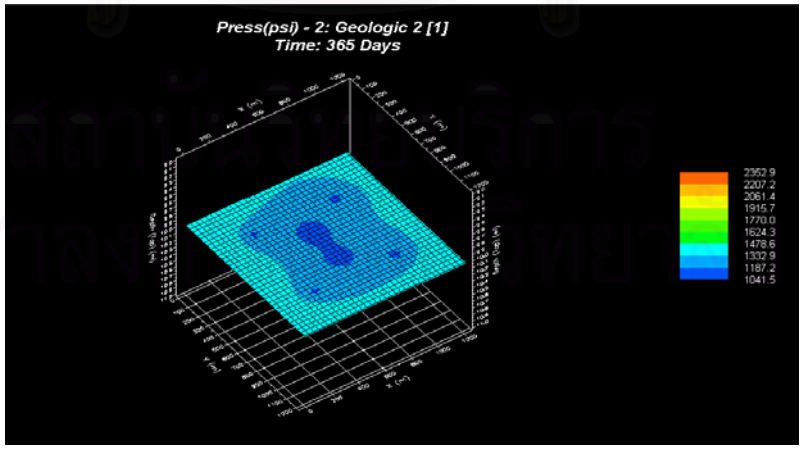

Figure 4.56: Pressure distribution after one year of production for simulation based on global upscaling for Reservoir I.

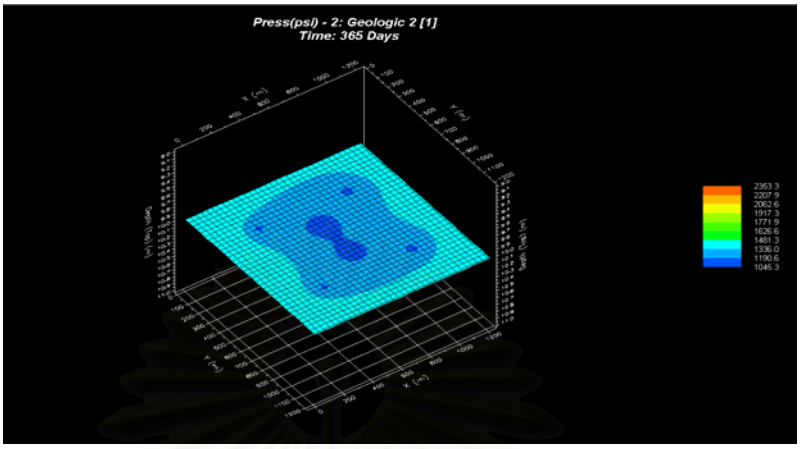

Figure 4.57: Pressure distribution after one year of production for simulation based on local upscaling for Reservoir I.

Figs. 4.58, 4.59, and 4.60 show the pressure distributions of fine-scale, globally upscaling and locally upscaling scenarios, respectively, for Reservoir II. These figures show that coarse-scale permeability distribution based on local upscaling provide similar results with coarse-scale permeability distribution based on global upscaling and the fine-scale permeability distribution.

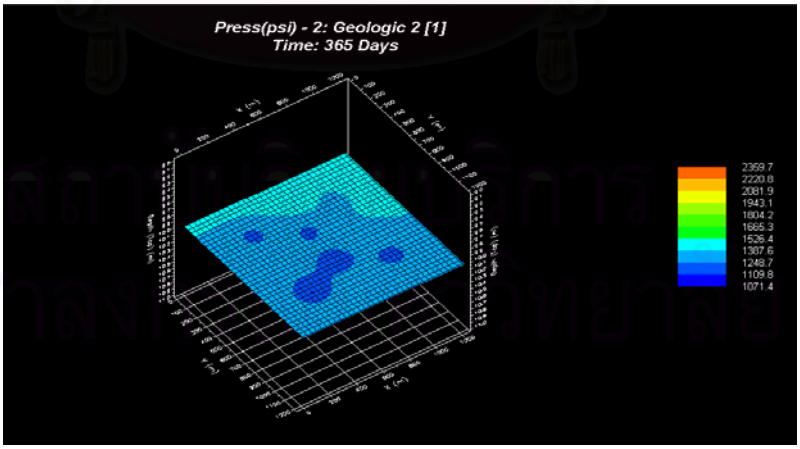

Figure 4.58: Pressure distribution after one year of production for fine-scale simulation for Reservoir II.

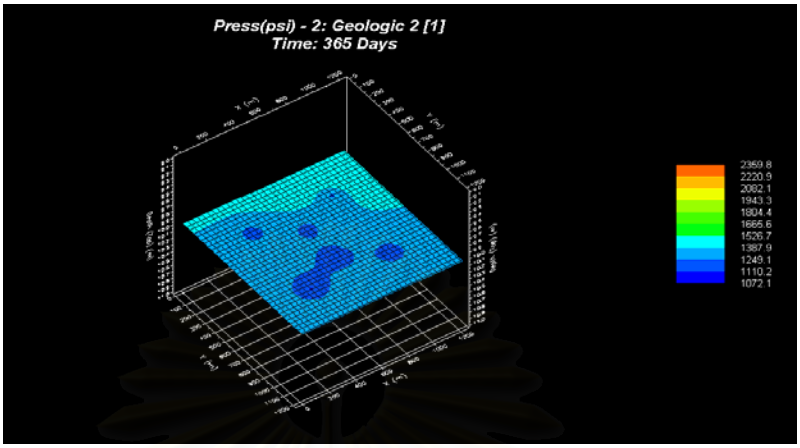

Figure 4.59: Pressure distribution after one year of production for simulation based on global upscaling for Reservoir II.

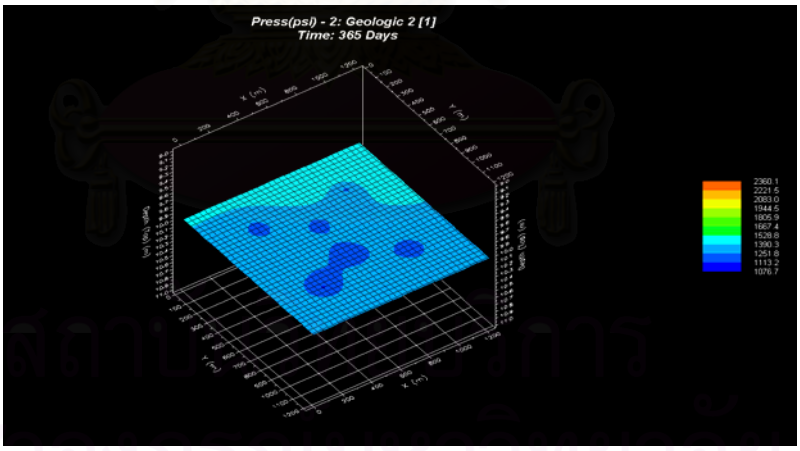

Figure 4.60: Pressure distribution after one year of production for simulation based on local upscaling for Reservoir II.

Oil rate, gas rate, and bottom hole pressure obtained from simulating the two reservoirs using globally upscaled and locally upscaled permeability values are similar to results obtained from fine-scale simulation. In addition, the pressure distributions after one year of production obtained from coarse-scale simulation based on global and local upscaling are similar to the results from fine-scale simulation. This indicates that the coarse scale permeability distribution determined from local upscaling approach is as good as the one obtained from global upscaling approach. The benefit of determining permeability distribution based on local upscaling is mainly a reduction in computational time.

CHAPTER V

CONCLUSIONS AND RECOMMENDATIONS

Tremendous number of cells is needed to describe fine scale heterogeneities of the reservoir. Such scale cannot be accommodated by a dynamic reservoir simulator really well. Thus, the number of grid blocks must be reduced by averaging the reservoir properties to fit with the capability of the reservoir simulator. Coarse-scale reservoir properties have to be determined. In addition, these coarse-scale reservoir properties have to provide similar result to the one from fine-scale simulation. The process of determining properties of larger grid blocks is called upscaling. Conventional methods used to generate coarse-scale reservoir properties are performed for the entire reservoir. Thus, the approach is global upscaling in this study. The disadvantage of this approach is long computational time spent on upscaling properties for the entire field. To speed up the process, this study introduces a new method to generate coarse-scale reservoir properties based on local upscaling. Local upscaling is applied only at data locations. Distribution of upscaled properties are then determined using Geostatistics.

In this study, three synthetic reservoirs were used to test the effectiveness of the proposed algorithm. In the first and second reservoir, 14 permeability values sampled from 14 vertical wells in 4,020 x 4,010 ft^2 of domain area were made up. Then, the variogram models which are spherical model with nugget of 0.00, range of 1,400 ft, and sill of 3,240 for Reservoir I and nugget of 0.00, range of 1,510 ft, and sill of 4,080 for Reservoir II, were determined. Krigging estimation was used to generate fine-scale permeability distributions for both reservoirs. Then, two coarse-scale permeability distributions were generated based on global and local upscaling for both reservoirs. For local upscaling approach, the new variogram models which are spherical model with nugget of 0.00, range of 1,600 ft, and sill of 2,820 for Reservoir I and nugget of 0.00, range of 1,530 ft, and sill of 4,230 for Reservoir II was determined. Krigging estimation was used to generate coarse-scale permeability distribution. In the third reservoir, 28 permeability values sampled from 16 vertical

wells and 3 horizontal wells in 2,000 x 2,000 ft^2 domain area were made up. Then, the variogram model which is spherical model with nugget of 0.02, range of 548 ft, and sill of 0.98 of normal score data were determined. Sequential Gaussian Simulation technique was used to generate 60 realizations of fine-scale permeability distribution. Then, 60 realizations of coarse-scale permeability distributions were computed based on global upscaling. For local upscaling, Krigging estimation was used to generate fine-scale permeability distribution. The new variogram model which is spherical model with nugget of 0.01, range of 538 ft, and sill of 0.99 of normal score data for the coarse properties was determined. Gaussian Simulation technique was then used to generate 60 realizations of coarse-scale permeability distribution.

The coarse-scale permeability values based on global and local upscaling for all reservoirs were compared using scatter plots. The scatter plots between coarse-scale permeability values based on global and local upscaling for all reservoirs show the strong correlations which are 0.996, 0.999, and 0.998 for Reservoir I, II and III, respectively. In addition, the results of reservoir simulation from coarse-scale permeability values based on global and local upscaling for Reservoir I and II were compared with the results from fine-scale simulations. However, Reservoir simulation was not performed for Reservoir III since there are too many realizations. The results of reservoir simulation in oil rate, gas rate, bottom hole pressure, and pressure distribution after one year of production from coarse-scale permeability values based on global and local upscaling for Reservoir I and II show similar results to those obtained from fine-scale permeability values. Local upscaling approach gives similar results compared with results obtained from global upscaling approach. Both of them still provide accurate results as compared with the results from fine-scale simulation.

In conclusion, coarse-scale permeability distribution based on local upscaling is an alternative approach of upscaling. The new approach can be used as effectively as the conventional global upscaling but consumes less computational time since upscaling is performed only at data locations.

It is worth pointing out that the range of permeability used in this study is between 30 and 220 md which is quite small. If there are more variations in permeability values, the results may be different. Further investigation is thus needed.

REFERENCES

1. Beckner, D. Li and B., and Kumar, A. A New Averaging Technique for Scaleup of Multimillion-Cell Geologic Models. SPE 56554, 1999.
2. Lozano, J.A., Costa, L.P., Alves, F.B. and Silva, A.C. Upscaling of Stochastic Models for Reservoir Simulation-An Integated Approach. SPE 36205, 1996.
3. King, P.R., The Use of Renormalization for Calculating Effective Permeability, Transport in Porous Media 4 (1989): 37-58.
4. Begg, S.H., Carter, R.R., and Dranfield, P., Assigning Effective Values to Simulator Gridblock Parameters for Heterogeneous Reservoirs, SPERE, November (1989):455.
5. Muskat, M., Flow of Homogeneous Fluids Through Porous Media, New York, McGraw-Hill, 1937.
6. Cardwell, W.T. J.R., and Parsons, R.L., Average Permeability of Heterogeneous Oil Sands, Trans. AIME, No.160, 1945:34-42.
7. Warren, J.E. and Price, H.S., Flow in Heterogeneous Porous Media, Society of Petroleum Engineers Journal (1961): 153-169.
8. Tang, R.W., Behrens, R.A., and Emanuel, A.S., Reservoir Studies Using Geostatistics to Forecast Performance, SPE18432, 1989.
9. Christie, M.A., Upscaling for Reservoir Simulation, SPE37324, 1996.
10. Malick, K.M., Boundary Effects in the Successive Upscaling of Absolute Permeability, Master's Thesis, Stanford University, Standford, CA, 1995.
11. Kelkar, M., Applied Geostatistics for Reservoir Characterization, Class Notes, The University of Tulsa, tulsa, Oklahoma, 1996.
12. Petrel Oslo, Petrel Workflow Tools. Oslo, Norway, Technoguide Continental Europe AS, 1996.
13. Research and Technology Services, FrontEnd/Reduce++ Online Users Manual, Shell International E&P, Rijswijk, 2001.
14. Shell E&P Technology Applications and Research, Spider Users Manual, Shell International E&P, Rijswijk, 2002.

VITAE

Pakarang Yimpoonsap was born on September 24, 1977 in Bangkok province, Thailand. He received his B. Eng. in Chemical Engineering from the Faculty of Engineering, King Mongkut University of Technology at Thonburi in 1998. He has been a graduate student in the master degree program in petroleum engineering of the Department of Mining and Petroleum Engineering, Chulalongkorn University since 2000. Currently, he works as a drilling engineer at Chevron Offshore (Thailand) Limited.